KNMI Climate Change Scenarios 2006 for the Netherlands

KNMI Scientific Report WR 2006-01

Bart van den Hurk, Albert Klein Tank, Geert Lenderink, Aad van Ulden, Geert Jan van Oldenborgh, Caroline Katsman, Henk van den Brink, Franziska Keller, Janette Bessembinder, Gerrit Burgers, Gerbrand Komen, Wilco Hazeleger and Sybren Drijfhout

This electronic document is a corrected update of the hardcopy version, published on 30 May 2006 together with a list of errata.

Abstract

Climate change scenarios for the Netherlands for temperature, precipitation, potential evaporation and wind for 2050, and for sea level rise for 2050 and 2100 have been constructed using a range of data sources and techniques. The scenario variables have been defined after consultation with a number of potential scenario users.

General Circulation Model (GCM) simulations which have become available during the preparation for the upcoming Fourth Assessment report (AR4) of IPCC have been used to derive scenarios of sea level change in the eastern North Atlantic basin and wind speed in the North Sea area. The GCM simulations also were used to span a range of changes in seasonal mean temperature and precipitation over the Netherlands. It was found that most of this range could be related to changes in projected global mean temperature and changes in the strength of seasonal mean western component of the large scale atmospheric flow in the area around the Netherlands. Therefore, temperature and circulation were used to discriminate four different scenarios for temperature, precipitation and potential evaporation, by choosing two different values of global temperature change and two different assumptions about the circulation response. The construction of the extreme precipitation and temperature values and the potential evaporation values was carried out using an ensemble of Regional Climate Model (RCM) simulations and statistical downscaling on observed time series. Additional scaling and weighting rules were designed to generate RCM sub-ensembles matching the seasonal mean precipitation range suggested by the GCMs.

The circulation steering parameter has a great impact on the number of precipitation days, the seasonal mean precipitation, and the intensity of extreme precipitation exceeded once every 10 years. Also potential evaporation is affected greatly by the assumed circulation change. Changes of daily mean wind speed exceeded once per year are rather small, compared to the typical interannual variability of this variable. Sea level change scenarios are constructed using a combination of GCM output and a literature survey of sea level change contributions from changes in terrestrial ice masses. For 2100 the scenarios span a range between 35 and 85 *cm*.

This report contains a detailed description of the motivation and rationale of the new KNMI'06 climate scenarios for the Netherlands, and provides a detailed description of the methodology used for each group of variables. A summary table (Table 8-1) lists all final scenario values. The last part of the manuscript provides guidelines for the use and interpretation of the scenario values. Also an index is provided with a justification of the statements made in a popular brochure on the KNMI'06 climate scenarios.
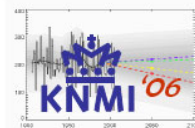
GENERAL DESCRIPTION

1 Introduction

1.1 Quick reading guide

This manuscript contains a description of the construction of the new climate change scenarios 2006 for the Netherlands, identified as the **KNMI'06 climate scenarios**. It is probably too detailed for people interested in a specific feature or component, and simultaneously there can be many details missing. The group of readers who want a broad overview of the rationale of the construction of the scenarios and some more details about a certain group of variables are advised to read Section 3, in particular Section 3.2. Table 1-1 gives an index of sections where the different groups of variables are discussed.

The remainder of this report provides the technical and scientific documentation of the KNMI'06 scenarios. After a description of the context and methodological justification, a brief overview of the history of climate scenarios at KNMI is given in Section 2. The rationale and methodology to arrive at the four scenarios are detailed and documented in Section 3. The resulting quantitative changes are presented for temperature and precipitation, potential evaporation, wind, and sea level in Sections 4 to 7. After the final summary (Section 8), Section 9 is devoted to remarks on how these quantitative numbers can and should be interpreted in applications. Suggestions for future research directions are described in Section 10. Section 11 contains references justifying each of the statements made in the brochure "Climate in the 21st century; Four scenarios for the Netherlands" (KNMI, 2006).

1.2 Context and Motivation

Information on regional and local climate variability and extremes is of great practical importance for living conditions and almost all human activities. Nature and man have adapted to the conditions of local climate so closely that large deviations of it may cause considerable damage. As a result, detailed information on climate change is required for impact and adaptation studies in the Netherlands.

Climate change is a subject of intense scientific research. When the Fourth Assessment Report (AR4) of the Intergovernmental Panel on Climate Change (IPCC) will be published in 2007 it will condense results from thousands of scientific publications into a general assessment of the current knowledge about the climate system and the man-induced changes to it. Despite this wealth of information, regional and local climate change predictions are still hard to make due to the complexity of the climate system. A regional manifestation of climate change is subject to many interacting processes affecting atmospheric circulation and region-specific responses of physical processes. The KNMI Climate Scenarios 2006 presented in this report have been formulated on the basis of current knowledge and uncertainties with the ambition of providing planners with the best possible advice. They provide an update of the previous generation climate scenarios (Können, 2001), as described in Section 2.

Potential future evolutions of the climate (so-called "projections") are explored with the help of sophisticated global climate models (General Circulation Models, GCMs). These models differ considerably in their projections, for regional scales in general and for the Western European region in particular. Uncertainties arise from imperfect models, internal variability of the climate system, and unknown future evolutions of anthropogenic forcings of the climate system. To capture the possible range of future climate change an ensemble

approach is required in which boundary conditions, initial conditions and model formulations are varied.

A means of dealing with uncertainty is the construction of a small collection of climate *scenarios*. Climate scenarios are relevant, plausible and internally consistent pictures of how the climate may look like in the future (IPCC, 2001). *Relevant* means that they must allow the evaluation of climate change effects under conditions relevant for decision making. In many impact assessment applications the robustness of strategies is analyzed, and this assessment can only be done when the possible range of conditions for which the application is being evaluated is wide enough. *Plausible* means that the scenarios should reflect a future that is considered to be possible. The definition of what is plausible is somewhat subjective: very extreme changes may be very unlikely but not totally impossible, and in some cases it may be relevant to make an assessment of the consequence of this extreme, yet unlikely, event. *Internally consistent* implies that different physical processes that are quantified in the scenarios are likely to be occurring simultaneously. In practice, multiple variables (e.g., temperature, precipitation, wind) affect an application, and the change of these variables should thus be projected in a consistent manner.

Different applications or sectors in society may require different climate information or scenarios. The selection and specification of scenario variables and the selection of projection time frames depend on the requirements of the users and thus on the actual dialogue process with stakeholders. For this reason, scenarios are some times called "social constructs" (Müller and Von Storch, 2004; Von Storch, 2006).

Table 1-1: Overview of variables in the KNMI'06 climate scenarios. The section refers to the chapter where the variables are described in detail. A brief explanation of the rationale and sources of information per group of variables is given in Section 3.2.

Summer (JJA)	Winter (DJF)	Section
Mean summertime temperature	Mean wintertime temperature	4.4
Mean temperature of yearly warmest summer day	Mean temperature of coldest winter day	4.5
Mean summertime precipitation	Mean wintertime precipitation	4.4
Number of summertime precipitation days	Number of wintertime precipitation days	4.4
Mean precipitation on summertime precipitation day	Mean precipitation on wintertime precipitation day	4.4
Local precipitation daily sum exceeded once every 10 years	10-day precipitation daily sum exceeded once every 10 years	4.5
Summertime potential evaporation		5
	Daily mean wind exceeded once per year	6.2
Not seasonally dependent		
Mean sea level rise		7.8

The existence of different user groups implies that "general" climate change scenarios are not necessarily useful for all. On the other hand, the construction and publication of an unlimited number of scenarios is not desirable, since the construction of a coherent set of

impacts for different sectors is then no longer feasible. Some grouping is thus required, in order to serve as many users as possible with a limited and coherent set of future inventories.

The scenarios that are addressed in this study are a group of general climate change scenarios constructed by KNMI for the Netherlands for the target periods around 2050 and 2100. The scenarios include values of changes of a set of variables, where relevant per season, in particular winter (December, January and February) and summer (June, July, August). The scenarios consist of values for the changes in both climatological means and extremes on the daily time scale. The variables included in the KNMI climate scenarios are listed in Table 1-1. The construction of these scenarios is described in detail in this manuscript.

General climate change scenarios for the Netherlands have been issued before by Können (2001; see also Kors et al., 2000, Kabat et al., 2005 and Section 2). Similar regional climate change scenarios have been developed for many larger and smaller regions of the world, e.g. the United States (Giorgi et al., 1994; MacCracken et al., 2003), the United Kingdom (Hulme et al., 2002), Switzerland (Frei, 2004) and Southern Africa (Arnell et al., 2005). The reason to present new general climate change scenarios for the Netherlands at this moment is a combination of questions from stakeholders and newly available knowledge on the climate system.

We will first discuss some aspects of our current understanding of the climate system (Section 1.3), and available methods to make assessments of future evolutions of the (regional) climate (Section 1.4). This is followed by a brief description of the interaction with stakeholders, and the approach chosen for scenario development (Section 1.5).

1.3   Understanding climate and climate change

The state of the climate system is constantly changing. The combination of multiple time scales related to the solar cycle, heat exchange between ocean, land and atmosphere, and other physical processes is able to generate regional variations on many time scales (CLIVAR, 1995). An example that even on 30-year time scales climate displays substantial and unpredictable variability is given by Selten et al. (2004). Additional change comes from variations in forcings of the atmosphere and ocean, both natural (such as variations in solar strength and variations in atmospheric dust load due to volcanic eruptions) and anthropogenic (such as anthropogenic emissions of greenhouse gases and changes in land use).

The climate system is characterized by a large number of processes acting on different temporal and spatial scales. The first order climate response to enhanced greenhouse gas concentrations may be regarded as a radiative adjustment leading to a change of the temperature distribution through the atmosphere: higher temperatures near the surface, cooler temperatures in the higher troposphere and stratosphere. This response is accompanied by a complex chain of higher order effects, including changes in snow and ice cover, the hydrological cycle, ocean currents, atmospheric circulation patterns and distribution of storage reservoirs for heat, moisture and carbon.

As an additional complication, the processes also interact with each other, causing many different feedbacks, both positive and negative (Komen, 2001). A quantitative assessment of the effects of these forces and processes requires the use of numerical models, such as GCMs. Much effort has gone into their development and validation, e.g. under the umbrella of the Coupled Model Intercomparison Modelling project, CMIP (Meehl et al., 2000, 2005; Covey et al., 2003). The many validation studies that have been carried out have given

valuable insight in the abilities and shortcomings of these models in reproducing the observed climate of the twentieth century (Boer et al., 2000; Stott et al., 2000). As it turns out some climate variables (e.g., global mean temperature) are better simulated than others (e.g., regional precipitation).

Even with a well calibrated GCM, simulation of the future climate is subject to considerable uncertainty. Projections are made with climate models which are forced with external variables, such as volcanic dust load, solar insolation and anthropogenic emissions and land use changes. The anthropogenic forcings are closely related to socio-economic developments, which are difficult to predict. To overcome this problem a set of widely agreed greenhouse gas emission scenarios have been constructed (IPCC, 2000; these scenarios are known as the SRES scenarios). Climate models are then used to translate each emission scenario into a climate change scenario.

Another important source of uncertainty comes from the internal dynamics of the climate system. It is well known that deterministic weather prediction is not possible beyond a horizon of one or two weeks due to the chaotic nature of the atmospheric flow. However, the mean (climatic) state of the flow has some predictability (Lorenz 1975; Palmer, 1993; Shukla, 1998), especially when "external" factors such as solar insolation or the atmospheric composition are changing. Climate predictability remains limited (Tennekes, 1990, Komen, 2001), as there is always the possibility of unexpected features (Komen, 1994), for example, when certain thresholds are exceeded (Manabe and Stouffer, 1988; Schaeffer et al., 2002; Rial et al., 2005).

Recently, several studies have addressed the problem of limited predictability using an ensemble of model simulations. In this approach uncertainty related to initial conditions and/or parameter values is mapped into uncertainty in the future state of the system. In weather prediction the ensemble approach is operational (Molteni et al., 1996; Buizza et al., 2005), resulting in an estimate of the probability distribution of future weather variables, a few days later. This approach has been successfully extended to seasonal prediction (Palmer et al., 2004), where the mean state of the climate system is predicted with coupled atmosphere/ocean models. Similar work is done for predictions on a longer, decadal time scales. A regional multi-model study of climate change was presented by Vidale et al. (2003). In the Dutch Challenge project (Selten et al., 2004) ensemble projections for the 21st century were made with a global coupled atmosphere/ocean model. The result showed significant (internal) decadal variability of the mean state, in good agreement with the magnitude of observed decadal variations. Another example is the so-called perturbed physics ensemble (Allen et al., 2000; Murphy et al., 2004), where the perturbations were generated by varying key model parameters within their range of uncertainty. The studies give valuable insights in the limitation of predictability on seasonal to decadal time scales.

In summary, the assessment of the future evolution of (regional) climate is subject to many uncertainties:
- the unknown evolution of anthropogenic activities and natural forcings and the degree to which these will change the greenhouse gas concentrations in the atmosphere or the land cover;
- the limited quality of present-day climate models, owing to limited process and system understanding and limited computer resources;
- lack of knowledge about the climate response to future atmospheric concentrations and land use;
- the inherent internal variability of the climate system.

Predictions of anthropogenic climate change are hampered by these uncertainties. Model ensemble studies (Murphy et al., 2004) are a viable method for exploring uncertainty, but they will never provide absolute certainty, simply because the models involved may share common deficiencies.

For making a systematic outlook of future climate, a hierarchy of climate models at various spatial resolutions and empirical/statistical techniques is the most suitable tool. IPCC (2001) concludes in their Third Assessment Report (TAR) that "the combined use of different techniques may provide the most suitable approach in many instances. The convergence of results from different approaches applied to the same problem can increase the confidence in the results". This is the methodology followed in this report for developing the climate scenarios for the Netherlands.

1.4　Available tools for assessing future climate

The climate change scenarios for the Netherlands are based on a hierarchy of GCM model output, high resolution nested Regional Climate Model (RCM) simulations, and empirical/statistical downscaling using local observations in the Netherlands.

Coupled atmosphere-ocean GCMs are the most suitable tools to simulate the global climatic response to anthropogenic forcings, as they represent the current state of our understanding of the global climate system in a quantitative, consistent and integrated structure. The present construction of climate change scenarios for the Netherlands is based on a multi-model ensemble approach, where use is made of many recent model simulations, and where the use of each model is based on a careful expert-judgement of the quality of that particular model. An important source of information is the database of global GCM results, made available by the Climate Model Diagnosis and Intercomparison (PCMDI) group at Lawrence Livermore National Laboratory, in collaboration with the JSC/CLIVAR Working Group on Coupled Modelling (WGCM) and their Coupled Model Intercomparison Project (CMIP; see `http://www-pcmdi.llnl.gov/ipcc/about_ipcc.php`). This database contains results from control runs for the present climate and from transient runs for the 21st century forced with a set of SRES emission scenarios.

An ensemble of GCM simulations driven by a range of greenhouse gas emission scenarios is compared to observations to make a selection of GCMs that adequately simulate the important climate features in the Netherlands and surroundings. Projections with this set of GCMs are grouped into four different scenarios, where variations in global mean temperature and in the response of the regional atmospheric circulation are used to discriminate between the scenarios.

The typical grid resolution in state-of-the-art GCMs is still too coarse to examine effects of local topography and land use, and to quantify local extreme events. In a process called dynamical downscaling, GCM-simulations are used as boundary condition for high resolution Regional Climate Models (RCMs), where information on mesoscale effects and small-scale temporal and spatial variability of meteorological variables is generated. Again, an ensemble approach is followed where multiple RCM/GCM combinations are used. The main source of information here are results from the European PRUDENCE project (Christensen et al., 2002) including the KNMI Regional Climate Model RACMO2 (Lenderink et al., 2003). The PRUDENCE archive (`http://prudence.dmi.dk`) mainly contains time-slice runs for the period 2070-2100 based on the SRES A2 scenario. However, the PRUDENCE RCM output cannot be used directly to construct scenarios for time frames or circulation changes that are not included in the database. Therefore, we used an indirect "scaling" approach by combining existing GCM and RCM outputs in an optimal way. By verification

and qualitative expert judgement of the RCM results, a selection of models used for each scenario is made.

The combined GCM/RCM scaling approach only produces meaningful changes for a limited number of indices related to the means and the extremes of climate variables of interest, in particular temperature and precipitation. Many applications, however, need a more complete description of the probability density functions or time series representative for future climate conditions for these climate variables. Therefore, where possible, additional information on spatial and temporal variability is added by a transformation of a set of observation time series from Dutch weather stations covering the 20th century. This transformation, for example, yields changes in the number of cold and warm days or 10-day precipitation amounts.

Sea level scenarios are directly derived from the GCM simulations and recently published results. For sea level rise, we use all GCM model output available at PCMDI to estimate the effect of thermal expansion of the ocean on sea level. Estimates of the contribution of melting land ice are based on the recent literature. For the wind scenarios we use a selection of GCMs with a good representation of large scale flow over Europe. High resolution RCMs do not add relevant information on this variable.

1.5   The scenario structure and consultation of scenario users

Climate change is represented by changes in many different climate indices, related to the means and the extremes on different temporal and spatial scales. It is practically impossible to represent the range spanned by the full set of indices by a limited set of scenarios. Therefore a selection has been made in order to focus the scenarios on the indices that are most relevant to society. Part of this selection was based on a user consultation involving individuals and institutions involved with planning in the Netherlands in the following sectors: water, nature/ecosystem, energy, agriculture, transport and infrastructure, industry, financial services and public health. With some of these sectors already intensive contacts were maintained over the last few decades; contacts with others were new. In several presentations and meetings information on climate change was provided, and information needs were expressed by the audience.

Table 1-2: Values for the steering parameters used to identify the four KNMI'06 climate scenarios for 2050 relative to 1990. The scenario labels are explained in the main text.

Scenario	Global Temperature increase in 2050	Change of atmospheric circulation
G	+1°C	weak
G+	+1°C	strong
W	+2°C	weak
W+	+2°C	strong

On the basis of these discussions the list of variables included in the climate scenarios was fine-tuned, resulting in the list in Table 1-1. The climate scenarios mainly focus on changes for 2050, since most potential users of the scenarios do not have a longer planning horizon. To complete the picture of the future climate, the changes of the climatological mean and daily extremes included in the scenarios need to be accompanied by information on natural year-to-year variability. This is effectuated by presenting scenario values in conjunction with observed time series in which variability on interannual and longer time scales is included (see Section 9.7).

The criterion for discriminating the actual four scenarios is based on the GCM projections. Inspection of GCM output for the B1, A1B and A2 scenarios shows a range in mean global mean temperature rise between 1990 and 2050 of approximately +1°C to +2°C. For the first half of the 21st century the uncertainty due to different emission scenarios is smaller than the uncertainty induced by the differences between individual GCMs driven by the same emission scenario. To tag the different scenarios to elementary underlying assumptions, it was decided not to relate the climate scenarios to emission scenarios, but simply to the increase in global mean temperature by 2050. Global mean temperature increase is thus the first criterion to discriminate the four scenarios. The values for global temperature increase and atmospheric circulation change chosen to discriminate the four scenarios for the Netherlands are summarized in Table 1-2. They represent a "moderate" increase of the global temperature of +1°C in 2050 relative to 1990, and a "strong" increase of +2°C in 2050. These temperature increases are consistent with the previous generation climate change scenarios for the Netherlands (Können, 2001; see Section 2).

A further analysis of GCM and RCM output for typical regional quantities revealed the importance of changes in circulation patterns over Europe for the climate in the Netherlands. It was found that for a given global temperature rise the range of future climate conditions for the Netherlands could be very well spanned by specification of differences in the simulated circulation change. Two anticipated circulation regime changes are included in the scenarios: a *strong change of circulation*, which induces warmer and moister winter seasons and increasing the likelihood of dry and warm summertime situations, and a *weak change of circulation*. Both regimes are presented for the +1°C and +2°C global temperature increases, producing a total of four scenarios (see Figure 1-1). Table 1-2 gives an overview of the scenario labels. "G" is taken from the Dutch word "Gematigd" (= moderate), while "W" is taken from "Warm". "+" indicates that these scenario's include a strong change of circulation in winter and summer.
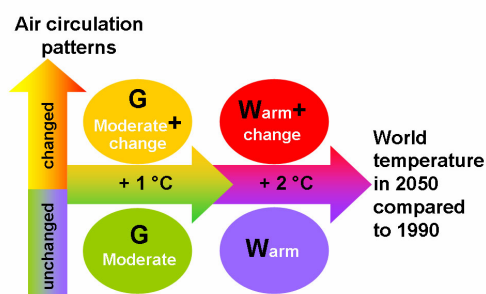
Figure 1-1: Schematic overview of the four KNMI'06 climate scenarios. For the legend, see Table 1-2.

Specific scenario values for the global temperature change and the circulation change were chosen in such a way that they represented the underlying variability of GCM results for Western Europe well, without overemphasising the extreme members in the GCM projections. This will be explained in more detail in Section 4.

For mean sea level rise in the North Sea, which is not clearly related to regional patterns of atmospheric circulation, a different approach was chosen. In fact, only two scenarios are distinguished (high global temperature and low global temperature rise) and for each

scenario the uncertainty range is quantified based on an analysis of all available GCM output and results from the recent literature. Sea level scenarios are given for both 2050 and 2100.

2   History of KNMI climate change scenarios

The practice of KNMI climate change projections dates back to 1991 with a project that was funded by the National Research Programme on Climate Change (NRP). Klein Tank and Buishand (1995) and Buishand and Klein Tank (1996) transformed observed precipitation records into time series representative for the future climate, which were useful for climate change impact studies. This transformation makes use of regression relations between precipitation and other climate variables (temperature and surface air pressure). The rationale is that information on large scale temperature and pressure changes can be used to derive local precipitation changes. The method allows for a modification of the sequence of wet and dry days by assigning a probability of rain to each day.
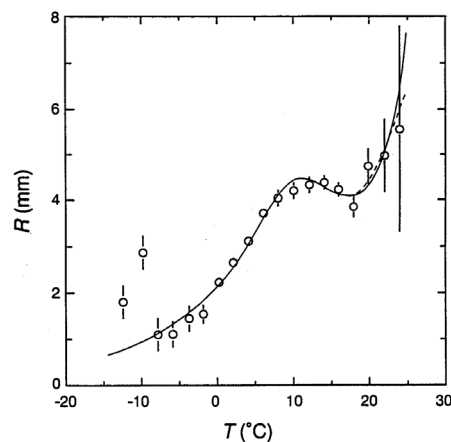
Figure 2-1: Relation between mean daily precipitation amount (R) and mean temperature in De Bilt (T) for wet days between 1906 and 1981 (from Buishand and Klein Tank,1996).

National and regional water authorities extensively used these transformed time series. The project was followed by a more formal suite of climate change scenarios, prepared in the context of 'Water Management in the 21st Century' (WB21) (Kors et al., 2000; Können, 2001). In these scenarios, only global temperature rise is considered as the independent driving variable, and a low, central and high value were adopted. For precipitation, observed relationships between temperature and precipitation intensity were used (Figure 2-1). These scenarios were constructed after the publications of the Second Assessment Report (SAR) of IPCC. It was assumed that local temperature change was equal to global mean temperature change. Sea level rise scenarios were derived from model calculations published in the SAR, and adjustments were included to account for land subsidence in the coastal area of the Netherlands. A collection of primary scenario variables is given in Table 2-1.

An essential assumption in the WB21 scenarios is that the scaling relations derived from the observations would not change under climate change conditions. This implies that the frequency distribution of circulation patterns (and associated precipitation days) would not change either. The appearance of the Third Assessment Report of IPCC did not give rise to a modification of the WB21 scenarios (Beersma et al., 2001).

After the first publication of the WB21 scenarios in 2000 (Kors et al., 2000), a number of additional scenarios was constructed, as requested by several users. The scaling relations applied for these additional scenarios were similar as in the original WB21 scenarios. In one

scenario, it was assumed that the global temperature increase would be accompanied by a strong decline of the Atlantic thermohaline circulation (Section 7), thus giving a relatively strong cooling of Northwest Europe (based on Klein Tank and Können, 1997). Another scenario was based on evidence from early GCM and RCM simulations for Europe, in which higher temperatures would lead to strong drying of the continent during summer, which in turn would lead to enhanced warming and reduced precipitation. In a later study by Beersma and Buishand (2002) this dry scenario has been transformed into a more sophisticated scenario that was constructed in the context of the National Drought study (RIZA, 2005). In that scenario, a seasonal variation in evaporation and precipitation changes was based on RCM results.

Table 2-1: Collection of variables according to the WB21 scenarios and later variants of these scenarios (Können, 2001; Beersma and Buishand, 2002).

Variable	low	central	high	change of Atlantic circulation	high dry
Annual mean temperature in 2050 (°C)	+0.5	+1	+2	-2	+2
Annual mean precipitation (%)	+1.5	+3	+6	-6	-10
Summer precipitation (%)	+0.5	+1	+2	-2	-10
Winter precipitation (%)	+3	+6	+12	-12	-10
10day precipitation sum (%)	+5	+10	+20	-20	-10
Return period of 1/100 yr daily precipitation sum (yr)	90	78	62	-	200
Annual evaporation (%)	+2	+4	+8	-8	+8
Sea level rise (cm)	+10	+25	+45	-	+45
Intensity of high wind speed and gales (%)	±5	±5	±5	-	0 – -10

A notable feature of the WB21 scenarios is that the sign of the changes in the mean and extreme precipitation is the same (see Table 2-1): an increase in mean precipitation implies an increase of the intensity of extreme precipitation events (or equivalently a reduction in the return period). Reversely, the dry scenario (with reduced summer precipitation) shows an increased return period of extreme precipitation as well. This feature is not necessarily realistic. Many recent (model based) projections of future climate indicate that reduced precipitation during summer is likely to be associated with small changes or increased levels of extreme precipitation at midlatitude land areas (Christensen and Christensen, 2003). This is one of the motivations for a revision of the climate change scenarios for the Netherlands, which is outlined in the next chapters.

3 Outline of the methodology

3.1 Important factors for climate change in Western Europe

The change of the regional climate of Western Europe and local climate of the Netherlands is determined by a chain of processes acting and interacting on global, regional and local scales. On the global scale the radiation balance plays a major role. Uncertainties are the future emission levels, and the level of response of the radiation balance to these greenhouse gases and aerosols. Also heat uptake by the oceans, large scale radiation feedbacks through clouds, water vapour and surface albedo (snow and ice) are key issues. The global change in the radiation balance is reflected in the global temperature rise. The change of the global temperature per W/m² increase in radiative forcing (directly related to enhanced greenhouse gas concentrations) is often referred to as 'climate sensitivity'. Global warming induces changes in atmospheric circulation which, together with local processes, leads to local

climate change in the Netherlands. Uncertainty increases when the level of regional detail increases. For example: projections of changes of global mean temperature have a smaller uncertainty than projections for a specific region in the world.

This somewhat simplistic picture of the chain between global scale warming and regional scale climate effects is embedded in the methodology followed to construct the KNMI'06 climate scenarios (Figure 3-1). Global climate models are used to diagnose the global temperature rise and circulation effects above Europe. Regional climate models and local observations are used to construct regional climate scenarios.
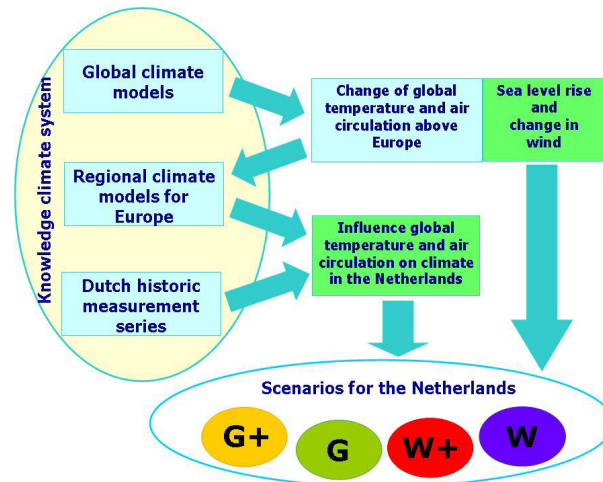
Figure 3-1: Schematic presentation of the methodology used for the construction of the KNMI'06 climate scenarios. The blue rectangles describe the sources of scenario information in the green rectangles. The arrows symbolise the information flow. Information about the climate system at global, regional and local scales was used for the climate scenarios.

In the KNMI'06 climate scenarios global mean temperature rise will be used as one of the two steering parameters. The global mean temperature rise is derived from projections of GCMs. Since the Third Assessment Report (TAR) of IPCC (2001), a wide range of state-of-the-art coupled atmosphere ocean GCM simulations have been executed and the main results have been made accessible to the scientific community for preliminary analyses to support the Fourth Assessment Report (AR4) of IPCC. This report will appear in 2007, and draft versions of the report are currently under review. A selection of these AR4 model results can be accessed via the KNMI Climate Explorer (`http://climexp.knmi.nl`).

Figure 3-2 shows the global mean temperature rise, calculated for four greenhouse gas emission scenarios (SRES B1, A1B, and A2, and a scenario with 140 years of 1% CO_2 increase per year) and by a collection of GCMs. The selection of models and emission scenarios is considered to reflect nearly the full range of realistic future temperature projections, and is described in detail in Section 4.2. The projected global temperature rise is in close agreement with the projections in TAR: between roughly 1.5 and 4.5°C increase in 2100 compared to the mean 1980 – 2000 temperature (which is almost the same as the mean of the reference period 1975 – 2005 that we will use). Both the methodology and the selection of models and emission scenarios are different for TAR and AR4. Therefore, the TAR maximum temperature rise of 5.8°C in 2100 is not present in Figure 3-2. For 2050 the temperature rise is between 1 and 2.5°C (Figure 3-3).
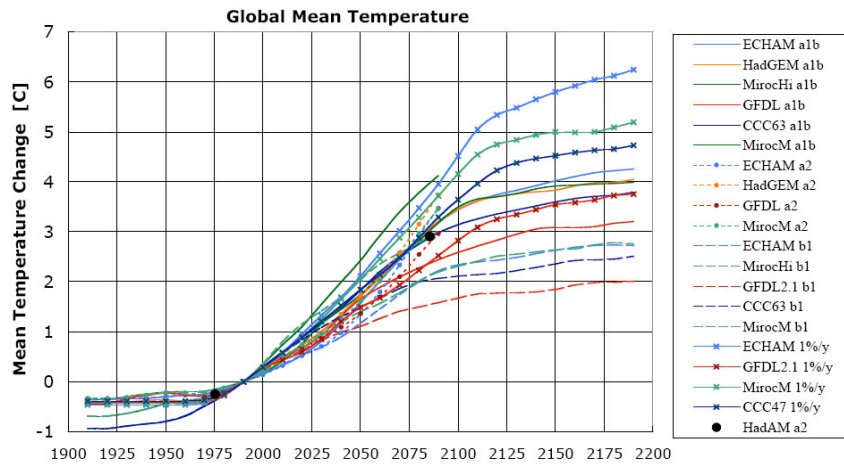
Figure 3-2: Time series of global mean temperature change for a wide range of GCM simulations, all driven by four different greenhouse gas emission scenarios. References to the models displayed are given in Table 4-1. For further explanation see main text.

The projected global temperature rise is not necessarily the same as the regional temperature rise in Western Europe. This can easily be seen in the observations of the past century. Van Oldenborgh and Van Ulden (2003) show that during the 20th century the temperature in De Bilt follows the rise in the global mean, but multiplied by a factor 1.4. This is mainly due to the position close to the land mass of Eurasia, which has warmed much more than the global mean. An increase of the frequency of south-western wind regimes affected the late winter and early spring seasons since the late 1980's. It is unknown whether the change in (south-western) wind directions has a partly anthropogenic origin, or whether natural variability may entirely explain this signal (Selten et al., 2004).
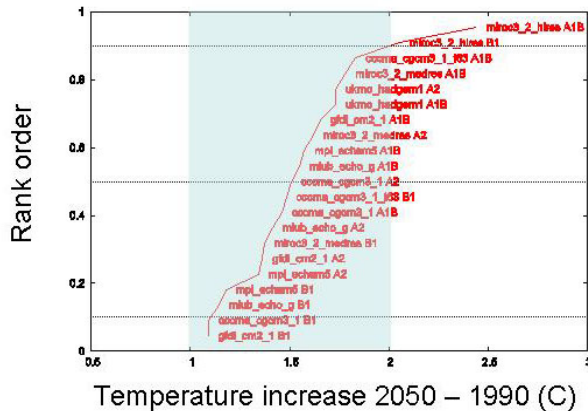
Figure 3-3: Cumulative frequency distribution of the model-predicted global temperature rise between 2050 and 1990. The shading indicates the KNMI-scenario values.

An observational illustration of the strong link between the strength of the western circulation and (seasonal mean) temperature and precipitation in the Netherlands is given in Figure 3-4. Here the strength of the western circulation is expressed as the seasonal mean westward component of the geostrophic wind (U_{geo}). Results are presented for seasonal mean temperature and precipitation in De Bilt for winter (DJF) and summer (JJA). The figure shows that a systematic change in the mean value of U_{geo} is associated with a clear change in

the mean temperature and precipitation characteristics. The circulation effect is that western wind generally brings moister air which is warmer in winter and cooler in summer.
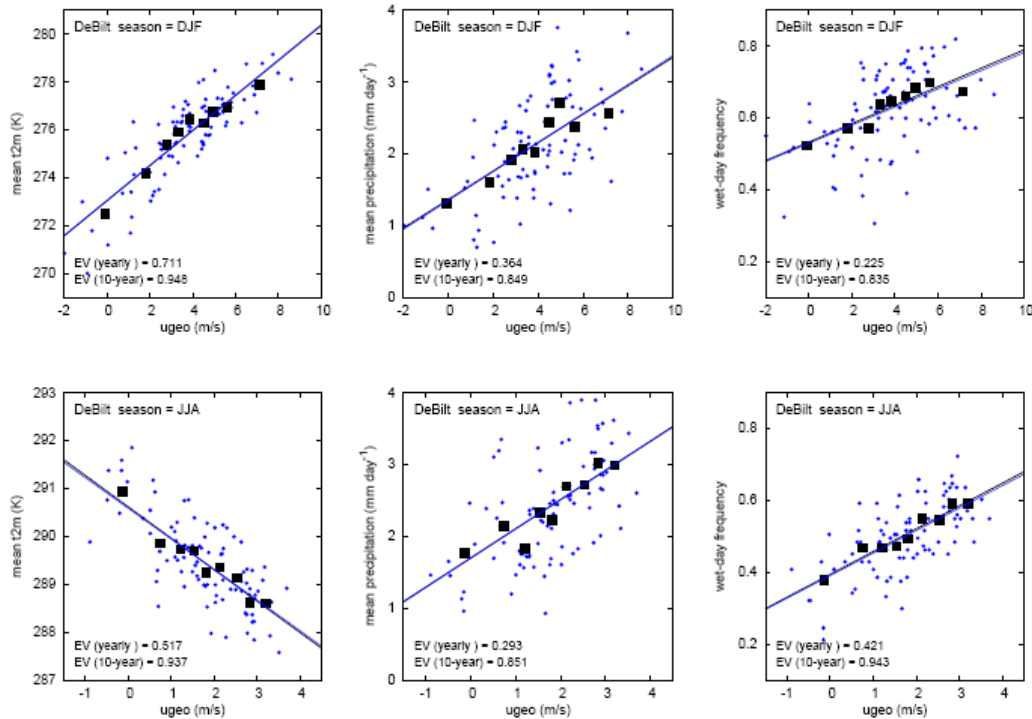
Figure 3-4: Observed relation between the strength of the east-west component of the geostrophic wind and the seasonal mean temperature (left), mean precipitation (middle) and wet day frequency (right) in winter (DJF, top) and summer (JJA, bottom). Shown are observations derived from surface pressure data from Jones et al. (1999) in the area $45 - 55^{\circ}N$, $0 - 20^{\circ}E$, and precipitation and temperature at De Bilt. All observations reflect the period $1911 - 2000$. Each symbol represents a single year. The black squares indicate the averages of the 10 year intervals in this period.

Future projections with a selection of GCMs also show that various indices of the West-European circulation regime are subject to considerable change under conditions when greenhouse gas concentrations increase according to the SRES A1b emission scenario (Van Ulden and Van Oldenborgh, 2006). The atmospheric circulation response to enhanced greenhouse warming over North-western Europe is generally a stronger westerly circulation in winter, and a more easterly circulation in summer.

In addition to global temperature rise and atmospheric circulation statistics, some local scale processes play a major role for the local climate. A pronounced example of a local scale process is the land-atmosphere interaction that can lead to large scale summer drying and temperature rise (e.g. Schär et al., 1999). Also the high surface albedo of snow and ice causes major changes to the local energy balance, and thereby on the temperature. Other examples of local phenomena affecting local climate are the presence of land-sea contrasts, topography, interactions between clouds, radiation and aerosols, subtleties affecting nocturnal boundary layers etc. In the KNMI'06 climate scenarios these processes will be dealt with by application of a local "downscaling" technique using RCMs. This issue is elaborated in Section 4.4.

Also for sea level rise, effects on the circulation and the thermal structure of the ocean imply that sea level projections for the North Sea may differ significantly from the global means. Figure 3-5 shows satellite-derived observations of mean sea level change between 1993 and 2004. Although the observational record is still rather short, it is evident that sea level rise varies strongly between regions. In this observational record sea level changes in the North Sea area do not seem to deviate systematically from the global mean. GCM simulations for future climate conditions do reveal differences between GCMs in warming and freshening of the North Atlantic, the response of the Thermohaline Circulation (THC, Gregory et al., 2005) and the associated North Atlantic sea level change (see Section 7).
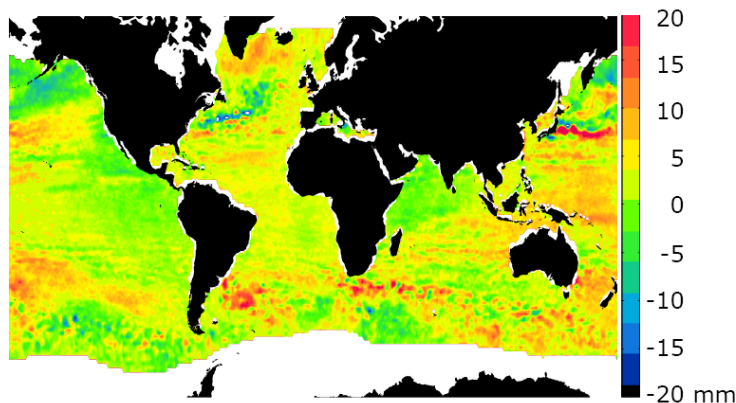
Figure 3-5: Mean sea level change between 1993 and 2004, derived from satellite altimetry observations (based on Leuliette et al., 2004).

3.2 Overview of scenario variables and their construction

The list of variables that is included in the KNMI'06 climate scenarios is a mixture of changes in the mean climate and variables representative for changes in daily climate extremes (see Table 1-1).

The scenario values are constructed with a range of tools and methodologies, briefly explained here. More detail is given in the sections listed in Table 1-1.

The values for the changes in **seasonal mean temperature and precipitation**, **number of precipitation days** and **mean precipitation on a wet day** are obtained from a combination of GCM and RCM output. First, GCM output of the seasonal mean temperature and precipitation in the Netherlands is normalized by the global mean temperature in the GCM projections (Section 4.2). This reveals a range of possible mean changes in the Netherlands for a given global temperature change. Next, for an ensemble of available RCM simulations, yearly output of any seasonal mean variable X (referring to the seasonal mean temperature, precipitation etc.) in the domain around the Netherlands is correlated with a circulation index (U_{geo}). RCM runs were available for two 30-year time slices: a control period (1961 – 1990) and a future climate scenario run (2071 – 2100) driven by GCMs with a clear signal of elevated CO_2-concentrations in the global mean temperature. The change of X between these two time slices is expressed as a linear combination of a change induced by a changed circulation ΔU_{geo} and a circulation independent change, considered to reflect a direct response to a change in global temperature ΔT_{glob}. For each RCM and each 30-year simulation period, regression coefficients c_X^{circ} and c_X^T where thus found, expressing the sensitivity of X to a change in U_{geo} and T_{glob}, respectively. For each climate scenario (identified by specific values of ΔT_{glob} and ΔU_{geo}) the coefficients c_X^{circ} and c_X^T from the set of available

RCMs were weighted in a way that the changes in seasonal mean temperature and precipitation are consistent with the changes projected by the GCMs (Section 4.4). The choice of weighting factors is largely based on qualitative judgment of the available RCM simulations.

A transformation of observations is used to translate the climate change signal derived from the GCM/RCM scaling approach into future time series at the different Dutch stations. With these transformed time series we construct values for the change in the **yearly warmest summer day and coolest winter day**. Also, the number of cold days below 0°C in winter and warm days above 25°C in summer is estimated (see for instance Figure 9-2). For precipitation, we constructed the changes in **daily summer precipitation and 10-daily winter precipitation sum exceeded once every 10 years** from these transformed time series. Daily summer precipitation is relevant for regional water management, whereas wintertime 10-day precipitation sums are an important input for discharge estimates of the larger rivers (e.g. Asselman et al., 2000). These 1 in 10 year quantities were determined by fitting Generalized Extreme Value distributions through the yearly maxima of the transformed time series.

For **potential evaporation** (Section 5) the same weighting factors were used as for the mean seasonal temperature. The seasonally integrated quantity is relevant to estimate the maximum possible water shortage ($P - E_{pot}$) in agricultural and domestic water applications.

Wind speed is given as a change of the daily mean wind exceeded on average once per year, which is considered to be an extreme wind speed quantity that can directly be retrieved from the available (GCM) information without statistical extrapolation. This is a value that can be exceeded during hundreds of hours in historical records, and can therefore not be considered to be a measure of extreme winds relevant for emergency flood conditions. The retrieval of high-order statistics needed for these applications (return levels of 1/10.000 years are required for the Dutch coastal defence) is the subject of additional research. The wind speed scenarios are derived directly from GCM output, since the available RCM output is shown to not add significant information on the scenario variables. Results from four selected GCMs are analysed for a number of grid points covering the North Sea. The GCMs are grouped into models that do give a systematic change of U_{geo} during winter, and models that do not simulate such a change. From all grid points and models the output was collected into a probability distribution expressing the likelihood of a change of the annual maximum daily mean wind (Section 6.2). It is found that the width of these distributions is considerably wider than the mean climate change signal. To span a likely range of future wind conditions, it was decided to include the 10% and 90% quantile values of these distributions in the scenarios.

Sea level scenarios were also constructed using GCM data. A large group of GCMs (24) was selected and analysed in terms of the relation between global mean sea level rise due to thermal expansion, global mean temperature, and the difference between the global mean and the Northeast Atlantic sea level rise. In addition, estimates of other contributions such as the melting of glaciers and ice caps were collected using the TAR and other relevant literature. The uncertainties in sea level rise for a given global mean temperature change are considerable. For two global mean temperature values a low and a high estimate of the corresponding sea level rise are included in the KNMI'06 climate scenarios (Section 7.8).

3.3   Target years and seasons

As in the previous generation scenarios, climate change scenarios are given relative to 1990. For most variables, scenarios for 2050 are defined. A note on the definition of reference and

target periods is appropriate here. For the KNMI'06 climate scenarios we describe the changes in the climatological target period *around 2050* relative to a climatological baseline period *around 1990*. Both for the target and baseline period a 30-year period is used to serve as climatology. Thus, in the following the climate scenarios for 2050 describe the changes in the period 2036 – 2065 relative to the period 1976 – 2005.

Primarily summertime and wintertime values are presented, with summer consisting of June, July and August (JJA) and winter of December, January and February (DJF). Spring and autumn are dealt with only in a few specific cases. Consistent scenarios for these transition seasons are the subject of future research.

Not included in these scenarios are changes in the interannual variability of seasonal mean values, in spite of the high relevance of this feature. A further discussion on this subject is given in Section 9.7.

For sea level scenarios, most planning activities extend beyond the target year 2050. Moreover, differences between sea level scenarios in response to different global greenhouse gas emission scenarios generally do not become apparent before 2050 (IPCC, 2001). For these reasons, sea level scenarios will also be presented for the target year 2100, as well as an outlook for the period beyond the 21st century.

CONSTRUCTION OF SCENARIOS

4   Regional scenarios for precipitation and temperature

4.1   Introduction

Temperature and precipitation scenarios are constructed by combining information from global GCM simulations, regional RCM output and local observational series. First, the changes projected in the GCMs between the periods around 1990 and around 2050 are used to determine the possible range of changes in the *seasonal mean* precipitation and temperature. Section 4.2 gives a description of GCM projections for Western Europe.

Global model output is considered to be not reliable enough to produce changes in the extremes at daily time scales due to the coarse resolution of the global models. Therefore, regional climate model output and local observations were used to translate the changes in the seasonal means into changes of, for instance, the wet-day frequency, extreme daily precipitation events, and precipitation on a wet-day. Regional model runs were available for only a limited number of GCM projections. Not the entire range of relevant GCM projections was covered by the available RCM ensemble. Therefore, a scaling procedure was designed to determine the wet-day frequency and extremes for all cases. This scaling involved the use of the two scenario steering parameters (the global temperature rise and an index of the circulation). These large-scale steering parameters are calculated from the GCM simulations. The scaling variables are described in detail in Section 4.3, whereas the RCM-downscaling is further detailed in Section 4.4.

A further refinement of temperature and precipitation extremes included the derivation of changes in extremes with relatively long return periods (10 years). For this, 20th century observational records from 13 synoptic weather stations in the Netherlands were used and

transformed using the quantities derived from the RCM downscaling. This is described in Section 4.5.

A summary of the temperature and precipitation features is given in Section 4.6. These scenarios are only indicative for the multi-year mean characteristics of seasonal mean and likelihood of extreme precipitation and temperature.

4.2   Global model output for Western Europe

Prior to addressing the impact of climate change on the Western European circulation, Van Ulden and Van Oldenborgh (2006) evaluated the performance of the geostrophic circulation calculated by a suite of AR4 GCMs for present day climate conditions. Many GCMs appeared to have systematic biases that cause systematic errors in the surface pressure and circulation patterns. A selection of eight GCMs with reasonable circulation patterns was made to estimate the change of the circulation indices in response to an enhanced greenhouse gas concentration. From these eight models, three appeared to be low-resolution versions of the same models in the selection of eight, and these were removed from the sample. A selection of five models with an adequate skill in terms of large-scale pressure patterns remained, and this selection is listed in Table 4-1.

Table 4-1: Overview of the GCMs used for the construction of the KNMI'06 climate scenarios for temperature, precipitation and wind.

Name	Resolution	Reference	Remarks
ECHAM5	T63, L31	Jungclaus et al. (2005)	
CCC63/CCCMA	T63, L31	Flato (2005)	
GFDL2.1	2.5°×2°, L24	Delworth et al. (2006)	
HadGEM	1.875°×1.25°, L38	Johns et al. (2004)	not used in wind scenarios
MIROCHi	T106, L56	K-1 model developers (2004)	only data up to 2100 available

Figure 4-1 and Figure 4-2 show that even for seasonally mean values a large range of results is calculated by the different GCMs. The differences are partly an expression of natural variability of temperature and precipitation on timescales of 30 years, captured by the various GCM simulations. They also result from the different representations of many local and remote processes in the different models, which cause a systematic difference of the model results.

The overall temperature signal (Figure 4-1) in winter is stronger at higher latitudes and over continental areas. In summer, a fairly clear North-South gradient appears present across Western Europe. Temperature changes in the Netherlands vary widely between the models, between +0.5°C (GFDL2.1 DJF) and +3°C (MIROCHi JJA).

For wintertime precipitation (Figure 4-2) a general increase is projected over most of Northern and Western Europe, and a reduction over the Mediterranean. However, the spatial pattern over the Netherlands and its surroundings is rather scattered, and a clear spatial gradient cannot be detected. Also summertime precipitation decreases clearly stronger in Southern Europe. For the Netherlands summertime precipitation changes in south-western direction are stronger than in north-eastern direction in some GCMs.
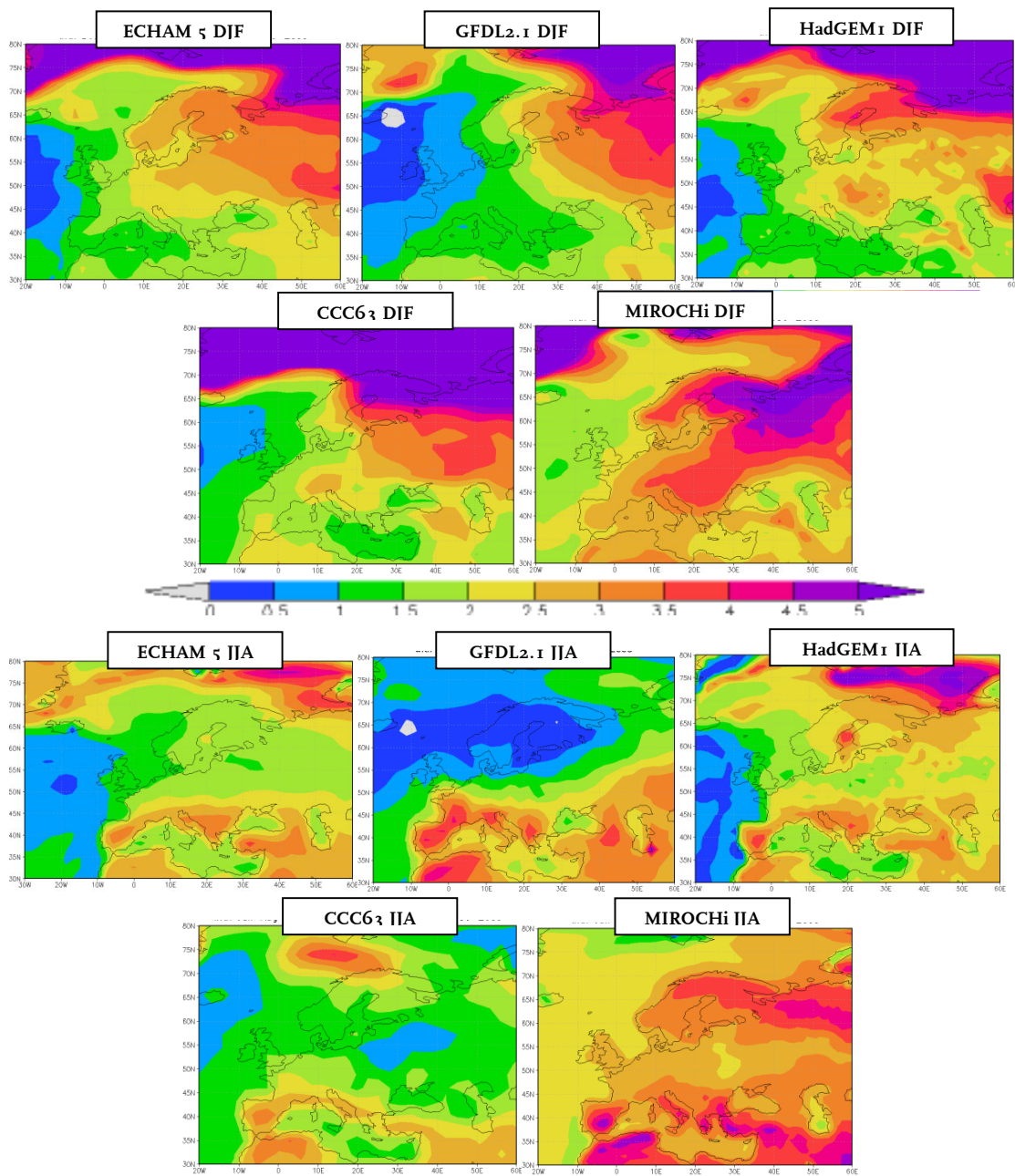
Figure 4-1: Spatial patterns of temperature changes (K) in DJF (top 5 panels) and JJA (bottom panels) of the 5 analysed GCMs. Shown are the response of the SRES A1b simulations around 2050 (2035-2065) relative to 1990 (1975-2005). See Table 4-1 for the references to the displayed models.

The north-south gradient in the precipitation response is consistent with the effects of elevated atmospheric water vapour concentrations in a warmer climate. A mean atmospheric transport of water takes place from the divergence zones at the subtropical subsidence latitudes (20° - 35°N) to the convergence zones at higher latitudes. Higher water vapour contents have the potential to increase this net latitudinal transport. A possible manifestation of this mechanism is a systematic northward movement of the Azores high pressure area, which promotes dry conditions in the western part of the European continent between

roughly 40° and 50°N. Although there is still considerably scientific debate about this mechanism, small systematic changes of the hydrological cycle are particularly apparent in the transition zones between divergence and convergence areas, which give rise to large relative changes in particularly southern Europe.
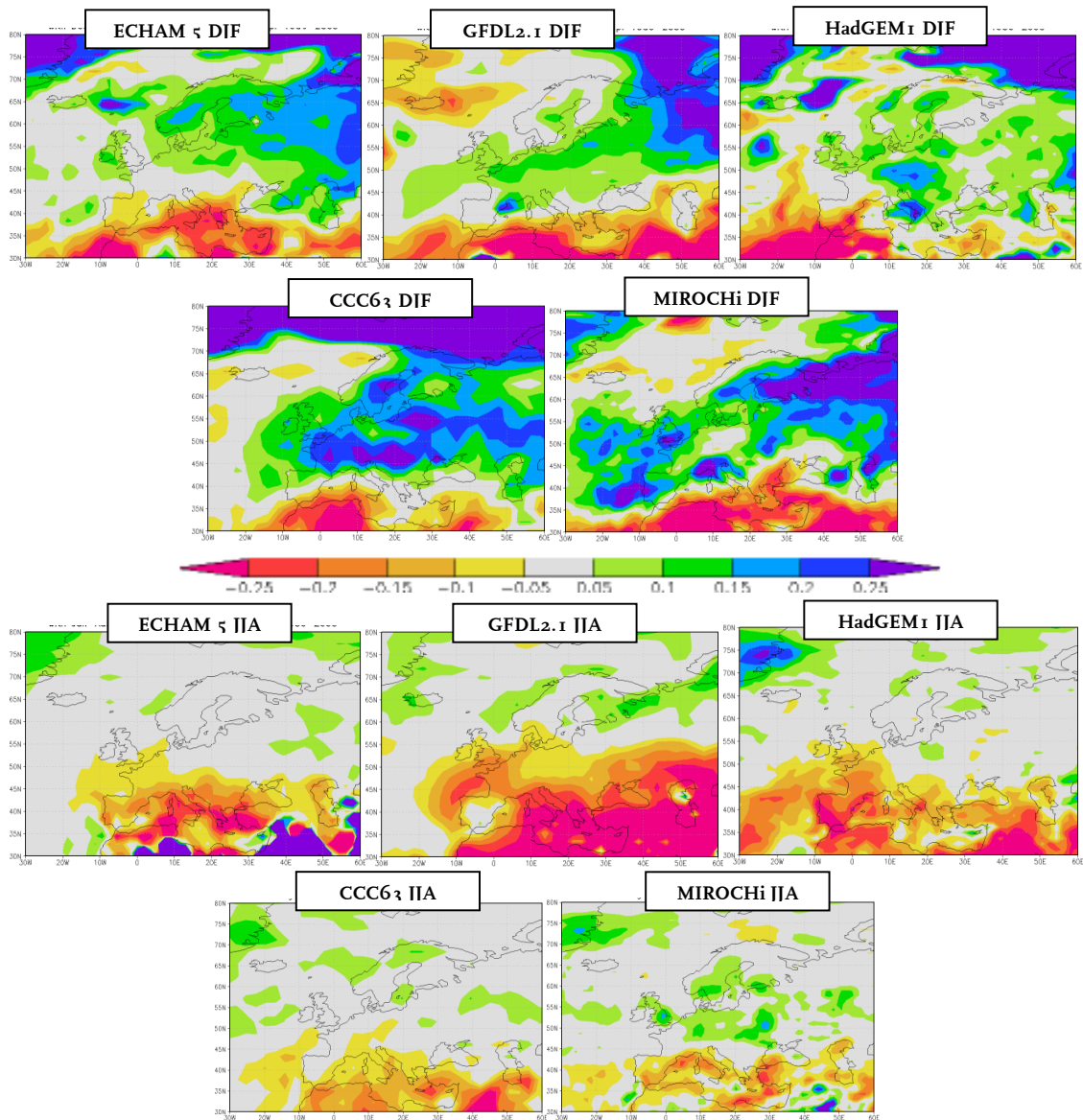
Figure 4-2: Spatial patterns of precipitation changes (fraction) in DJF (top 5 panels) and JJA (bottom panels) of the 5 analysed GCMs. Shown are the response of the SRES A1b simulations around 2050 (2035-2065) relative to 1990 (1975-2005). See Table 4-1 for the references to the displayed models.

The correspondence between the seasonal global mean temperature rise (Figure 3-2) and seasonal mean temperature and precipitation change in the Netherlands is shown in Figure 4-3. Here all available simulations with different versions of the five selected GCMs for four different greenhouse gas emission scenarios are used. Model data for the gridbox covering

the Netherlands (with centre near the location of Eindhoven, 51°N, 6°E) are considered representative for the Netherlands. Time series output is filtered using a 30-year running mean filter. The figure shows changes relative to the period 1976 – 2005.
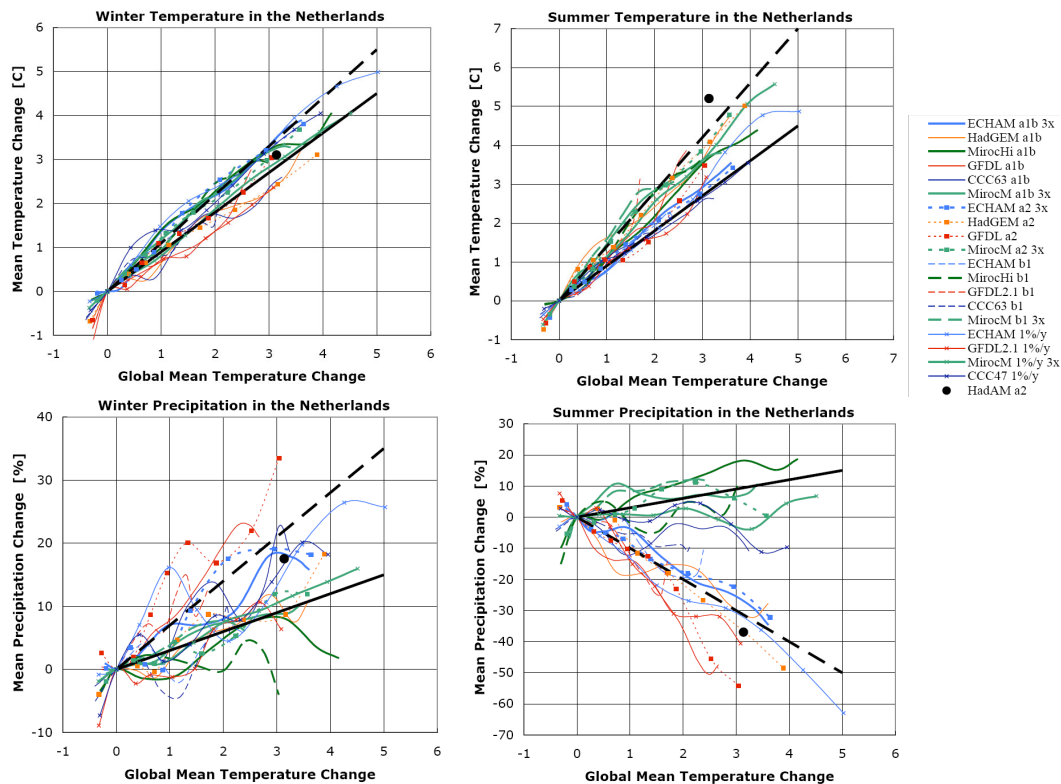
Figure 4-3: Projected change of seasonal mean temperature (top) and precipitation (bottom) for winter (left) and summer (right) in the Netherlands as function of global mean temperature rise, as simulated for the period 1990-2200 (see Figure 3-2). The black straight lines indicate fixed scaling relationships (see text).The black dots represent the value of HadAM3H, used for most PRUDENCE RCM simulations described in section 4.4.

The (time filtered) results support an approximately linear dependence between global and local seasonal mean temperature change, both in summer and winter. The range of this relation spanned by the included GCMs is a result of variations in regional atmospheric circulation and local processes between the models. It is used as an indicator for the range that should be spanned by the KNMI'06 climate scenarios. For wintertime the local temperature varies between 0.9 and 1.1 °C per °C global temperature rise for most models, whereas for summer the local temperature varies between 0.9 and 1.4 °C/°C. The high positive values of local temperature are likely a result of strong continental summer drying (see further on). For precipitation the GCMs generate a much wider range of local effects of global temperature rise. In winter the local precipitation change varies between +3 and +7%/°C, with low values for the GCMs with little circulation change and high values for a stronger circulation change (see below). In summer even the sign of the precipitation change is different between the GCMs: between +3 and –10 %/°C. Here the low value is obtained for GCMs with a strong circulation response. The positive summertime precipitation response is mainly due to a family of the MIROC GCMs, which run at a relatively high

spatial resolution and display a small circulation change. These numbers for the scaling behaviour largely span the range of future model projections. They will be used in the following section to constrain the results of the RCM downscaling/rescaling procedure.
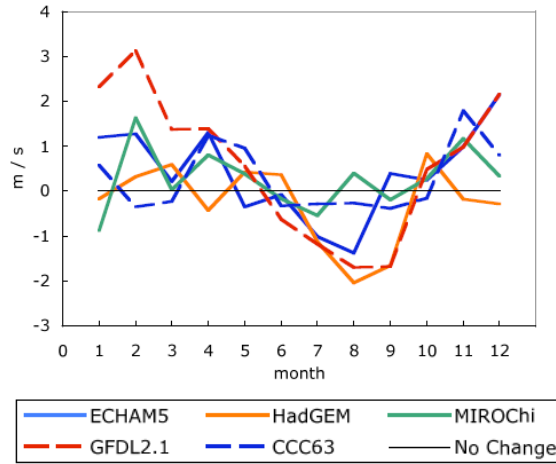
*Figure 4-4: Change in the monthly mean westward geostrophic wind over Central Europe (U_{geo})
between a control period (1960 – 2000) and future (SRES A1b) greenhouse gas scenario
simulation (2060 – 2100) for a selection of models (Van Ulden and Van Oldenborgh, 2006).*

4.3   Large scale steering parameters

Based on Figure 3-2 and associated analyses, the global mean temperature change around 2050, to be used as the first scenario steering parameter, is +1 and +2 °C (see Section 3.2). Based on the GCM output for Western Europe described in the previous paragraph, a second steering parameter is defined that characterizes atmospheric circulation. This steering parameter is largely based on the work by Van Ulden and Van Oldenborgh (2006), who found that the zonal geostrophic forcing (U_{geo}) explain most of the variance in seasonally mean temperature in summer and winter (excluding the transition periods at the beginning of these seasons). U_{geo} is defined as the geostrophic wind speed calculated from gradients in the surface pressure in a fairly wide area surrounding the Netherlands (45 – 55°N, 0 – 20°E). Also for mean precipitation U_{geo} is a strong indicator for circulation-induced variability, although the geostrophic vorticity also plays a significant role here.

We also analysed the degree to which circulation indices explained the variance of seasonal mean precipitation and temperature in the PRUDENCE RCMs, mostly driven by the HadAM3H GCM (see Section 4.4). Although the use of both U_{geo} and geostrophic vorticity leads to somewhat better correlations, the use of the seasonal mean zonal geostrophic wind U_{geo} alone as circulation steering parameter enables an adequate representation of circulation induced contributions to the seasonal mean temperature and precipitation variability in Western Europe. Therefore, U_{geo} is selected as circulation steering parameter for the KNMI climate scenarios.

Figure 4-4 shows the response of U_{geo} to an A1b emission scenario for the period 2060 – 2100 relative to a control climate (1960 – 2000). The general trend is an increase in U_{geo} during the late autumn, winter and early spring months, and a reduced U_{geo} during mid- and late summer, with June and Sep-Oct serving as transition periods. In all seasons the monthly mean vorticity and meridional geostrophic wind is generally reduced (not shown).

In Figure 4-4 two models (GFDL2.1 and ECHAM5) show this general summertime and wintertime response. Two other models (MIROCHi and CCC63) show a fairly small circulation change in both winter and summer. HadGEM, finally, shows a small response in winter but strong in summer. From this small ensemble it is not possible to make firm statements about the correlation between winter and summer responses.
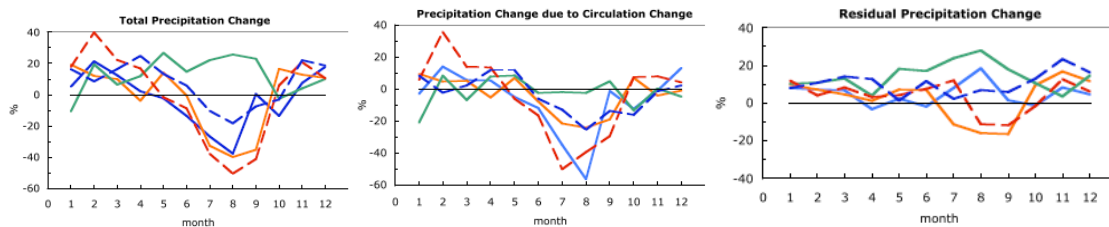
Figure 4-5: Precipitation change in Central Europe calculated from GCM simulations for the period 2060-2100 assuming an SRES A1b scenario compared to a control simulation (1960-2000). Shown is the total change (left), the change explained by changes in the circulation (middle panel) and the residual precipitation change, attributed to enhanced greenhouse warming (right). The legend is given in Figure 4-4 (Van Ulden and Van Oldenborgh, 2006).

Figure 4-5 shows a decomposition of the change of the monthly mean precipitation in Western Europe deduced from the AR4 GCM simulations. The total precipitation change between the control climate and the (2060 – 2100) A1b simulations is approximated by the sum of a term proportional to the change in circulation and a residual term that is associated with other factors resulting from the enhanced greenhouse forcing. During the winter months the total change in precipitation is consistently positive for the GCMs, and the sign of the circulation induced change varies between the models. The residual term is consistently positive. In summer the scatter in the residual term is much larger, while the circulation induced term ranges between a zero and negative precipitation change.
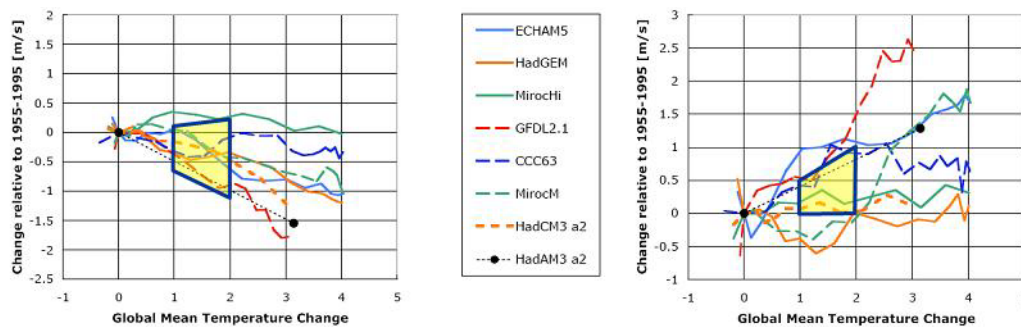
Figure 4-6: Change in U_{geo} as function of the change in simultaneous global temperature increase for each of the considered GCMs for (left) summer and (right) winter. The coloured shapes identify the selected steering parameter for the scenarios (Table 4-2).

From the analyses above the following conclusions are deduced.
- A change of circulation in West-Europe in response to enhanced greenhouse gas concentrations (as clearly shown by 2 GCMs in Figure 4-4) implies a stronger zonal flow in winter, and weaker in summer.

- In winter the tendency to stronger zonal winds is associated with an increased mean temperature and precipitation in Western Europe. In summer the effect of a decrease of the zonal wind strength is generally associated with higher temperature, and lower mean precipitation.

The change in U_{geo} as depicted in Figure 4-4 refers to the 40-year mean period at the end of the 21st century. The change of the circulation over Western Europe is a combined manifestation of natural variability and the (time-varying) effects of increased greenhouse gas concentrations. To account for the relation between global climate change and West European circulation, the values of the steering parameter U_{geo} were correlated with the simultaneously projected global temperature change (Figure 4-6). The range of these values reflects the variability in the response of the regional circulation regime between the different GCMs: in winter some models give a strong increase of the advection of relatively warm moist air from the West, whereas others show a much smaller change. In summer some GCMs promote dry warm conditions by increasing the strength of the eastward component of the geostrophic forcings, whereas others – again – show a smaller response. This variability is represented in the KNMI'06 climate scenarios by selecting two values of ΔU_{geo} for each season and for each temperature regime. The resulting values are listed in Table 4-2. These values are optimized in order to project the RCM results for the seasonal mean temperature and precipitation within the GCM range as shown in Figure 4-3. This optimization is mainly based on the time slice 2071 – 2100 where both RCM and GCM results were available. Therefore, the selected values for U_{geo} are somewhat biased to the correlation with increased global mean temperature in the range between 3° and 4°C. Not the entire range of U_{geo} values corresponding to +1°C and +2°C global temperature increase in the GCM runs is covered by the selected values, in particular during winter.

Table 4-2: Overview of values of ΔU_{geo} (m/s) used to construct the KNMI'06 climate scenarios.

Season	Circulation change	+1°C	+2°C
Winter	yes	+0.5	+1.0
Winter	no	+0.0	+0.0
Summer	yes	-0.6	-1.2
Summer	no	+0.1	+0.2

4.4   Regional temperature and precipitation

GCM simulations for future climate are valuable to assess the effects of anthropogenic CO_2-emissions on global mean temperature and atmospheric and oceanic dynamics, but their predictive skill for regional climate change is still rather poor. In addition, they do not provide information on small scale features, like for example summertime convective precipitation events. Therefore, relatively high resolution RCMs have been used to generate regional scale changes of precipitation and temperature from the GCM results. The RCMs are provided with lateral and SST boundary conditions from the host GCM. In most cases, also atmospheric CO_2 concentrations in the RCM interior follow the global mean SRES scenarios. An overview of the regional climate variables derived from the RCM output is given in Table 4-3.

The suite of RCM simulations used for the KNMI'06 climate scenarios is produced in the context of the European PRUDENCE project (Christensen et al., 2002). In this project dynamical downscaling was applied using 10 RCMs and 3 GCMs, all run for two 30-year time slices: a control period 1960 – 1990 and a future period 2070 – 2100, assuming two

different SRES emission scenarios (A2 and B1) (Jacob et al., 2006). One of the PRUDENCE models was the KNMI RCM RACMO2 (Lenderink et al., 2003).

Prior to assessing the RCM results of the future climate runs, an extensive evaluation of the skill of RCMs for present day climate conditions was carried out. RACMO2 appeared to have a good skill in calculating precipitation climatology in the Rhine area (Van den Hurk et al., 2005b), in mean and interannual variability of summertime temperature (Lenderink et al., 2006), and in the reproduction of large scale geostrophic forcing (Van Ulden et al., 2006). A relatively large soil hydrological memory makes the RACMO2 model less sensitive to excessive summertime drying (Lenderink et al., 2006), and the capacity of the soil to absorb anomalies in precipitation and evaporation compare well to large scale observational analyses for the Rhine basin (Van den Hurk et al., 2005a). Analyses of the remaining PRUDENCE RCMs highlighted unrealistic behaviour in precipitation and temperature for a minority of models. This gave rise to excluding one RCM, leaving 8 RCM simulations nested in results from the HadAM3H atmosphere model (Jones et al., 2001), and 2 RCMs driven by two different runs of the ECHAM4 coupled climate model (see Table 4-4).

Table 4-3: List of variables for which the future climate changes are derived from the RCM downscaling procedure. All variables are derived separately for winter (DJF) and summer (JJA) seasons.

Variable	Temperature	Precipitation
Seasonal mean	●	●
Median (50%-percentile)	●	●
Wet day frequency		●
Precipitation on wet day		●
10% & 90%-percentile	●	
99%-percentile		●

All driving GCMs for PRUDENCE have at least been forced with the A2 SRES emission scenario, and some also with B1. As expected, large differences in simulation setup and model formulation caused significant differences in (regional) climate and circulation response. HadAM3H was an atmosphere-only model with sea surface temperature (SST) forcing in the A2 run prescribed from a control SST dataset modified by climate sensitivities from a coarse resolution coupled climate simulation with HadCM3. ECHAM4/OPYC is a fully coupled climate model integration, but the two simulations are different realizations (Christensen and Christensen, 2006) with a fairly similar SST response but a very different change in the winter-time atmospheric circulation over Western Europe. Both ECHAM4 and HadAM3H models generate a global temperature rise of about 3.3°C by the end of 2100, but the response of the Atlantic SST in the HadAM3H was about 1 °C lower than the SST response in the ECHAM4 simulations (based on qualitative inspection of near surface air temperatures). Partly due to this difference in SST response, ECHAM4 generates a much milder and wetter winter climate with higher values of U_{geo} than the HadAM3H simulations (Räisänen et al., 2004). Thus, even for a similar change of the circulation index in different GCMs, variations in the upwind SST response have a strong impact on the temperature and precipitation changes. These effects have been taken into account in the downscaling procedure. Basic scaling properties between global temperature and West European temperature and precipitation from HadAM3H are indicated in Figure 4-3.

Most RCM-simulations were carried out using the HadAM3H simulation, which enables to highlight differences induced by different dynamical and physical approaches in the RCMs.

Many seasonal mean features of West European climate change, as projected by the ensemble of RCMs, are dominated by the large scale forcing GCM, rather than determined by the local physics of the RCM (Déqué et al., 2006). The ECHAM4 driven RCMs were shown to have a considerably poorer performance of seasonal mean precipitation over the Rhine area than the HadAM3H driven RCMs in the reference simulations (Van den Hurk et al., 2005b).

Table 4-4: Overview of RCMs used for the dynamical downscaling. The two ECHAM4 simulations are two different GCM runs.

Acronym	Model name and Reference	HadAM3H	ECHAM4/OPYC
DMI	HIRHAM (Christensen et al., 1996)	•	• (1)
ETH	CHRM (Vidale et al., 2003)	•	
GKSS	CLM (Steppeler et al., 2003)	•	
METO	HadRM3H (Hulme et al., 2002)	•	
ICTP	RegCM (Giorgi and Mearns, 1999)	•	
KNMI	RACMO2 (Lenderink et al., 2003)	•	
MPI	REMO (Jacob, 2001)	•	
SMHI	RCAO (Räisänen et al., 2004)	•	• (2)
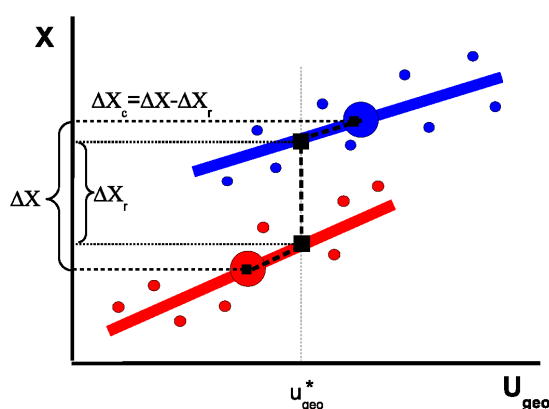
Figure 4-7: Illustration of the technique used to separate the change of a variable X into a change related to the mean circulation change (ΔX_c) and a residual change (ΔX_r). X is plotted as function of the mean circulation index U_{geo}. The 30 seasonal values of X from the RCM simulation are given by the dots, blue for the control run, and red for the future (A2) simulation. The large symbols represent the 30 yr mean. The dependence of X on U_{geo} estimated from the regression method is given by the solid red and blue lines. The offset between these two regression lines at a reference value of the circulation U_{geo}^* (indicated by the black dashed line) determines the residual change, and two separate transects following the two regression lines (which may have a different slope) represents the circulation dependent change.

There are a few important exceptions that justify the use of RCMs in scenario development: summertime hydrological features (low precipitation and high temperatures associated with soil drying), and the representation of temperature and precipitation extremes.

Summertime hydrological regimes vary widely across the RCMs due to strong differences in the strength of the regional hydrological cycle and moisture buffering capacity in the soil (Van den Hurk et al., 2005a; Lenderink et al., 2006; Vidale et al., 2006). Most RCMs driven by the HadAM3H show a strong summertime reduction of precipitation partly due to a positive drying feedback. Figure 4-3 shows that HadAM3H projects a strong reduction in summertime precipitation (12%/°C, assuming a linear dependence on global mean temperature), and most RCMs tend to inherit and amplify this drying response. RACMO2 simulations of summertime precipitation have a good skill for present day climate conditions, which results in a good representation of the mean and variability of the seasonal mean summer temperature (Lenderink et al., 2006).

The relatively high resolution in RCMs allows a better quantification of the tails of the distributions of temperature and precipitation. Strong differences between RCMs are highlighted in these tails. For instance, Kjellström et al. (2006) showed that the differences in extreme summer and winter temperature in an RCM ensemble driven by the same GCM can be large. Frei et al. (2006) gave similar conclusions for precipitation extremes.

Ideally, the set of RCM runs would have been distributed homogeneously over a range of GCM simulations that covers the inherent uncertainty in the climate response in the Atlantic and Eurasian regions. However, the AR4 GCM projections discussed in Section 4.2 have not been downscaled with RCMs: the available RCM experiments used HadAM3H and ECHAM4/OPYC as boundary condition instead. This implies that a regional interpretation of GCM simulations must be (indirectly) obtained by using scaling relationships. This technique originally stems from weather forecasting (see e.g. Lorenz, 1969). These relationships describe a major part of the variability of relevant variables X (listed in Table 4-3) as a linear function of the large scale steering parameter (U_{geo} and T_{glob}). Changes in these steering parameters are then translated into changes of the variable under consideration:

$$(4.1) \qquad \Delta X = c_X^{circ} \Delta U_{geo} + c_X^T \Delta T_{glob}$$

The regression factors c_X^{circ} and c_X^T were derived from the interannual variability in a collection of RCM time slice simulations for control and future climate conditions (see Figure 4-7). The regression factors were not obtained in a straightforward way by performing a regression on seasonal mean temperature and circulation. Instead, the procedure involves two steps:

- For both the control and future simulation a single regression of the variable X on the mean circulation was made. Since we are interested in climatic timescales, we used a 3 month season as a minimum time period. Thus, for each year we computed X and the mean circulation for the considered season. This procedure gave 30 data points for the 30-year simulations, for which a least square fit was computed. In addition, two methods using seasonal data of separate 10 year periods were used, to increase the statistical sample. In total this gave three estimates of the relation of X on the circulation. In practice, the three estimates were fairly similar. The regression factors were cross-checked with observations (as for instance indicated in Figure 3-4), to verify the relation between circulation indices and regional climate variables from the RCMs.
- The response of X between the control period and the future period was separated into a part related to the circulation change and a residual part. This was done by correcting the control and future simulations back to a reference value $U_{geo}*$ using the relations estimated under the previous step (see Figure 4-7), essentially comparing

years with similar circulation statistics in both the control and future simulation. The sum of the corrections due to circulation change was defined as the circulation dependent change ΔX_c, and the residual part as ΔX_r. The regression factors are given by:

$$(4.2) \qquad c_X^{circ} = \frac{\Delta X_c}{\Delta U_{geo}} \text{ and } c_X^{T} = \frac{\Delta X_r}{\Delta T_g}$$

with ΔU_{geo} the circulation change in the RCM integration, and ΔT_g the global temperature change from the GCM model that was used to force the RCM integration. When the circulation dependencies in the control and future simulations are not the same, the outcome is dependent on the value of $U_{geo}*$. Since this is an arbitrary choice we take two values of $U_{geo}*$ to obtain a quantification of the uncertainty related to this choice.

In total the outcome of the above procedure gave for each RCM simulation consisting of a control and future period, in total six estimates of the regression coefficients in Eq.(4.1) (two values of $U_{geo}*$ and three regression methods). The spread in the six estimates gives a quantification of the uncertainty in the separation procedure. The spread between the RCMs is the result of the differences in the representation of physical and dynamical processes between the RCMs.
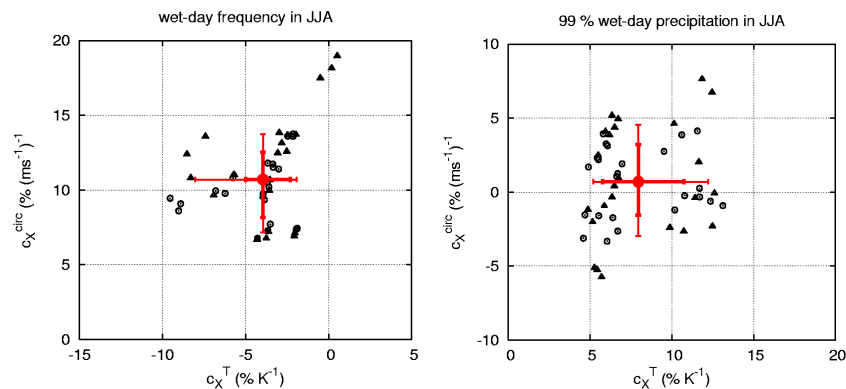
Figure 4-8: Regression coefficients c_X^{T} and c_X^{circ} for the change in (left) wet-day frequency and (right) 99% percentile of daily precipitation in summer, derived from 8 PRUDENCE RCMs all driven by the HadAM3H GCM simulations for present day (1971-2000) and A2 scenario (2071-2100) forcing. The black symbols indicate the results of the statistical regression methods to solve Eq. (4.1) for each RCM from the ensemble. Triangles are results from the control simulation, circles from the A2 simulation. The red error bars represent the mean (red dot), and the 10%, 20%, 80% and 90% percentiles of these estimates.

An illustration of the total spread of the results is given in Figure 4-8, which shows an example of the resulting circulation dependent and independent change for the summertime wet day frequency (WDF) and the 99% percentiles of daily precipitation for the collection of RCMs. In addition to the separate data points, horizontal and vertical error bars denote the mean, and the 10%, 20%, 80%, and 90% percentiles of these estimates.

Plots similar to Figure 4-8 are made for all variables listed in Table 4-3 (not shown). From these analyses, it was revealed that for most variables the spread between the RCMs is small or distributed evenly around the ensemble mean. However, for other measures (for example

for the 99% percentiles of daily JJA precipitation), RCM results appear to be very different and sometimes even cluster in two groups. In those cases, the average behavior is not supported by any of the individual model results, and it makes sense to assign different sets of RCMs to different regimes. Based on our understanding of these results, we decided to assign different weights of each RCM to different scenarios (Table 4-5). The rationale of this qualitative choice of weights is explained next.

Table 4-5: Weights applied to the various RCMs from Table 4-4. The same weights are applied for the +1 °C and +2°C scenarios.

Season and scenario	Weight for RACMO2	Total weight for the 7 remaining HadAM3 RCMs	Total weight for the 2 ECHAM4 RCMs
Winter, all scenarios	1	7	8
Summer, G and W	1	0	0
Summer, G+ and W+	0	7	1

For winter we do not make a separation in two different RCM ensembles, since differences in representations of local physical processes play a much smaller role than in summer (Van Ulden et al., 2006). Due to the dominance in winter of the westerly winds, the Atlantic SSTs strongly influences the climate of the Netherlands. The SSTs in HadAM3H in the 2071 – 2100 time slice (originating from HadCM3) lag the global temperature rise by about 2°C. SST in ECHAM4 is about 1°C warmer. Since the temperature lag of the Atlantic SST from HadAM3H is rather large in comparison to the GCM ensemble (van Ulden and van Oldenborgh, 2006), this effect was compensated by giving both ECHAM4 driven RCM integrations a weight of 4, to give a similar weight to the ECHAM4 and HadAM3H ensembles.

For summertime conditions, different weights are chosen to express the difference in the degree of a drying feedback, impacting on the precipitation climate. The results from RACMO2 were used to derive climate scenarios values for the summertime regime with small circulation change (giving rise to wetter conditions), whereas the ensemble of other RCMs was used for the dry regime induced by a strong circulation change. In this scenario, all RCMs (including the ECHAM4-driven models) are given a similar weight. The RCAO ECHAM4 integration was not used, because this integration displays a very large circulation response which makes the separation method prone to errors.

In all cases multiple RCM grid points around the location of De Bilt were used for the calculations. Every grid point covers an area of approximately 50×50 km. For temperature (both mean and quantiles) 2×2 grid points were used (De Bilt located in the north-western grid point). All GCM results used for the KNMI'06 scenario's show a spatial gradient in the temperature response: coastal areas show a smaller warming than inland areas in winter (approximately 0.5°C), whereas a North-South gradient is present in summertime warming (Figure 4-1). The consistency of these gradients between the GCMs is fair, and is generally captured in any RCM nested in a GCM. The selection of a 100×100 km downscaling domain implies temperature scenarios that are representative of the mean change in the Netherlands away from the coast.

For precipitation this limited number of 4 grid points is not considered representative, since the short spatial correlation scale makes the precipitation values susceptible to significant noise. Another complicating factor is that the change in precipitation is not uniform over the domain of interest and this pattern is not consistent among the GCMs (Figure 4-2). In winter the maximum response in the surroundings of the Netherlands can be either in the centre, to the north, east or south of the country. In summer the maximum response of the models with a negative response (all except MIROCHi and CCC63) is consistently stronger in south-west direction. Also the GCMs used in PRUDENCE show a clear northeast-southwest gradient in the response of mean summer precipitation to a change in the greenhouse gas forcing.

To increase the statistical significance of the values for precipitation, 11×11 grid points (500×500 *km*) were used for the scaling relations of the precipitation variables (Figure 4-9). This sample covers the variability of the spatial patterns of the precipitation response of the GCMs, and the gradients of Figure 4-2 are averaged out in the scenarios. The pooled data allowed better estimates of the extremes. Again, De Bilt is located in the northwest of this domain. The continental coverage of included grid points reduces the subtle land-sea effects present in the GCM and RCM model results. The averaging area is large enough to consider the precipitation scenarios representative for the Netherlands and a large portion of the non-Alpine Rhine catchment.
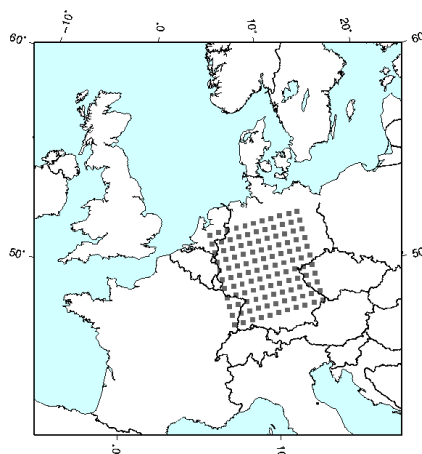
Figure 4-9: Spatial distribution of 11×11 RCM grid points used for the downscaling procedure.

A summary of the dependency of mean precipitation and mean temperature on the circulation (based on U_{geo}) is given in Figure 4-10. RCM results are separated between RACMO2 and a weighted combination of remaining RCMs as defined in Table 4-5. RACMO2 control simulations are carried out using both the PRUDENCE HadAM3H control run and ERA40. Also shown are observed regression factors for a number of 30-year periods in the 20th century.

A few issues are worth noting here. First, the circulation dependence in observed records of (in particular) summertime precipitation shows a large variability throughout the 20th century, and perhaps a trend. This implies that U_{geo} is not a very firm predictor for mean summertime precipitation, since the natural variability is large. Summertime precipitation is a fairly local process, and not as strongly governed by geostrophic forcing as for instance temperature. A second point is the poor correspondence between observations and PRUDENCE control RCM results for wintertime temperature. RACMO2 driven by ERA40 gives a much better resemblance. The deviation from observations is strong in the RCM runs

with HadAM3H boundaries, which suggests that the prescription of SSTs might play a role. Third, summertime responses of RACMO2 are quite different from the mean of the model ensemble: both temperature and precipitation is less sensitive to U_{geo} but the climate change impact is stronger in RACMO2. Uncertainties of these scaling factors mainly have an impact on the scenarios with circulation change (G+ and W+).

For the A2 simulations the dependency on the circulation increases in summer. It is likely that the enhanced land-sea temperature contrast plays a role in the increase in circulation dependency: a larger temperature contrast makes the temperature in the Netherlands more depending on the mean wind direction. Processes that are considered to contribute to this enhanced land-sea temperature contrast are large scale continental soil drying and increased incoming shortwave radiation (Lenderink et al., 2006). In winter, there is a tendency for a decrease in dependency on the circulation, which most likely is a consequence of a decrease in land-sea contrast due to a smaller role of snow induced land cooling (Kjelström, 2004).
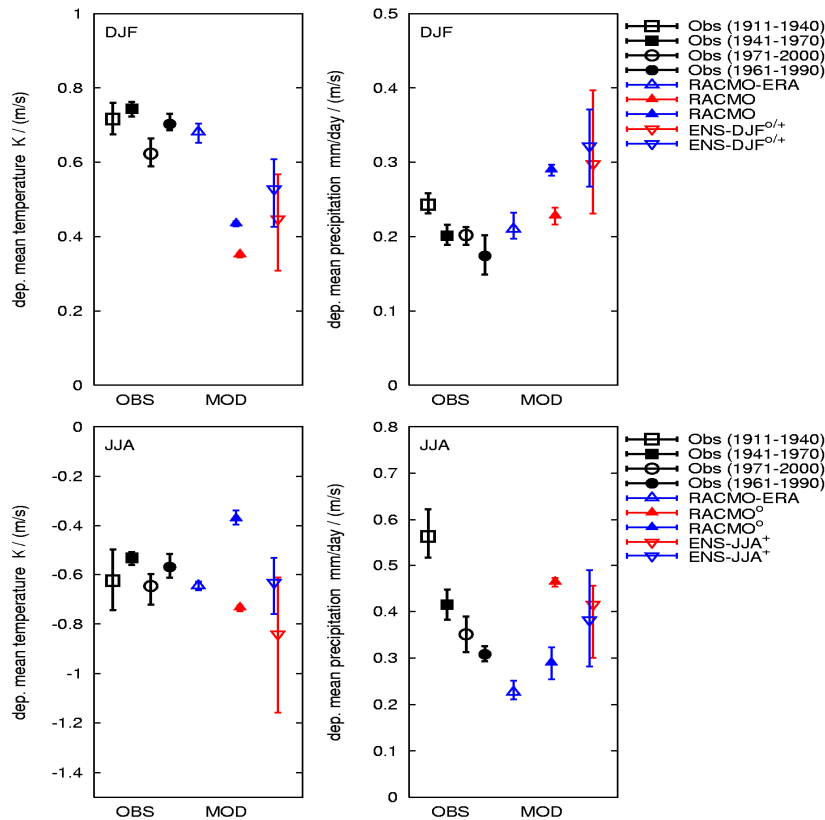
Figure 4-10: Best estimate of the linear slope between U_{geo} and a range of climate variables, derived from observations, control simulations and A2 simulations. Left panels: mean temperature [K/(m/s)]. Right: mean precipitation [mm/day / (m/s)]. Top panels: winter. Bottom: summer. The observations are taken from station De Bilt, and are divided into four different periods during the 20th century. Blue symbols refer to 1960-1990 control simulations of the PRUDENCE RCMs, red symbols to the 2070-2100 A2 simulations. The upward triangles (Δ) are RACMO simulations used for the G and W scenarios, whereas downward triangles (∇) are mean slopes from an ensemble of RCMs, grouped to form the input for the scenarios G+ and W+ (see Table 4-5). The RACMO control simulations are also carried out with ERA40 as boundary condition (filled blue triangle). Error bars denote 25-75 percentile ranges of the results, where the spread comes from the different fit methods and circulation indices briefly explained on page 29.

The weighted regression factors c_X^{circ} and c_X^T as given in Eq. (4.1) are combined with the steering parameters from Table 4-2 to get specific values of the scenario variables for the four KNMI'06 climate scenarios. The RCM runs used to derive these numbers are – as explained – driven by a limited number of GCMs and time slices. However, the selection of models and their weighting is optimized to reproduce the gross scaling expressions and sample the major portion of the range plotted in Figure 4-3. For mean summertime precipitation the spread in the KNMI'06 scenarios is smaller than the GCM spread in the +1 – +2°C range. This is partly a result of the followed procedure: the scenarios are derived by scaling PRUDENCE RCM runs representative for a global temperature change of +3.1 °C (A2 scenario 2070 – 2100) back to the lower steering values. However, individual outliers have been discarded on purpose as well. These outliers may be affected by exceptionally high SSTs and a small circulation change probably related to a smaller land-sea temperature contrast (MIROCHi), or excessive drying hydrology (GFDL2.1).

Table 4-6 gives an overview of the precipitation and temperature variables that are obtained by following the outlined procedure. Figure 4-11 and Figure 4-12 summarize the changes of the precipitation variables for the four scenarios, separately for winter and summer conditions. Also shown are error estimates, derived as the 20% and 80% percentiles from the ensemble of estimates based on the different models and different method used for that particular scenario.

Table 4-6: Summary of regional changes corresponding to the KNMI'06 scenarios obtained by scaling GCM projections with RCM output for precipitation and temperature variables.

Variable	G	G+	W	W+
summertime				
mean temperature (K)	+0.9	+1.4	+1.7	+2.8
10% warmest days (K)	+1.0	+1.8	+2.0	+3.6
10% coldest days (K)	+0.9	+1.1	+1.8	+2.2
mean precipitation (%)	+2.8	-9.5	+5.5	-19.0
wet day frequency (%)	-1.6	-9.6	-3.3	-19.3
mean precipitation on wet day (%)	+4.6	+0.1	+9.1	+0.3
median of wet day precipitation (%)	-2.5	-6.2	-5.1	-12.4
precipitation on 1% wettest days (%)	+12.4	+6.2	+24.8	+12.3
wintertime				
mean temperature (K)	+0.9	+1.1	+1.8	+2.3
10% warmest days (K)	+0.8	+1.0	+1.7	+1.9
10% coldest days (K)	+1.0	+1.4	+2.0	+2.8
mean precipitation (%)	+3.6	+7.0	+7.3	+14.2
wet day frequency (%)	+0.1	+0.9	+0.2	+1.9
mean precipitation on wet day (%)	+3.6	+6.0	+7.1	+12.1
median of wet day precipitation (%)	+3.4	+7.3	+6.8	+14.7
precipitation on 1% wettest days (%)	+4.3	+5.6	+8.6	+11.2

The wet day frequency in winter is only slightly sensitive to the choice of the circulation steering parameter, but the precipitation per wet day (and thus also the mean precipitation) is the major factor that changes between the circulation regimes. An increase of up to 7%/°C in the mean precipitation is projected to occur in the G+ and W+ scenarios, greatly influenced by giving a relatively high weight to the ECHAM4 runs with the strong SST response. The 99% quantile is less dependent on the circulation regime, but increases with increasing global temperature.

In summer (Figure 4-12) the wet day frequency is the main factor determining the seasonally mean precipitation. It is strongly affected by the choice of the circulation regime: the larger reduction occurs when circulation is assumed to change. From Figure 4-12 it appears that the difference between the two circulation regimes gives rise to a sign change in the mean precipitation response, consistent with Figure 4-3. The 99% precipitation on wet days increases in all scenarios, regardless the sign of the mean precipitation changes.
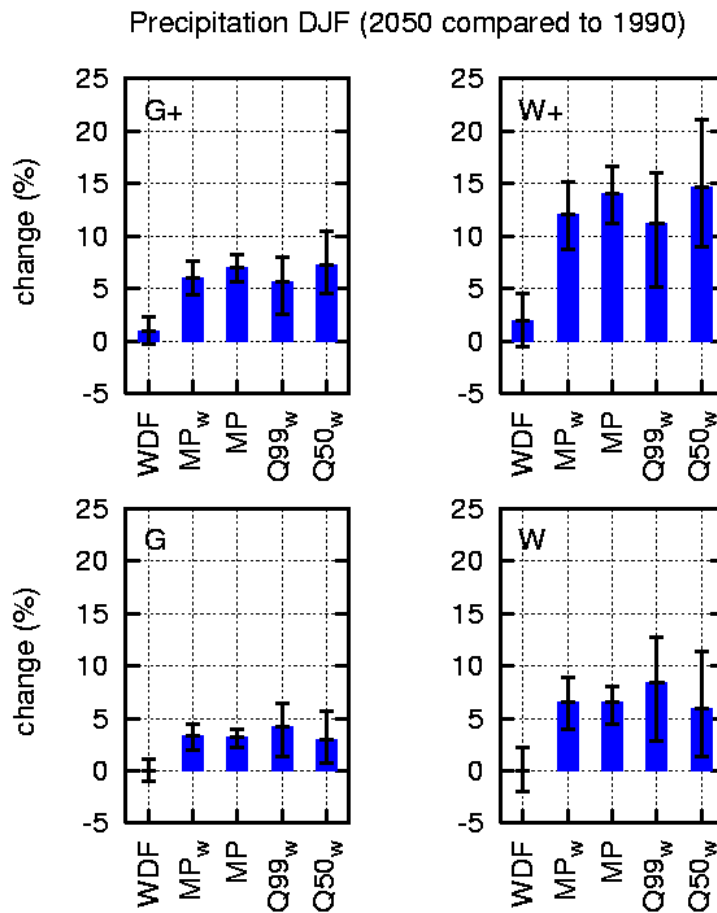
Figure 4-11: Precipitation variables for the winter scenarios derived using weighting factors from Table 4-5. The error bars denote the standard deviation generated by using various RCMs and regression techniques to calculate the circulation dependent and independent scaling factors. The error bars are the 20% and 80% percentiles from the ensemble of estimates based on the different models and different method used for that particular scenario. WDF = Wet Day Frequency, MP_W = Mean Precipitation on a wet day, MP = Mean Precipitation, $Q99_W$ = 99% percentile of precipitation on wet day, $Q50_W$ = median of precipitation on wet day.

The difference in extreme precipitation (on wet-days) between W and W+ is an illustration of the difference between RCMs used for the scenarios, not caused by the difference in circulation. Scenario W is based on a model (RACMO2) with sufficiently moisture supply to support strong convective precipitation events; W+ is based on models that have a stronger limitation by soil moisture. The large increase in extreme events in RACMO2 is in agreement with a similar increase in extreme events in the relatively high resolution MIROChi of +40% in the period 2080 – 2100. In addition, RACMO2 compares well to observations of the Rhine catchment area (see Figure 11-4 below). The large difference between the results of RACMO2 on one hand and a group of RCMs used for the W+ scenario on the other reflects the large uncertainty of particularly the summer precipitation scenario values (see also the large error bars in Figure 4-10). The values for the W scenario are derived from an RCM driven by the HadAM3H model that also drives the RCMs used for the W+ scenario. Strictly spoken, one cannot disentangle the uncertainties originating from the assumed circulation change or GCM selection on one hand, and from the range of local precipitation responses covered by the RCM ensemble on the other.
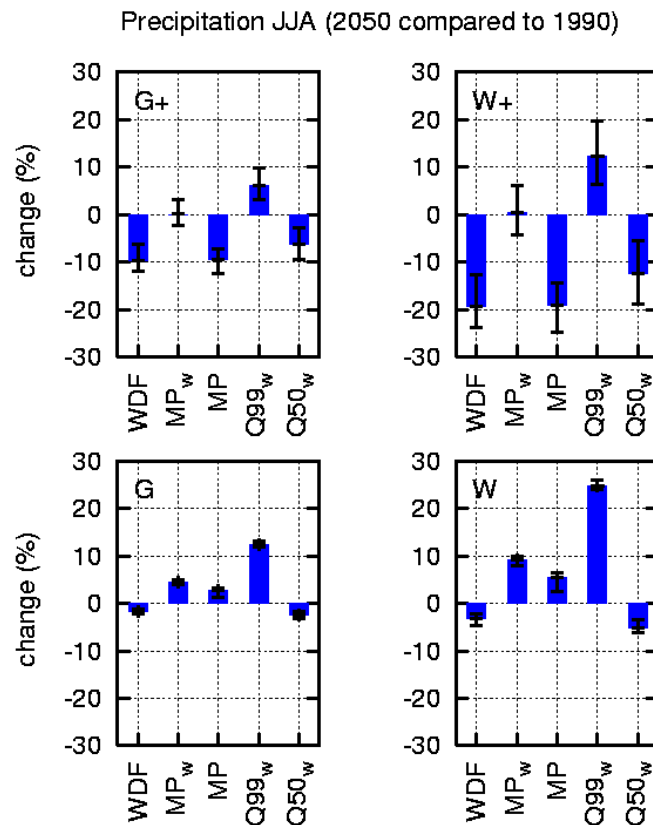
Figure 4-12: As in Figure 4-11 for the summer scenarios.

4.5 Time series transformation of precipitation and temperature

As discussed before, there is a need to downscale predicted changes by the GCM and RCM simulations, which are homogeneous over the Netherlands, to local information. This is done by transforming the observed time series at 13 synoptic stations in the Netherlands (Table 4-7). This procedure automatically compensates for a bias in the RCM results, and provides future time series to be used in impact models. The temperature and precipitation time series from these stations were transformed using the changes in quantiles listed in Table

4-6. The transformed time series are then analysed in terms of changes in return period of extreme events.

For **temperature**, a pragmatic linear quantile scaling is applied to transform a reference time series into a time series representative for one of the four climate scenarios. The 90%, 50% and 10% quantiles, given in the scenarios, are also calculated from the observations and denoted as $T_{90}{}^c$, $T_{50}{}^c$ and $T_{10}{}^c$, respectively. This is applied for each season separately. Each value of the temperature in the transformed temperature time series, T^f, is derived from the reference time series T^c using a scaling relation that uses the distance to the median of the observed and transformed time series:

$$(4.3) \qquad T^f = T_{50}^f + a\left(T^c - T_{50}^c\right)$$

where $T_{50}{}^f$ is given by $T_{50}{}^c + \Delta T_{50}$, and a is a scaling factor that is different for values smaller or higher than the median of the reference sample:

$$(4.4) \qquad a = \begin{cases} \dfrac{T_{90}^f - T_{50}^f}{T_{90}^c - T_{50}^c} & T^c > T_{50}^c \\[2em] \dfrac{T_{10}^f - T_{50}^f}{T_{10}^c - T_{50}^c} & T^c < T_{50}^c \end{cases}$$

Table 4-7: Overview of synoptic weather station in the Netherlands, used for the statistical downscaling.

Station name	latitude	longitude
West Terschelling	+53:13:01	+05:13:01
De Kooy/	+52:55:28/	+04:47:07/
Den Helder	+52:56:00	+04:45:00
Groningen	+53:11:05	+06:36:03
Ter Appel	+52:52:44	+07:03:39
Hoorn	+52:38:41	+05:04:05
Heerde	+52:23:46	+06:03:05
Hoofddorp	+52:18:40	+04:42:15
De Bilt	+52:06:05	+05:11:12
Winterswijk	+51:58:58	+06:42:02
Kerkwerve	+51:40:38	+03:51:53
Westdorpe/	+51:13:10/	+03:51:47/
Axel	+51:16:36	+03:54:32
Oudenbosch	+51:34:09	+04:31:53
Roermond	+51:10:56	+05:58:02

A simple bypass procedure was followed to estimate changes in the 1/year extreme values directly from the changes in the 10% and 90% quantile values according to the four KNMI'06 climate scenarios. The high temperature with a 1/year return period is more or less equal to the 99% percentile value (the warmest day out of 90 summer days), but this quantile value was not directly calculated from the RCM results given the short available time series. It was approximated by extrapolating the difference in the changes between 50% and 90% percentile values to 99%:

$$(4.5) \qquad \Delta T_{99} = \Delta T_{50} + \frac{99-50}{90-50}\left(\Delta T_{90} - \Delta T_{50}\right)$$

where T_{99}, T_{90} and T_{50} denote the 99%, 90% and 50% (median) values of temperature, respectively. Similarly the cold temperature with a 1/year return time was estimated. The results are listed in Table 4-8. In the scenarios with small circulation change the extremes scale roughly with the mean (and globally averaged) temperature change. However, a shift to more westerly circulation in winter, and especially to more easterly circulation in summer, gives rise to a stronger increase in the extremes than the mean.

For **precipitation** a slightly different scaling procedure is applied. First, a *change of the wet day frequency* is calculated on the basis of the change in wet day frequency in the scenarios. Based on an observed time series of precipitation with a frequency of rainy days given by W^c, a new time series with a wet day frequency W^f is created by random elimination ($W^f < W^c$) or creation ($W^f > W^c$) of precipitation days. Elimination is applied by setting the precipitation to zero for a fraction $1 - W^f/W^c$ of the wet days. Creation of wet days is applied by assigning a precipitation amount P' to a fraction $(W^f - W^c)/(1 - W^c)$ of the dry days. P' is given by the mean precipitation of the 3 days preceding or following the particular day in the reference time series. The W^f-adjusted time series of P^c is labeled P^* hereafter, and denoted as the reference precipitation.

Table 4-8: Scenarios of 1/year temperature extremes (°C).

Temperature variable	G	G+	W	W+
mean temperature change JJA	+0.9	+1.4	+1.7	+2.8
1/year warmest day JJA	+1.0	+1.9	+2.1	+3.8
mean temperature change DJF	+0.9	+1.1	+1.8	+2.3
1/year coldest day DJF	+1.0	+1.5	+2.1	+2.9

Subsequently, a change of the *precipitation intensity on wet days* is applied to the modified precipitation time series P^* by a quantile scaling technique, that uses an exponential rather than a linear transformation function (Leander and Buishand, 2006). The precipitation in the new time series P^f is calculated from the (wet day frequency adjusted) reference precipitation P^*:

$$(4.6) \qquad P^f = a\left(P^*\right)^b$$

Similarly, the 99% values in the modified time series are written as

$$(4.7) \qquad P^f_{99} = a\left(P^*_{99}\right)^b$$

Assuming constant scaling of P_{99}/P for both the future and (modified) reference time series, the following expression applies:

$$(4.8) \qquad \left(\frac{P^f_{99}}{P^f}\right) = \left(\frac{P^{*b}_{99}}{P^{*b}}\right)$$

The scaling factor b is derived iteratively in order to satisfy Eq. (4.8) and fitted on the time series of P^f. The factor a is defined by the required ratio of the seasonal mean precipitation in the scenario and the reference time series, listed as the change of the precipitation on wet days in Table 4-6:

$$(4.9) \qquad a = P^f / P^*$$

An example of the precipitation time series of De Bilt is shown in Figure 4-13. Time series for a single summer and winter season were transformed according to the W+ scenario. Changes in wintertime precipitation are generally positive ($b > 1$) whereas summertime precipitation adjustments vary per intensity ($b < 1$ or $b > 1$).
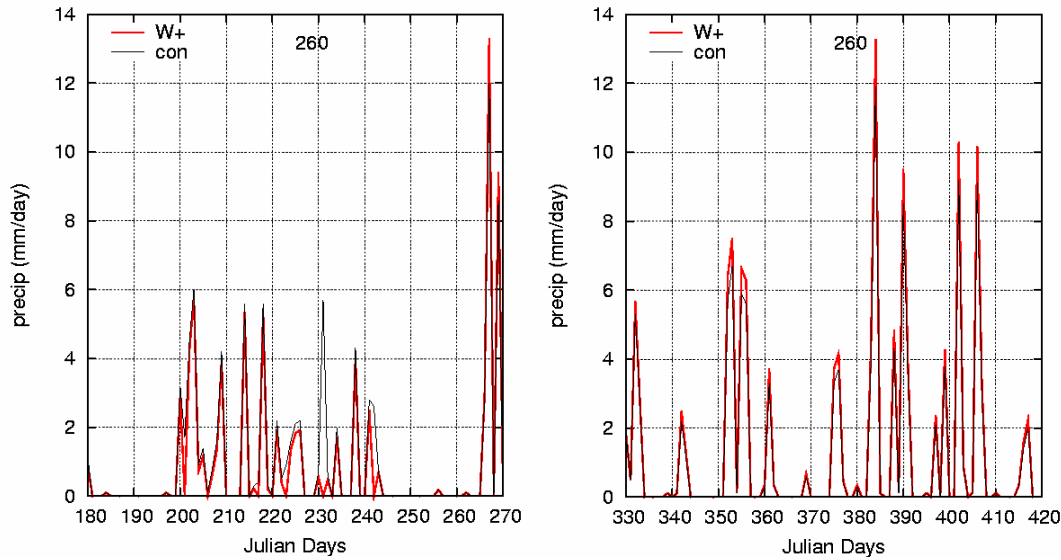
Figure 4-13: Example of control (black) and modified (red) precipitation time series for De Bilt for a summer (left) and winter (right) sample month, assuming the W+ scenario. In the summertime scenario it can be seen that the number of wet days is reduced (precipitation on days 200 and 234 is removed), that precipitation events with low intensity are reduced as well, and high intensity events (e.g. days 266 and 268) increased. For winter the changes are generally more uniform.

The perturbed time series were used to estimate changes in the return period of extreme precipitation with a given intensity y using a Generalized Extreme Value (GEV) distribution function of the probability F:

$$(4.10) \qquad F(y) = \exp\!\left(-\exp\!\left(-x\right)\right)$$

where x is a substitute for

$$(4.11) \qquad x = \ln\!\left(1 - \frac{\theta}{\alpha}(y - \mu)\right)^{-1/\theta}$$

with α, θ and μ shape parameters that are fitted to the distribution of yearly maximum events. A return time T can be deduced from this equation using

$$(4.12) \qquad T(y) = \frac{1}{1 - F(y)} \quad .$$
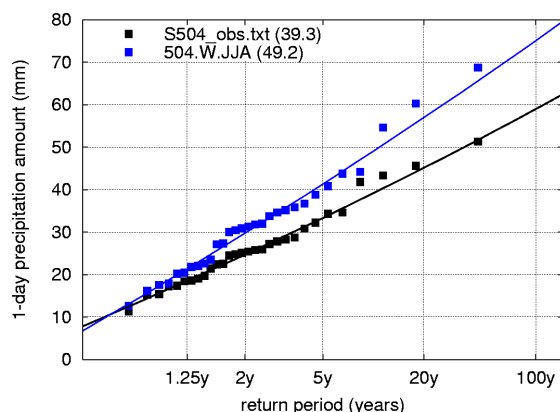
Figure 4-14: Extreme value distribution of summertime precipitation from the observations at station De Bilt (black) and from the modified time series according to the W-scenario (blue).

For 13 stations in the Netherlands Eq (4.10) was fitted to the observed and perturbed time series. Separate fits were constructed for summertime and wintertime conditions. Figure 4-14 shows an example of a fit for summertime precipitation in station De Bilt, both for the observations and the time series perturbed according to the W scenario. For all precipitation events occurring less than once per year the intensity is seen to increase, which was to be expected from the +24.8% precipitation increase for the 1% wettest days (Table 4-6).

Table 4-9: Relative change (%) of 10 year return levels of 1-day (JJA) and 10-day (DJF) precipitation sums for precipitation in the Netherlands. The 10 year return level of JJA 1-day precipitation is 43 mm, and 84 mm for 10-day precipitation in DJF.

Scenario	1-day sum JJA	10-day sum DJF
G	+13	+4
G+	+5	+6
W	+27	+8
W+	+10	+12

The GEV fits have been used to estimate 10 yr return period precipitation intensities for both 1-day and 10-day sums in summer and winter (Table 4-9) for the 13 stations in the Netherlands. For each station the change in extreme precipitation was first calculated from the fitted GEV distributions, and the 13 values were later averaged. Figure 4-15 shows the changes of the 10 year return levels for summer and winter 1-day to 10-day precipitation sums. Wintertime extreme precipitation is seen to increase similarly for all accumulation intervals (1 day, 5 days and 10 days), and the major difference between the scenarios is the temperature dependence. For summertime conditions the lower wet day frequency in the scenarios results in a general decline of the return levels as the accumulation period is increased from 1 day to 10 day precipitation sums. In the W+ and G+ scenarios this decline results in a sign change of the response: the 10 yr return level of 5- and 10-day precipitation is seen to decrease compared to the reference climate. The decline with increasing

accumulation length is related to the relatively low wet day frequency, which makes consecutive days with extreme precipitation fairly unlikely.
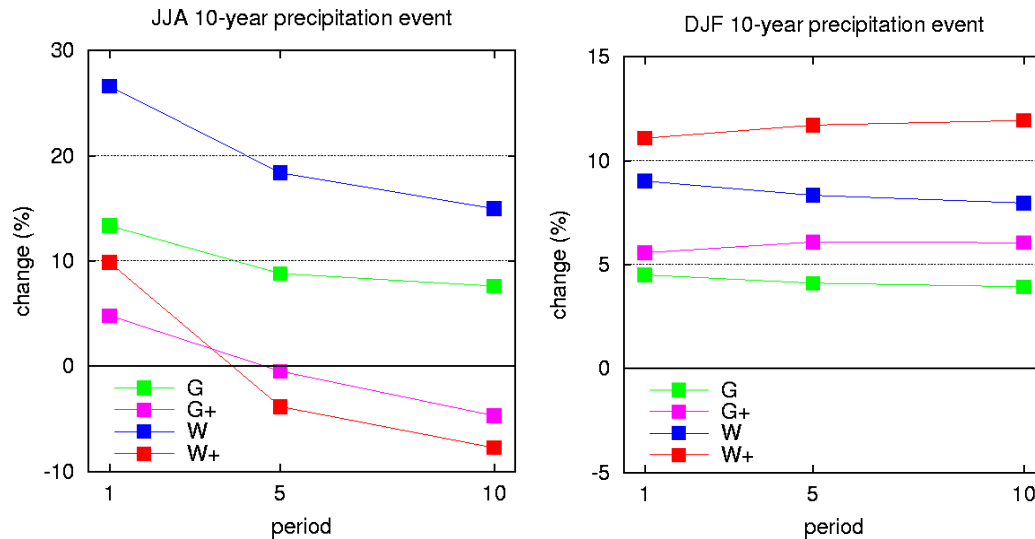
Figure 4-15: JJA (left) and DJF (right) changes in intensity for 1-day, 5-day and 10-day precipitation sums with a return period of 10 years for each of the scenarios. Calculations are based on observations for 13 stations in The Netherlands.

4.6 Summary of precipitation and temperature scenarios

From the scenario figures in Table 4-6 and Table 4-9 the following characteristics of precipitation changes are noted:

- In winter the wet day frequency changes are fairly small. In summer the decrease of the wet day frequency for the G+ and W+ scenarios is pronounced (10-20%).
- This implies that the mean precipitation increase in winter is mainly due to the precipitation on wet days, and this is strongly dependent on circulation. In summer a change to drier circulation types ($\Delta U_{geo} < 0$) tends to reduce the wet day frequency (and thereby the mean precipitation), but leaves the mean wet day precipitation virtually unchanged. In the wet regime the wet day precipitation increases considerably (4 – 9%), but the number of wet days hardly changes.
- Extreme precipitation changes in winter are close to changes in the mean precipitation. In summer extreme precipitation increases in all scenarios but this increase strongly depends on the scenario.

For temperature the following characteristics emerge:

- The circulation has a strong impact on the mean and coldest temperature in winter: for a warm circulation ($\Delta U_{geo} > 0$) the coldest days warm stronger than the mean, and the mean increases more than the global temperature of the scenario. For an unchanged circulation the coldest and mean temperatures increase similarly. This increase is smaller than the global mean temperature increase, probably owing to a relatively cool SST in the Atlantic in most GCMs. In the temperature observations of the last 25 years in the Netherlands the coldest days did not warm stronger than average (Klein Tank and Können, 2003), but further analysis is necessary to determine the circulation effect on these observed changes.

- In summer the circulation affects the temperature increase of the mean and warmest days very differently: a dry circulation regime is associated with a stronger than global mean regional temperature increase, and the extreme values increase even stronger. West circulations again cause a small difference between the increase in mean and extreme values, and a lower than global temperature increase.

5   Scenarios for potential evaporation

Evaporation is a highly relevant quantity in many hydrological, agricultural and civil applications. Also, it is a key process in the hydrological cycle. Evaporation is dependent on the availability of soil water, regulation of transpiration by vegetation (dependent on CO_2-concentrations), radiative forcing, temperature and humidity of the overlying atmosphere (governed by complex turbulent mixing, advection and convection processes), etc. Therefore, different approaches or models to generate projections of evaporation under future climate conditions can give widely varying results, owing to imperfections of models used or unforeseen changes in the relation between evaporation and ambient conditions. The present model projections do not allow a firm assessment of the changes in evaporation for the different climate scenarios.

Some of the complex interactions involving evaporation are bypassed when addressing *potential evaporation* instead, which may be defined as the maximum evaporation rate that can be supported by the atmospheric demand, assuming no feedback by atmospheric humidification. Stated differently, the potential evaporation is the maximum evaporation of a well-watered reference crop, and comparison to the actual evaporation serves as guidance for the amount of water that should be added to a crop to optimize growth. Potential evaporation is used in many applications that demand scenarios.
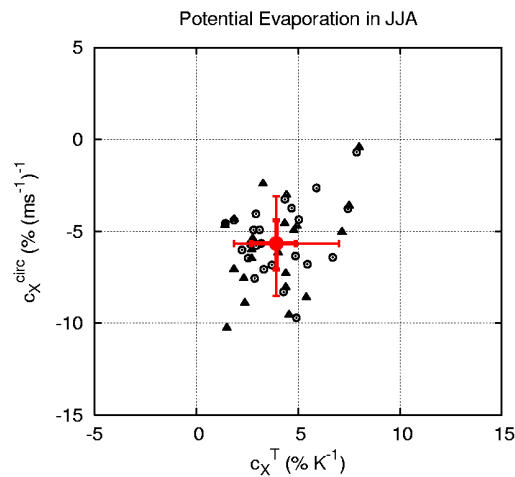
Figure 5-1: Regression coefficients for potential evaporation. Results are plotted for the models used in the G+/W+ scenario.

The KNMI'06 climate scenarios provide estimates for the change of potential evaporation in response to changing temperature and circulation. Potential evaporation LE_{pot} is calculated from the PRUDENCE ensemble models using the formulation by Makkink (1957):

$$(5.1) \qquad LE_{pot} = \alpha \frac{s}{s+\gamma} K^{\downarrow}$$

with $K^{\downarrow}$ the downward global radiation, *s* the rate of saturated vapour pressure with temperature, γ the psychrometric constant and α an empirical coefficient (= 0.65). Similar to the procedure for precipitation (illustrated in Figure 4-8) the change in LE_{pot} was related to changes in global mean temperature and ΔU_{geo}. The best fit was found by taking a 4% increase per °C temperature rise (similar to the value used in the WB21 scenarios by Können, 2001) and an additional –6% per *m/s* change of U_{geo} (defined positive for western wind), to account for the effect of dry summertime circulations on the potential evaporation (giving a negative correlation between E_{pot} and U_{geo}). Figure 5-1 shows the regression coefficients depicting the circulation dependent and –independent change for the RCM ensemble used for the G+ and W+ scenarios. The mean of RACMO2 (used in the G/W scenarios) is very close to the mean of this model ensemble, and therefore the same numbers were used for all scenarios. Table 5-1 gives an overview based on the steering parameters listed in Table 4-2.

Table 5-1: Scenarios for summertime (JJA) potential evaporation change.

	G	G+	W	W+
Potential evaporation (%)	+3.4	+7.6	+6.8	+15.2

An example of an application where a full annual cycle of precipitation deficit is analysed is given in Section 9.8. Here, basic assumptions about the scenario-dependent changes in precipitation and potential evaporation in all 4 seasons are made and applied.

6 Scenarios for wind

Wind speed is a quantity relevant for various applications. Extreme wind speed conditions that are able to generate excessive surges and waves determine the level of coastal defence. For this, 1/10.000 year wind speed events on time scales of a day or less should be estimated. This is elaborated for instance by Van den Brink (2005). For wind energy applications, extreme winds determine the operation practice of turbines. However, wind energy is proportional to the third power of wind speed, and thus the mean and frequency distribution of the cubed wind speed is a relevant quantity.
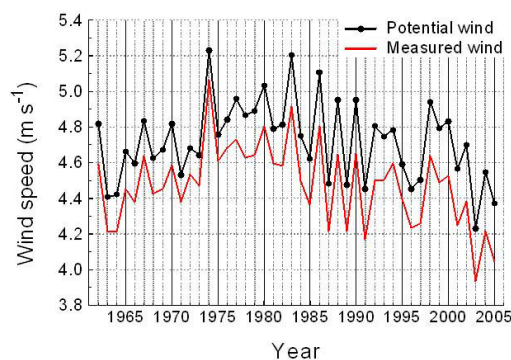
Figure 6-1: Observed mean and potential wind, averaged over the Netherlands.

For the KNMI'06 scenarios, no GCM runs were available that could be used to directly estimate 1/10.000 year wind speed events. Also GCM subdaily wind speed was not archived at PCMDI. As a compromise between available data and user requirements, the scenarios contain estimates of the daily mean wind speed that is exceeded on average once a year (i.e. it

has a return period of 1 year). Additional analyses with (much) larger model ensembles are considered necessary to give quantitative assessments of changes of more extreme wind speed variables. However, it is evident that the annual maximum daily mean wind speed is not of direct interest for the quantitative analysis of safety measures in which extreme wind plays a major role (coastal defence).

6.1   Observed and simulated wintertime wind and storms

Prior to addressing the potential impact of enhanced greenhouse gas concentrations on the wind and storminess near the Dutch coast, it is of interest to briefly consider the observed wind trends. Observations of wind speed averaged over 13 stations in The Netherlands show a decrease of the number of moderate to strong wind speed events between 1962 and 2002 (Smits et al., 2005). The results for moderate wind events (that occur on average 10 times per year) and strong wind events (that occur on average twice a year) indicate a decrease in storminess over the Netherlands between 5 and 10%/decade. Also the so called potential wind – which corrects measured winds for inhomogeneity over time in instruments, measuring heights and local surface roughness – shows a decrease since the mid seventies of the 20th century (Figure 6-1). However, the trends are not consistent for the different analysed stations, and the reason of this spatial variability is not well understood. Trends of near surface and geostrophic wind speeds found in ERA40 and NCEP/NCAR reanalysis data generally show the opposite: positive trends are found for nearly all wind speed classes (Figure 6-2).

Are the trends in mean and (moderate) strong winds related to the global warming in the recent decades? Lambert and Fyfe (2006) analyzed daily mean sea level pressure simulations from a wide range of AR4 GCMs to explore the frequency and intensity of winter cyclones. For the northern hemisphere they concluded that the number of storms will be reduced in response to an enhanced greenhouse gas concentration. On the other hand, the number of intense events (defined as cyclones with a core pressure < 970 *mb*) increases in the simulations.
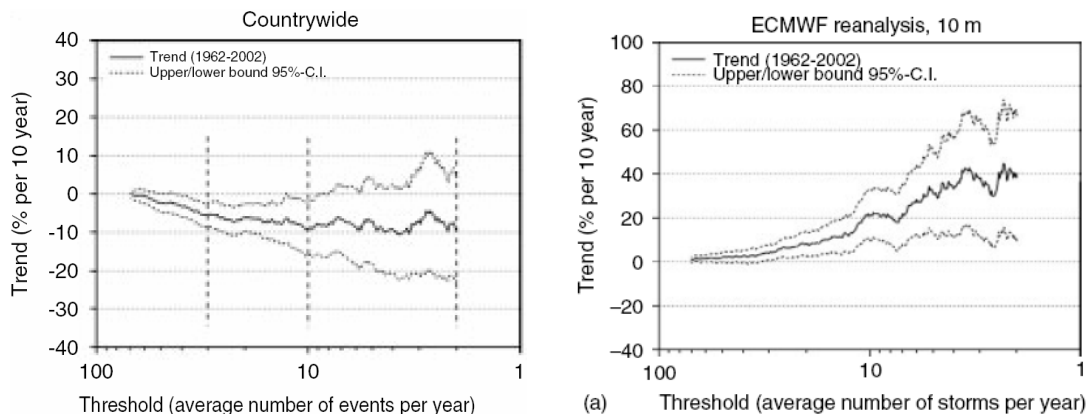
Figure 6-2: Trends (%/decade) in the annual number of storm events in the observations (left) and ERA40 (right) as a function of severity level for the Netherlands. Solid lines are the coefficients of the slope; dotted lines are the corresponding 95% confidence intervals (from Smits et al., 2005).

For the KNMI'06 climate scenarios we have analysed a subset of the models used by Lambert and Fyfe (2006), considering actual wind speed rather than surface air pressure as a proxy. The GCM-selection is identical to the set introduced in Table 4-1 used to generate the

steering parameters for temperature and precipitation scenarios. Only HadGEM was not included in the wind analysis, since daily data were not available.

Prior to our analysis, it was assumed that the coarse resolution in GCM simulations would underestimate the number of intense storms. Nested high-resolution RCM results would favour steeper pressure gradients, and thereby increase maximum wind speed. However, daily mean wind speed is not significantly altered using the RCM nesting approach. Figure 6-3 shows North-South cross sections of mean sea level pressure (MSLP) and $10\,m$ wind speed corresponding to the annual lowest pressure and highest daily mean wind. The depth of the lowest pressure is systematically different in ERA40 and the PRUDENCE model HadAM3H, but the nested RACMO2 runs do not consistently give rise to a deeper core pressure or steeper gradients. Difference in vertical resolution may be one of the reasons that the actual core pressure in RACMO2 is deepened compared to ERA40, but less deep when driven by HadAM3H. Van Ulden et al. (2006) show that particularly during winter the control of the lateral forcing on the inner dynamics in the PRUDENCE RCMs is strong. Therefore it was decided not to apply RCM downscaling for generating wind scenarios. This decision is confirmed by the results of Leckebusch et al. (2006).
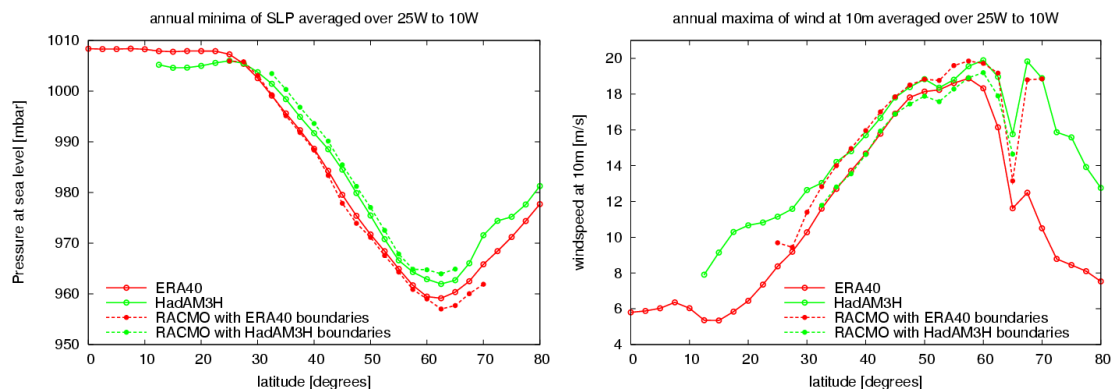
Figure 6-3: Cross section of (left) the average annual minimum mean sea level pressure and (right) the annual maximum wind speed at 10m height in the area 25-10°W and period 1960-1990. Shown are results from ERA40, the control run of HadAM3H, and two RACMO2 simulations driven by these GCM boundaries.

6.2   Wind scenarios

The wind scenarios are based on daily output from SRES A1b runs of the four selected GCMs. Simulations were available for the period up to 2300. The quantity considered is the yearly maximum of daily mean surface wind. Daily output was only available for distinct time slices: 1961 – 2000 for the control period, 2081 – 2100 for all models, 2181 – 2200 for all but MIROCHi, and 2281 – 2300 for ECHAM5 and GFDL2.1.

The four GCMs have a reasonable representation of the monthly mean wintertime pressure patterns over Western Europe (Van Ulden and Van Oldenborgh, 2006). A systematic bias is present in the distribution of annual maximum daily mean wind speed over the North Sea (Figure 6-4). However, the bias is similar in the whole range of extreme values, suggesting that information about the change in the extreme wind speed derived from the GCMs is still valuable. In the figure, also results from the 2081 – 2100 time slice are shown, to be discussed below.

Figure 6-5 shows the change in the mean 10 *m* wind speed between the control period and a +2°C scenario for the analyzed GCMs. The +2°C values are obtained from the time slice model output by assuming a linear relation between global temperature change and seasonal mean wind speed change. The results are grouped into the average of the models with a strong wintertime circulation change in the Netherlands (representative for the circulation change scenarios G+ and W+), and the (single) model that simulates a minor wintertime circulation change. At the lower midlatitudes (30°-45°N) all models consistently show a reduction of the mean surface wind over the Atlantic sector. At the higher midlatitudes (45°-65°N) all models also show a reduction of the mean DJF wind speed over the central and Western part of the North Atlantic basin, but a relative maximum is found in the Eastern sector of this basin. The location varies among the models (CCC63 showing the maximum above land), but the group average response (Figure 6-5, lower left panel) shows an increase of around 2% over the North Sea. This feature is in agreement with the positive wind speed changes in the three left panels in Figure 6-4.
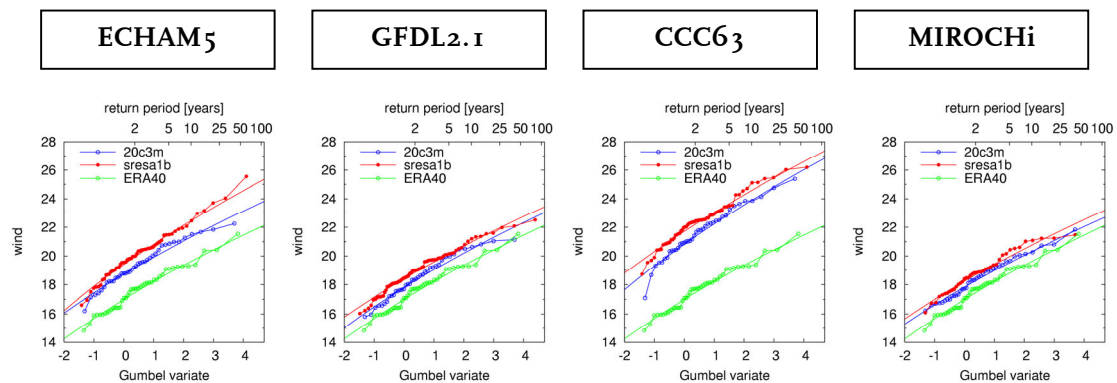
Figure 6-4: Distributions of annual maximum wind speed on a single grid point location over the North Sea (2.5 °E, 55 °N) of 4 GCMs. The Gumbel variate is a transformed rank order coefficient, related to the return period plotted in the top horizontal axis. Shown are the control simulation (blue line), SRESa1b simulation 2081-2100 (red line) and ERA40 (green line). The left three panels correspond to GCMs with a positive change of DJF ΔU_{geo}, the GCM from the right panel does not show such change.

In Figure 6-4, annual maximum 10 *m* wind speed in the North Sea area in one of the models (MIROCHi) run with the A1b scenario is seen to increase with approximately 0.45 *m/s* for all return values. The position of the point shown coincides with the relative maximum of 1.5% located in the North Sea (Figure 6-5, lower right panel). In the other A1b simulations shown in Figure 6-4 extreme 10 *m* wind speed increases by around 0.5 – 1 *m/s* (CCC63, GFDL2.1) or between 0.5 – 1.5 *m/s* (ECHAM5). The ensemble results are shown as a positive signal over the North Sea in Figure 6-5.

Figure 6-5 illustrates the spatial variability of the wind speed change in the individual GCMs, even when focusing on a relatively small area as the North Sea. For this reason, a group of grid point results is used to quantify the wind speed changes in the KNMI'06 climate scenarios. Annual maximum daily mean wind speed from all grid points in the area roughly covering the Netherlands and the North Sea (0°-10°E, 50°-60°N; see box in bottom right panel of Figure 6-5) is included. For each model and each grid point, this wind speed quantity is averaged for all available time slices. The mean values in the time slices are normalized by the values in the reference period (1961 – 2000) to obtain relative annual

maximum daily mean wind speed changes. These wind speed ratios are divided by the mean global temperature change in the particular episode and multiplied by two, to obtain a response corresponding to the +2°C scenarios for 2050. A frequency distribution plus a smoothing spline of the relative changes of annual maximum wind per 2°C global temperature rise is shown in Figure 6-6, where the same allocation of GCMs to scenario groups is used as in Figure 6-5. Means and 10/90%-percentile values are shown in Table 6-1. The distributions reflect the uncertainty related to the estimate of annual maximum daily mean wind speed associated with spatial variability of the wind speed changes (shown in Figure 6-5), and the model differences of the ensemble used for the G+ and W+ scenarios.
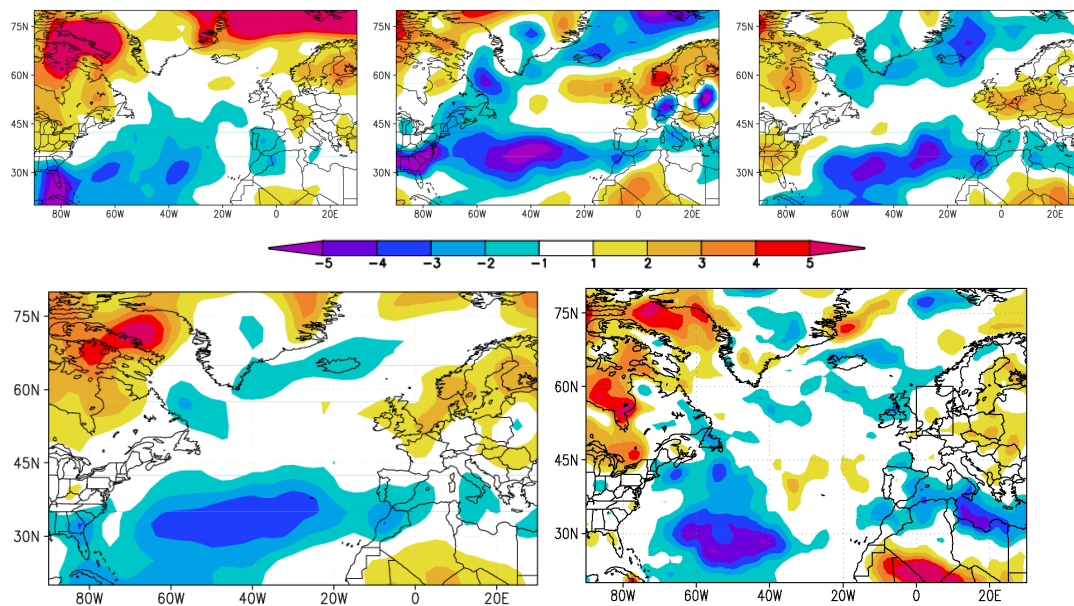
Figure 6-5: Relative change (%) in the annual maximum daily mean wind speed at 10 m height between the +2 °C scenario and the reference climate from the four GCMs. The mean wind difference is obtained by assuming a linear dependence of mean DJF wind change and global temperature increase, and scaling the GCM time slices back to a +2 °C global temperature increase. The upper row contains the models used for the G+ and W+ scenarios (CCC63, GFDL2.1 and ECHAM5). The lower left panel shows a composite of these three GCMs on the left, and the MIROCHi results (used for the G and W scenarios) on the right. The box in the lower right panel denotes the area from which grid point results are used for the scenarios.

In the group of models used for the G+ and W+ scenario the GFDL2.1 model gives a higher relative increase of annual maximum daily mean wind speed than the CCC63 model. The absolute change of the wind speed between the control and scenario simulations remains rather constant for all return values, shown as nearly parallel lines in Figure 6-4. This implies that *relative* wind speed change generally decreases as the return period becomes longer than once per year.

The mean values derived from the distributions plotted in Figure 6-6 are all centred around a value close to zero. Using the means of the distributions in Figure 6-6 as values in the KNMI'06 climate scenarios does not adequately span the uncertainty range of the wind speed changes derived from these GCM analyses. For that reason, we used the outer values of the 10% and 90% quantiles for the scenarios without and with circulation change, respectively, resulting in -1% for W and +4% for W+. The G and G+ scenarios are

constructed by dividing these values by 2 and rounding to integer values. Table 6-2 gives an overview of the scenario values.

Table 6-1: Change of annual maximum daily mean wind speed for the different scenarios in 2050, expressed in % change for 2 °C global temperature rise. Indicated are the mean and 10- and 90-percentile values of the distributions shown in Figure 6-6, all rounded to whole numbers.

Moment	no circulation change	circulation change
mean	+0%	+2%
10% quantile	-1%	-1%
90% quantile	+1%	+4%
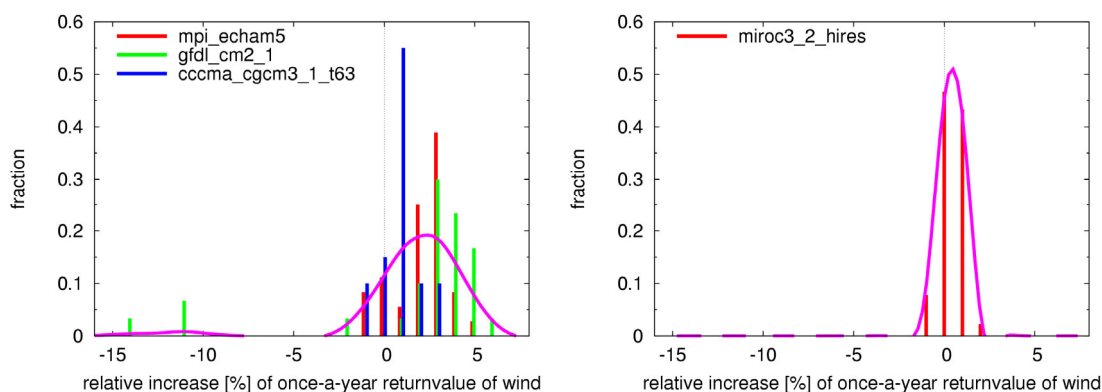
Figure 6-6: Frequency distribution of relative changes (%) of annual maximum wind speed corresponding to a +2 °C global temperature rise for (left) the collection of GCMs used for the G+ and W+ scenario, and (right) the MIROCHi model used for W and G. The vertical bars represent the relative number of grid points showing a given relative change.
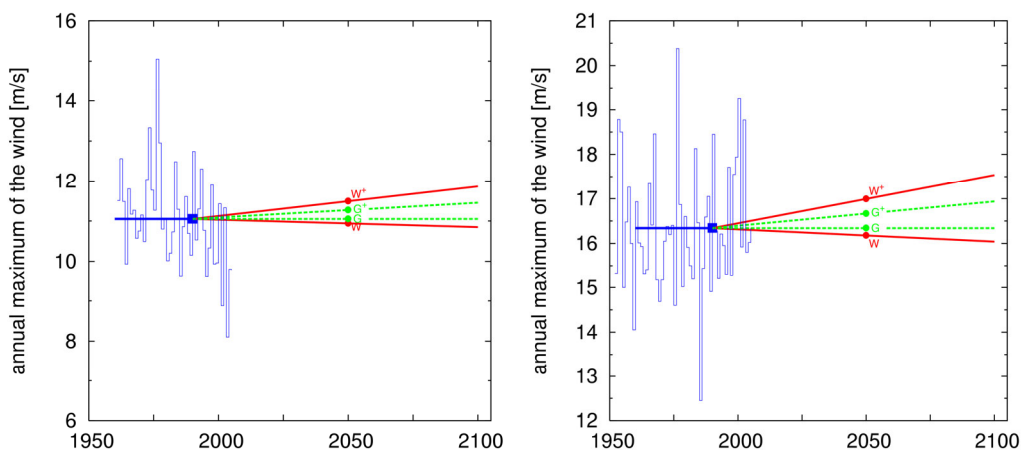
Figure 6-7: Example of annual maximum daily mean wind speed for De Bilt (left) and IJmuiden (right). Also shown are the scenario values for 2050.

The wind speed changes in the scenarios are small, certainly within the context of the interannual variability (see below in Figure 9-4). Figure 6-7 shows examples of DJF annual

maximum daily mean wind speed time series for two stations in The Netherlands (De Bilt and IJmuiden). The comparison between the two stations again highlights the considerable scatter of trends in maximum wind speed events. It is also clear that the wind scenarios give small changes compared to the typical interannual variability of the scenario variable.

Table 6-2: Scenarios for changes of the annual maximum wind speed in 2050 (% change).

Scenario	G	G+	W	W+
Change of annual maximum daily mean wind speed (%)	0	+2	-1	+4
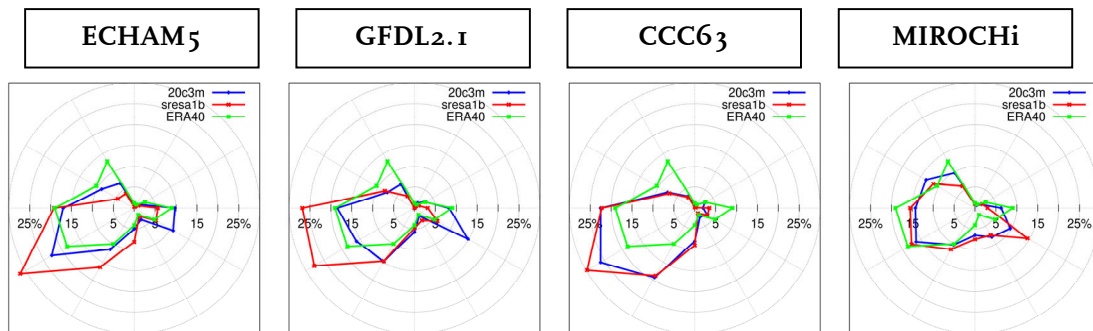
Figure 6-8: Relative distribution of the 10 highest daily mean wind speed values per year over the directional sector. Shown are results derived from ERA40 (green lines), control GCM simulations (blue) and SRES a1b runs (red).

6.3   Implications for North Sea surges

The GCM projected changes in extreme wind direction are less consistent than changes in wind speed (Figure 6-8). Most models show an increase of the daily mean wind speed exceeded 10 times per year from the southwest direction, but changes in the northwest direction (most relevant for the storm surges reaching the Dutch coast) are more ambiguous, varying from a reduction in the ECHAM5 model to no change in CCC63 and MIROCHi.
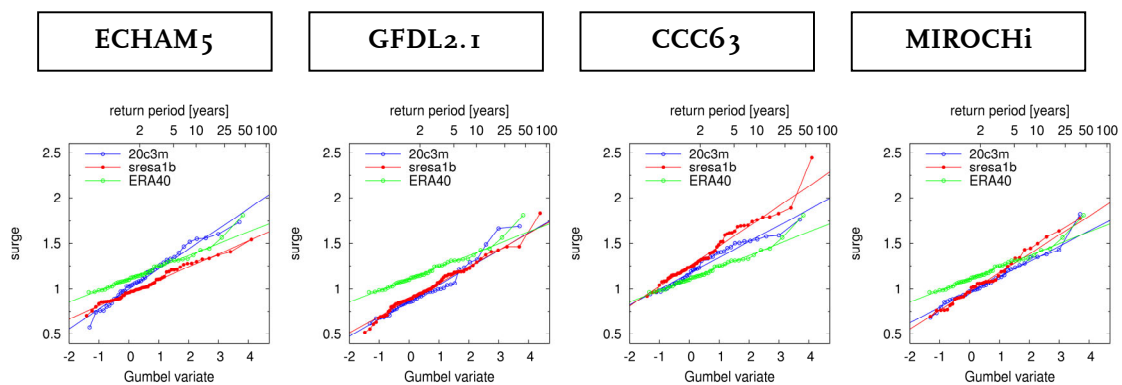
Figure 6-9: Extreme value distributions of surge levels calculated with a simple surge model and the daily wind records from the GCM simulations. Colour coding as in Figure 6-8.

From these wind statistics a simple parametric surge model (Van den Brink, 2005) is used to generate an estimate of the change in return value of the surge at the North Sea coast. For

this exercise, wind data from a collection of all GCM grid points within the area (0 – 10°E, 50 – 60°N) are used, which spans the typical region important for surge on the Dutch North Sea coast. In Figure 6-9 results of this simple surge model are plotted. Changes in the surge level are not consistent for the three GCMs used to construct the G+ and W+ scenarios: maximum surge levels are seen to decrease in ECHAM5 for SRES A1B conditions, CCC63 show an increase, and GFDL2.1 (and MIROCHi) show no significant change. The ECHAM5 model shows that an increase in annual wind speed (Figure 6-4) can coincide with a decrease of the surge (Figure 6-9) due to the change in wind directions (Figure 6-8).

Although the various grid points within the sector considered for the surge model are not uncorrelated (the highest values are most likely generated by the same synoptic system) the distribution of surge levels gives an indication of the variability of this quantity. Figure 6-10 shows the results for 1-year and 50-years return periods. The ensemble shows that the changes in the maximum surge levels are small on average, within a few % of the value generated with the control climate model output. Within the context of this simple analysis the wind speed scenarios combined with the modelled wind direction changes do not give rise to strong changes in the risk of North Sea surges. However, other methods to construct risk profiles (for instance, by selecting output from only the most extreme model (CCCMA)) can give rise to different conclusions.
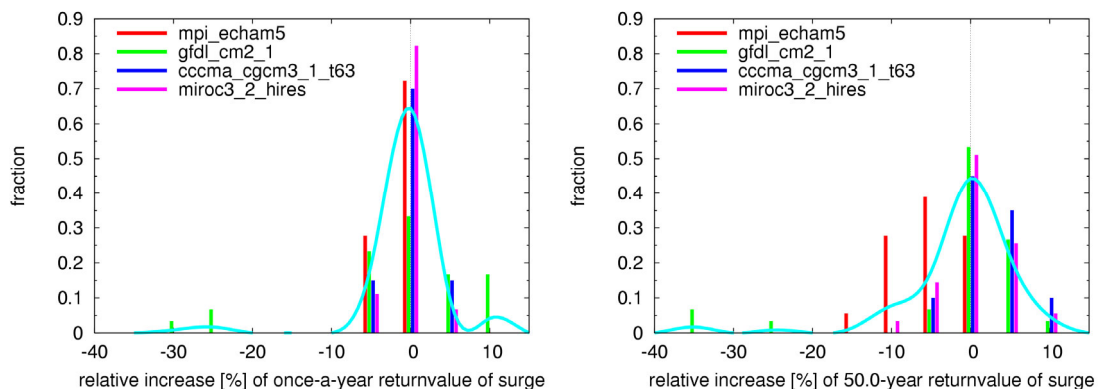
Figure 6-10: Probability distribution of relative changes of the surge level obtained from a sample of grid points in the area (0 – 10°E, 50 – 60°N) from the collection of GCMs. Shown are 1 (left) and 50 years (right) return values.

7   Sea level changes in the Eastern North Atlantic Basin

7.1   Constructing scenarios of sea level rise

The KNMI'06 climate scenarios for sea level rise (SLR) for the Netherlands are constructed for the target years 2050 and 2100 relative to 1990. Sea level changes in the 22nd century and beyond are discussed qualitatively. In constructing these scenarios, contributions from various sources are considered. For the period 1990 – 2005, observations for total SLR are used (see Section 7.3). From 2005 onwards, the main components contributing to SLR are considered separately:

- thermal expansion of sea water in the eastern North Atlantic Basin (Section 7.4);
- changes in glaciers and ice caps outside Greenland and Antarctica (Section 7.5);
- changes in the Greenland and Antarctic ice sheets, including glaciers (Section 7.6).

Remaining (small, uncertain) contributions are discussed in Section 7.7, before combining all elements to obtain scenarios for SLR in the Eastern North Atlantic Basin (Section 7.8).

Our estimate of the thermal expansion is based on the analysis of GCM runs that have been performed for the preparation of the 4th IPCC Assessment Report that is to appear. These runs have been made available to the scientific community in the course of 2005. For the other contributions we rely on results from published scientific papers. All major components of the SLR estimates depend on the global temperature rise achieved in the target periods considered. The rationale for choosing the relevant temperature values is discussed first in the next section.

7.2   Choice of values of global temperature rise

For the target year 2050, values of global temperature rise of +1°C and +2°C are used, similar to the other scenario variables. For 2100, the temperature selection is based on an analysis of AR4 GCM runs forced by the A1B, B1 and A2 emission scenarios (see Figure 7-1). The values of +2°C and +4°C correspond roughly to the 10% and 90% points of the probability distribution function of the temperature rise in 2100, and these are used for the moderate (G) and warm (W) scenarios, respectively. It should be noted, however, that a higher temperature increase for 2100 could eventually be justified, since the AR4 GCM runs do not account for the full uncertainty of the climate system. Sudden changes in the climate system induced by strong ice cap melting or complete collapse of the thermohaline circulation are also not included in this ensemble. Other feedbacks that are known to influence the climate system on century-long time scales, such as carbon cycle and vegetation feedbacks, are not or very crudely represented in all these models.
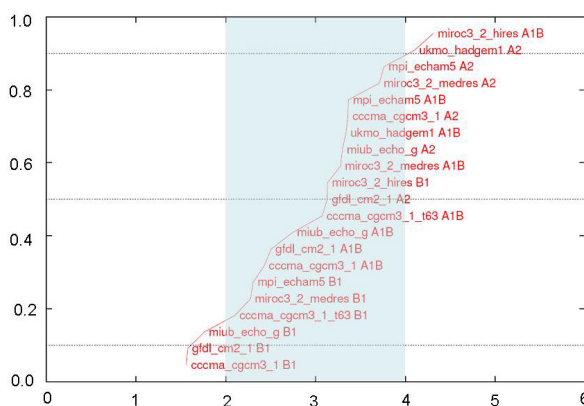
Figure 7-1: Global atmospheric temperature rise projected for 2100 (horizontal axis, in °C) by AR4 GCMs forced with A1B, A2 and B1 emission scenarios. Values on the vertical axis denote quantiles. The blue shading outlines the temperature range used for the scenarios for sea level rise.

7.3   Sea level rise between 1990 and 2005

For global mean sea level, the rise between 1975 and 2005 deduced from tide gauges is about 75 *mm* (Holgate and Woodworth 2004, Church and White 2006), which gives a contribution of 38 *mm* for the period 1990 – 2005, or approximately 2.4 *mm/yr* assuming a constant rate. Satellite radar altimetry estimates for the period 1993 – 2003 arrive at a somewhat higher value of 3.1 ± 0.8 *mm/yr* (Leuliette et al. 2004; see also Figure 3-5). For the Netherlands, sea level in the North Sea is more relevant than the global mean, but this quantity is also more erratic. Considering multi-year means, it is found that at time scales of

several decades, sea level at the coast of the Netherlands rises at a rate of about 2.5 ± 0.6 *mm/yr*, which is numerically the same as the rate of global SLR from 1975 to 2005. Hence a local SLR of 4 ± 1 *cm* at the Dutch coast is used in the scenarios for the period 1990 – 2005.

7.4   Thermal expansion in the eastern North Atlantic basin

To estimate the **thermosteric sea level rise**, GCM simulations for the A1B, A2 and B1 scenarios from the IPCC AR4 database were used, for the entire 21st century.

Three variables of interest were retrieved: global mean atmospheric temperature rise (ΔT_G), global mean thermosteric sea level rise ($TSLR_G$) and local thermosteric sea level rise ($TSLR_L$) in the area $[25°W, 10°E] \times [40°N, 65°N]$. The latter variable is used to construct specific scenarios for TSLR in the eastern part of the North Atlantic basin that reflect regional differences in TSLR (e.g., Levermann et al. 2005, Figure 3-5). Not all model data were used because of problems with technical availability of the required set of fields or obvious deficiencies in the model formulation (see Table 7-1).

Table 7-1: List of GCMs and the scenario runs used to assess the thermosteric component of SLR.

Model	Global thermosteric SLR	Local thermosteric SLR
BCCR BCM2.0		B1, A2
CCCMA CGCM 3.1	B1, A1B, A2	B1, A1B, A2
GISS AOM	B1, A1B	
GISS ER	B1, A1B, A2	
IAP FGOALS-g1.0		B1, A1B
INM CM 3.0	B1, A1B, A2	
MIROC 3.2 hires	B1, A1B	B1, A1B
MIROC 3.2 medres	B1, A1B, A2	B1, A1B, A2
MPI ECHAM5		B1, A1B, A2
MRI CGCM 2.3.2a		B1, A1B, A2
NCAR CCSM 3.0		B1, A1B, A2
NCAR PCM1		A2
UKMO HadCM3		B1, A1B, A2
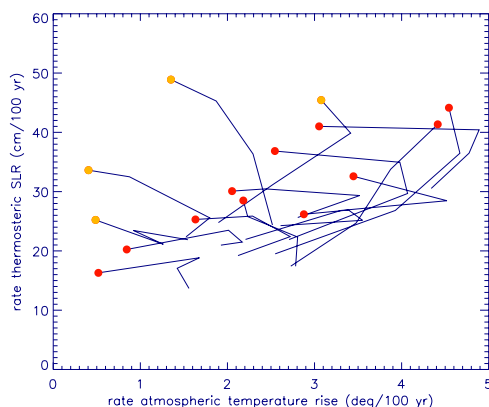
Figure 7-2: Relation between the rate of global mean atmospheric temperature rise and rate of global mean thermosteric SLR for GCM simulations driven by three different emission scenarios, for 20-year periods (circles mark the final period 2075 – 2095). Results from relatively coarse resolution simulations are marked by orange rather than red circles.

In the GCM projections, $TSLR_G$ and ΔT_G are not simply linearly related. This is clear from Figure 7-2, which shows the relation between the rate of global mean temperature rise and the rate of thermosteric sea level rise for all analyzed GCM simulations (to construct this plot, 20-year averages for 2015 – 2095 are used). In many cases the lines curve up and to the left

toward the end of the century (period 2075 – 2095, marked by circles). That is, the simulations show an acceleration of SLR even when the rate of global mean temperature rise remains the same or decreases, because of the slow response of the oceans to an atmospheric temperature rise. There is no pronounced difference in the rate of thermosteric sea level rise resulting from the B1 emission scenario (small rates of temperature rise) on one hand and the A1B and A2 emission scenarios (large rates of temperature rise) on the other. This is also a consequence of the slow response of the ocean to atmospheric temperature changes. In some low-resolution models, a low climate sensitivity of a GCM (small temperature change per unit greenhouse gas forcing) is accompanied by strong SLR per degree global warming (denoted as 'sea level sensitivity'). These are marked by orange circles in Figure 7-2. The temperature and sea level sensitivities of the other models are almost linearly related (red circles).
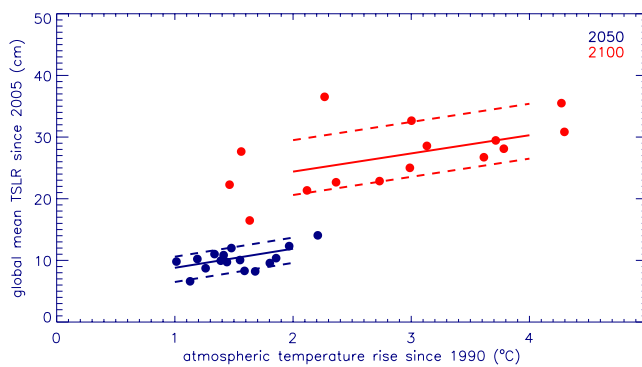
Figure 7-3: Global mean TSLR (relative to 2005) plotted against modelled global mean atmospheric temperature rise ΔT_G (relative to 1990) for GCMs driven by three different greenhouse gas emission scenarios. Values for 2050 (2100) are indicated in blue (red). Solid and dashed lines outline the median and 10% and 90% confidence values of linear fits of the dependence of TSLR on ΔT_G for these target years, respectively.

In Figure 7-3 the global mean thermosteric SLR ($TSLR_G$) in 2050 and 2100 (relative to 2005) is plotted against global mean temperature increase since 1990 for the transient GCM simulations. For the end of the 21st century, the GCMs project a wide range of global mean temperature rises between approximately +1.5°C and +4.5°C, while $TSLR_G$ projections vary only between approximately 15 and 35 *cm*. For 2050, the projected rises in global mean temperature are obviously smaller (between +1°C and +2°C), but again the range in $TSLR_G$ is fairly small (+5 to +15 cm).

Table 7-2: Estimates of global mean thermosteric SLR (cm) since 2005 as function of year and global temperature change since 1990, including the uncertainty ranges. The 10%, median and 90% uncertainty values are relative to the mean value.

SLR since 2005	low scenario		high scenario	
year (ΔT_G since 1990)	2050 (+1°C)	2100 (+2°C)	2050 (+2°C)	2100 (+4°C)
mean	8.8	24.4	11.9	30.3
Residuals relative to mean:				
10% quantile	-2.3	-3.8	-2.3	-3.8
median	0.0	-0.7	0.0	-0.7
90% quantile	+1.8	+5.1	+1.8	+5.1

Linear fits are used to describe the dependency of $TSLR_G$ on temperature change (solid lines in Figure 7-3). We assume an uncertainty that is independent of ΔT_G and we use the 10% and 90% quantiles as a measure of the uncertainties of this dependence. They are denoted by dashed lines in Figure 7-3. Thus one can read from this figure the lower and upper estimate for $TSLR_G$ at 2°C and 4°C temperature rise in 2100, and at 1°C and 2°C temperature rise in 2050. The results are shown in Table 7-2.

Table 7-3: Difference between Atlantic and global mean TSLR (cm), including the 10% and 90% uncertainty range.

Value	low scenario		high scenario	
year (ΔT_G since 1990)	*2050 (+1 °C)*	*2100 (+2 °C)*	*2050 (+2 °C)*	*2100 (+4 °C)*
median	+0.5	+0.1	+1.1	+0.1
10% quantile	-1.0	-1.7	-2.5	-3.8
90% quantile	+2.9	+6.8	+6.9	+14.8

Regionally, changes in thermosteric sea level rise can deviate substantially from the global mean value. In many simulations, sea level in the North Atlantic basin increases more than the global mean sea level. This is associated with variations in ocean heat uptake, freshening and circulation, which in the North Atlantic are strongly related to the strength of the thermohaline circulation (Van der Schrier et al., 2004). In most GCM simulations this circulation weakens (Schmittner et al., 2005; Hazeleger, 2005), although none give a total collapse. Besides an effect on thermosteric sea level, changes in the THC may also affect the local salinity and hence induce so called halosteric sea level changes. However, the variations in this component are generally much smaller than thermosteric changes (Antonov et al., 2002), and hence neglected.
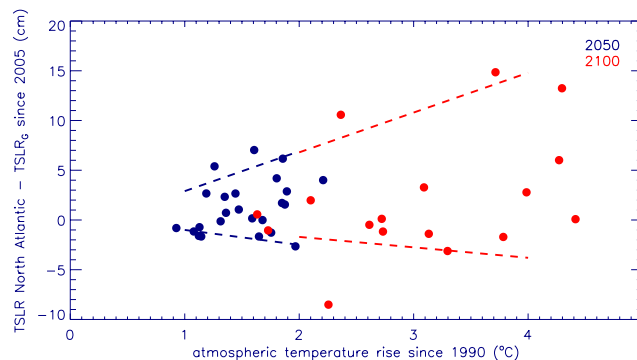
Figure 7-4: As Figure 7-3, but for the difference between TSLR in the eastern North Atlantic basin and the global mean value $TSLR_G$.

Figure 7-4 shows the difference in projected TSLR between the eastern North Atlantic Basin and the global mean value, again as a function of atmospheric temperature rise. While the mean only displays a weak dependence, more significantly, the scatter tends to increase with temperature rise. For this contribution we thus make a linear fit using the assumption that the uncertainties are proportional to the temperature rise since 1990. The 10% and 90% confidence intervals of the fit are indicated in Figure 7-4 by the dashed lines. Only one HadCM3 run falls far outside the uncertainty range for 2100. The upper bound of an additional TSLR of about 15 *cm* in the North Atlantic Basin for a 4°C temperature rise resulting from a weakening of the THC seems reasonable, considering the 25 − 30 *cm* local

sea level rise simulated for a totally collapsed THC (Levermann et al., 2005). Table 7-3 shows the median and 10% and 90% quantile values.

In combining the two contributions of the global mean *TSLR* (Figure 7-3) and additional local *TSLR* (Figure 7-4), the median values are added linearly, while the differences from the median to the 10% or 90% quantiles are added in quadrature to give the total uncertainty ranges. The final results are listed in Table 7-5 below.

7.5   Changes in glacier and ice cap changes outside Greenland and Antarctica

Estimates of the total ice volume currently stored in **glaciers and ice caps outside Greenland and Antarctica** ranges from 15 *cm* sea level rise equivalent (Ohmura 2004) to 24 *cm* sea level rise equivalent (Raper and Braithwaite 2005). The TAR estimate (Church et al. 2001) included glaciers and ice caps surrounding Greenland and Antarctica and is hence much larger (50 *cm*).

A way to characterize the response of glaciers to atmospheric warming is by means of the effective sensitivity *B* of the rate of sea level rise to global temperature increase. The present value of *B* is estimated to be of the order of 0.5 ± 0.25 *mm/yr/K*, based on recent papers (e.g., Ohmura 2004, Raper and Braithwaite 2006). Assuming a current deviation of 1 °C over the equilibrium temperature of the glaciers, the total contribution of the glacier melt can be crudely assessed. If the total sea level equivalent ice volume *V* in 2005 is around 20 *cm* (with an uncertainty range between 10 and 40 *cm*), and assuming *B* to be proportional to the ice area *A*, and that $V \sim A^{1.375}$ (van de Wal and Wild, 2001), the sea level rise in 2050 due to glacier melt is estimated to be 2.9 *cm* (uncertainty range 1.5 – 4.3 *cm*) for a temperature rise of 1 °C, and 3.9 (2.0 – 5.7) *cm* for 2 °C temperature increase. In 2100 the SLR from glacier melt is 7.4 (4.3 – 10.8) *cm* for the 2 °C scenario, and 10.5 (6.1 – 14.5) cm for the 4 °C scenario (see Table 7-5 below).

In studies by Gregory and Oerlemans (1998) and Raper and Braithwaite (2006) a much more sophisticated approach is used where reference glaciers are forced with GCM output. In the latter study, for example, glaciers are allowed to approach a new equilibrium as their environment warms. This effect decreases the sea level rise from glaciers. However, they use a GCM with a small global warming and start with a melt rate at the low end of the estimates presented by Raper and Braithwaite (2006).

7.6   Changes of Greenland and Antarctica ice sheets

As a starting point, estimates for the present-day sea level change due to the melting of the Greenland and Antarctic ice sheets are taken, including the glaciers and small ice caps around their edges. At present both ice sheets are shrinking. The **Greenland ice sheet** shrinks by 50 to 100 *Gt/yr*, equivalent to a sea level rise of $0.21 \pm .07$ *mm/yr* (Krabill et al. 2004; Rignot and Kanagaratnam 2006; Velicogna and Wahr 2005). Compared to the whole 1961 – 2003 period for which observations exist this implies an acceleration of the shrinking over the last decade; the forty year average being 0.05 ± 0.12 *mm/yr*. Estimates for the mass change of the **Antarctic ice sheet**, including glaciers and small ice caps around its edges, vary between a growth of 50 *Gt/yr* and a loss of 200 *Gt/yr*, equivalent to a sea level rise of 0.21 ± 0.35 *mm/yr*. There is a possible, but statistically insignificant acceleration of the shrinking; for the whole 1961 – 2003 period the estimate is 0.14 ± 0.42 *mm/yr* (Rignot and Thomas 2002; Rignot et al. 2005; Zwally et al. 2006). On the basis of these values we estimate that, taken together, both ice sheets shrink and contribute to a sea level rise of 0.4 ± 0.4 *mm/yr*.

Projections of the change of the Greenland and Antarctic ice sheets for the 21st century are highly uncertain (Huybrechts et al., 2004; Gregory and Huybrechts, 2006). The measurements are too sparse, and time series too short to asses the acceleration rate of the contribution to sea level rise as temperature rises. The data do suggest accelerated mass loss of the Greenland and Antarctic ice sheet over the last decade, although acceleration for the Antarctic sheet seems less dramatic. Model assessments are not wholly compatible with this picture. In models increased precipitation counteracts the increased ablation. For the Greenland ice sheet the net balance points to increased mass loss for rising temperatures, but for the Antarctic ice sheet models suggest a decrease of mass loss, or even mass gain when temperature increases. The estimate of the temperature dependence of the ice sheet mass balance from 18 coupled climate models forced with an AR4 scenario is 0.18 ± 0.14 $mm/yr/K$ for Greenland, and -0.31 ± 0.24 $mm/yr/K$ for Antarctica with respect to local temperature changes (Gregory and Huybrechts, 2006). So, both model studies and observations indicate a positive sensitivity of the Greenland ice sheet to increasing atmospheric temperatures. However, the sign of the sensitivity for Antarctica is undetermined (negative from model simulations, positive from recent observations). Hence, we assume that the mean sensitivity of the Antarctic ice sheet is zero. For the combined Greenland and Antarctic ice sheets we estimate a positive effective sensitivity of 0.2 ± 0.4 $mm/yr/K$ to global temperature rise.

Both the present-day rate of sea level rise of 0.4 ± 0.4 mm/yr and the above estimate for the sensitivity are used to determine the median and the lower bound of the contribution of the ice sheets to sea level rise in the 21st century for the different scenarios. For large temperature increases strong increases of melting may occur, especially for the Greenland ice sheet (e.g., Overpeck et al., 2006). Also, both the Antarctic and Greenland ice sheets may feature unstable glaciers and large amounts of calving. Accelerated ice flow in both ice sheets could dramatically increase their contributions, but quantitative projections are almost impossible to make. Climate simulations of the last interglacial period (130,000 years ago) by Otto-Bliesner et al. (2006) show that for climate conditions with a global mean temperature of +4°C compared to present-day climate the current Greenland ice sheet had melted to about half its current size (3.4 m sea level equivalent), but this process took many centuries. To incorporate such uncertainties in our scenarios, we base our estimate of the upper bound of contribution on the results of Ridley et al. (2005). They assessed a mass loss that saturated to values of 5 mm/yr for the Greenland ice sheet, after temperature increases of 4°C or more. Hence, we assume that the upper bound of the mass loss linearly increases from the present day estimate to 5 mm/yr at the moment that a 4°C temperature increase is accomplished. Unresolved processes, like calving, could even increase this number, but these are considered to have a relatively low likelihood.

Table 7-4 gives an overview of the range of SLR contributions of melting of the Greenland and Antarctica ice sheets. Shown are the median values and the upper and lower bounds of the range. The contribution to the final SLR scenarios is included in Table 7-5.

Table 7-4: Median and upper and lower bounds of the contribution from Greenland and Antarctic ice sheets, including glaciers and small ice caps at their edges, to SLR (cm) during the 21st century. The contributions from the present-day melt rate and the rapid calving are added in quadrature.

Contribution	low scenario		high scenario	
year (ΔT_G since 1990)	2050 (+1 °C)	2100 (+2 °C)	2050 (+2 °C)	2100 (+4 °C)
median	2.1	5.4	2.6	7.3
lower bound	0.1	-0.3	-0.1	-1.9
upper bound	5.8	19.2	+9.1	32.9

The upper bounds for the high scenarios are a factor four higher than the highest estimates of change over the last few years. This factor reflects both the error margins in the current measurements and the possible acceleration as the world warms.

7.7   Other contributions

During the 20th century the contribution of **permafrost** to SLR was of the order of 3 *mm/century* (Church et al. 2001), with a considerable uncertainty. The results of Lawrence and Slater (2005) imply a value of 5 *mm/century* for a model simulation. The **response of ice sheets to paleoclimate change on the time scale of ice ages** is estimated to be in the range of 0 – 20 *mm/century* (Peltier 2002; Lambeck 2002), considerably smaller than the central value of the TAR (Church et al. 2001). Anthropogenic contributions to **change in land water storage** may give a contribution of the same order of magnitude, but even the sign of this contribution is uncertain (Church et al. 2001). Effects of changes of the **sedimentation** are not well quantified. It is assumed that the global mean effect is negligible.

This gives a total estimate of 2 ± 2 *cm* for sea level rise in 2100 from these contributions, and half this value in 2050. The relative uncertainty is large, but the absolute uncertainty is small compared to the uncertainty in the main contributions to sea level rise.

7.8   Scenarios for total sea level rise in the eastern North Atlantic basin

The sea level scenarios are constructed by combining the observed sea level rise between 1990 and 2005, the thermosteric sea level rise since 2005 (Figure 7-3), the difference between global mean and North Atlantic sea level rise (Figure 7-4) and the various terrestrial components (Section 7.3 – 7.7). Two temperature scenarios are constructed for two target periods (2050 and 2100).

Table 7-5: Components for mean sea level rise (cm) for two time periods (2050 and 2100) and two temperature scenarios (low and high). Listed are the low and high values of a range determined by 10%/90% confidence limits for all components.

Component	low scenario		high scenario	
year (ΔT_G since 1990)	2050 (+1 ℃)	2100 (+2 ℃)	2050 (+2 ℃)	2100 (+4 ℃)
Observed 1990 – 2005	3.0 – 5.0	3.0 – 5.0	3.0 – 5.0	3.0 – 5.0
total thermosteric from 2005	6.8 – 12.5	20.2 – 32.7	8.9 – 19.3	24.7 – 45.5
global mean thermosteric since 2005 (Table 7-2)	6.5 – 10.6	20.6 – 29.5	9.6 – 13.7	26.5 – 35.4
Δ (Northeast Atlantic – global mean) (Table 7-3)	-1.0 – 2.9	-1.7 – 6.8	-2.5 – 6.9	-3.8 – 14.8
terrestrial water storage				
glaciers and ice caps	1.5 – 4.3	4.3 – 10.8	2.0 – 5.7	6.1 – 14.5
Greenland + Antarctica (Table 7-4)	0.1 – 5.8	-0.3 – 19.2	-0.1 – 9.1	-1.9 – 32.9
other	0.0 – 2.0	0.0 – 4.0	0.0 – 2.0	0.0 – 4.0
Total	**15.6 – 24.6**	**34.9 – 59.5**	**19.6 – 33.9**	**42.0 – 84.0**

Even for a given global mean temperature, the SLR projections show a large variation between models and assumptions. All estimates of thermosteric and terrestrial sea level rise are associated with considerable uncertainty ranges. We therefore present *ranges of SLR per global mean temperature scenario*. The ranges are calculated as a summation of 10% and 90%

confidence levels of the GCM analyses of the thermosteric component, and the reported uncertainty values of the other components discussed in Section 7.7.

Table 7-5 lists all contributions of the sea level rise scenarios. The 10% and 90% quantile values of the global mean and Atlantic difference contributions are combined by a non-linear error summation (assuming dependence between the various error sources):

$$(7.1) \qquad z_h = z_{m1} + z_{m2} + \sqrt{\left(z_{h1} - z_{m1}\right)^2 + \left(z_{h2} - z_{m2}\right)^2}$$

with z_h the final scenario value (for instance, the high end of the range), z_{h1} and z_{h2} the high end of the ranges of the separate contributions, and z_{m1} and z_{m2} the medians of the two contributions. Table 7-6 summarizes the final scenario values. The final figures are rounded to 5 *cm*, because of the large uncertainties. The intermediate results are given to 1 *mm*.

The uncertainty ranges represent approximate 80% intervals. This means e.g. that the probability that for the +4°C scenario the sea level rise is above 85 *cm* in 2100 is estimated to be of the order of 10%. Assuming that the uncertainties scale as in a two-side Gaussian distribution, 90% uncertainty margins would be obtained by multiplying the 80% margins by a factor 1.3.

Table 7-6: Scenarios of sea level rise (cm) for two target periods, two global temperature scenarios and two different sea level sensitivities (SLR per degree global warming). All values are rounded to 5 cm.

Sea level sensitivity	low scenario		high scenario	
year (ΔT$_G$ since 1990)	*2050 (+1 °C)*	*2100 (+2 °C)*	*2050 (+2 °C)*	*2100 (+4 °C)*
Low	15	35	20	40
High	25	60	35	85

7.9   Long-term changes

In the TAR, SLR has been considered for periods after 2100. While it is very likely that the rate of sea level rise will increase during the 21st century, it will level off later and decrease after global warming has stabilized. The most important conclusion of the TAR was that both thermal expansion and melting of the Greenland ice sheet will continue for centuries after the concentrations of greenhouse gases have stabilized. Projections given in the TAR show that given the large margins of uncertainty one may linearly extrapolate the *bounds* of the projections of sea level in 2100 up to 2300. Subsequent studies (Meehl et al., 2005; Alley et al., 2005) have confirmed this behavior. It is likely that thermal expansion in the 22nd and 23rd century will be somewhat larger than in the 21st century (Meehl et al. 2005). In addition, one can expect non-linear behavior in the various contributions from land ice. This implies that the bounds and the median value of sea level rise evolve fairly linearly, resulting in a range of SLR between 1.0 and 2.5 *m* in 2300.

8   Summary of the scenario values

All scenario variables are given in Table 8-1.

Table 8-1: KNMI'06 climate change scenarios for 2050 relative to 1990.

Variable	G	G+	W	W+
summertime values				
mean temperature (K)	+0.9	+1.4	+1.7	+2.8
yearly warmest day (K)	+1.0	+1.9	+2.1	+3.8
mean precipitation (%)	+2.8	-9.5	+5.5	-19.0
wet day frequency (%)	-1.6	-9.6	-3.3	-19.3
precipitation on wet day (%)	+4.6	+0.1	+9.1	+0.3
10yr return level daily precipitation sum (%)	+13	+5	+27	+10
potential evaporation (%)	+3.4	+7.6	+6.8	+15.2
wintertime values				
mean temperature (K)	+0.9	+1.1	+1.8	+2.3
yearly coldest day (K)	+1.0	+1.5	+2.1	+2.9
mean precipitation (%)	+3.6	+7.0	+7.3	+14.2
wet day frequency (%)	+0.1	+0.9	+0.2	+1.9
precipitation on wet day (%)	+3.6	+6.0	+7.1	+12.1
10yr return level 10-day precipitation sum (%)	+4	+6	+8	+12
yearly maximum daily mean wind speed (%)	0	+2	-1	+4

Sea level sensitivity	low scenario		high scenario	
year (ΔTG since 1990)	*2050 (+1 ℃)*	*2100 (+2 ℃)*	*2050 (+2 ℃)*	*2100 (+4 ℃)*
Low	15	35	20	40
High	25	60	35	85

GUIDANCE

9   Guidance for use

Deliberately, the KNMI'06 climate scenarios are not associated with a certain probability of occurring, and no 'most likely' scenario is identified. The scenarios are designed to serve a diverse user community, and a wide range of applications. This section gives some guidance on how to use and interpret the scenarios for these various applications.

9.1   Impact-studies and adaptation- and mitigation-studies

The KNMI'06 scenarios are designed in such a way that for most quantities of interest they enclose the major fraction of the spread of GCM projections with four "angular points" (points at +1°C and +2°C on lines in Figure 4-3). By comparing the effects of the four scenarios it will be possible to determine a wide range of impacts and robustness of various adaptation measures.

For explorative studies it can be sufficient to use just a selection of the KNMI'06 scenarios (e.g. the warmest, wettest and/or driest scenario). With this selection it can be determined if climate change has a significant impact on a sector, or if a certain measure may have the desired effect, and, consequently, if further research is needed.

In specific situations the information in the four KNMI'06 scenarios may not be sufficient. For example, for the Dutch coastal defence changes in extreme wind speeds from the North-West are highly relevant, because they may cause storm surges that increase the risk of floods. By law it is determined that the dikes and dunes should be sufficiently high to protect against events that can occur once every 10.000 years. Information on such wind extremes is not provided standard in the climate scenarios. In such cases potential users can contact KNMI to explore the possibilities to deliver tailored climate information or tailored climate scenarios.

The results of the types of studies mentioned above can play a role in the development of policy and strategies. In this phase often one or more climate scenarios are chosen to evaluate adaptation and/or mitigation measures. Climate change is one factor determining the optimal choice, together with economic, planning and societal factors.

9.2   Likelihood and relevance

In various consultation meetings scenario users express the desire for an expert judgment on the likelihood of the various scenarios. Yet, quantitative judgment is not provided, although they are all considered to be likely enough to be explored for policy making and impact assessment purposes.

Probability density functions for future global temperature, based on ensemble GCM simulations, are gaining increasing attention in the literature (e.g., Murphy et al., 2004; Stott et al., 2005), but the local West-European implication of global temperature change is inherently noisy due to the large uncertainties in atmospheric circulation response. It will take time to increase the credibility of the models and probabilistic tools before such procedures will be mature enough for practical planning purposes.

The most likely climate scenario is not always the most relevant scenario for users. Some users are mainly interested in extreme situations, which are less likely but may be more relevant. Also, the hypothetical probability distribution of potential future climate conditions does not show a clear maximum, and this per definition implies that a wide range of future climate conditions are equally likely.

9.3   IPCC and MNP story lines and KNMI'06 climate scenarios

The Third Assessment Report (TAR) of the Intergovernmental Panel on Climate Change (IPCC) was accompanied by a Special Report on Emission Scenarios (SRES), where storylines of economic, social and technical development are translated into emissions of greenhouse gases. The story lines are separated into families, as outlined in Figure 9-1.

The Netherlands Environmental Planning Agency (MNP) uses similar driving forces and names for their story lines and related emission scenarios. However, the 4 story lines (A1, A2, B1, and B2) are translated to the Dutch situation. In B1 the effect of global climate policy is included explicitly.
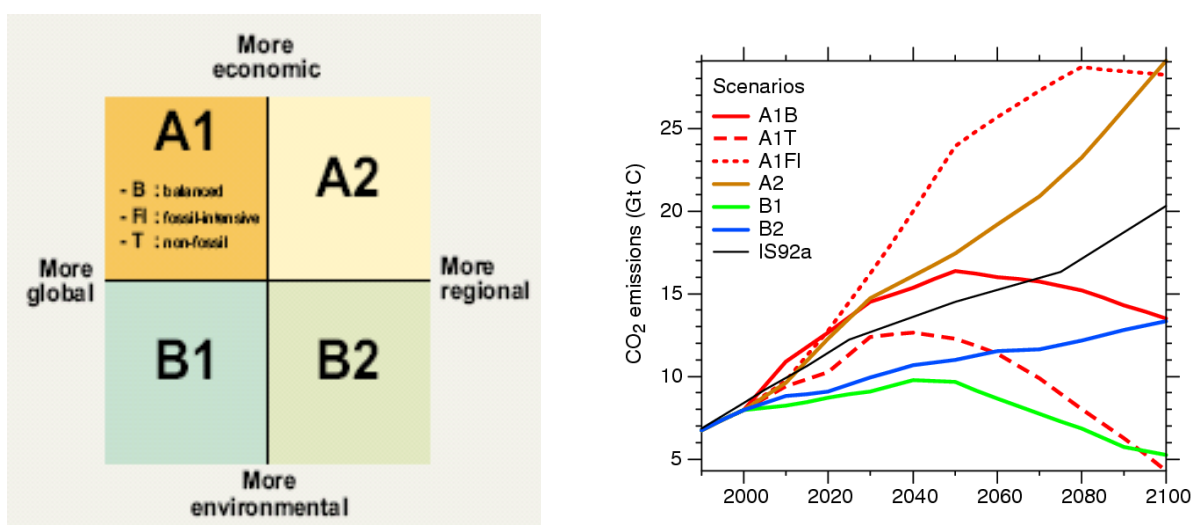
Figure 9-1: IPCC story lines (or socio-economic scenarios) for the future (left) and matching CO₂ emission scenario families (right) (Source: IPCC, 2001).

The KNMI'06 climate scenarios are not based on these storylines. The ranges of global temperature increase per storyline overlap considerably in the period until the middle of the 21st century (see Table 9-1). Therefore, climate scenarios based on these storylines do not show large differences. Most of the uncertainty about global temperature rise until 2050 is dominated by a lack of knowledge of the climate system, expressed by a wide range in GCM simulations with a common emission scenario. Uncertainty about emissions of greenhouse gases plays a smaller role, and starts to yield significant divergence only after 2050.

Table 9-1 Band width of projected global temperature rise (°C) calculated using the 7 models used for IPCC TAR (figures 9.14 and 9.15).

SRES Scenario	Range*** for 2030	Range for 2100	Estimated range for 2050*	Relevant ** scenario's for 2050	Relevant ** scenario's for 2100
A2	0.54-0.92	2.75-4.75	1.2-2.0	W, W+	W, W+
B1	0.57-0.96	1.4-2.6	0.8-1.4	G, G+	G, G+
B2	0.69-1.12	1.9-3.4	1.0-1.8	G, G+	G, G+
A1Fl	0.63-1.03	3.25-5.6	1.4-2.3		
A1B	0.64-1.04	2.1-3.8	1.1-1.8	W, W+	W, W+,G, G+
A1T	0.78-1.24	1.8-3.3	1.1-1.8		

* Based on linear interpolation between values for 2030 and 2100.
** "Relevant" means that the KNMI'06 scenarios are within the bandwidth of the emission scenario in TAR.

A link between the storylines and the KNMI'06 climate scenarios may however be given. If the global temperature rise used in a given KNMI'06 climate scenario is within the temperature range associated with a story line (see Table 9-1), the KNMI'06 climate scenario is considered relevant for this storyline. The band widths in Table 9-1 were determined with the help of data from the Third Assessment Report of IPCC (2001).

9.4   Dealing with uncertainty

"The true purpose of scenarios is to illuminate uncertainty, as they help in determining the possible ramifications of an issue (in this case, climate change) along one or more plausible (but indeterminate) paths" (Fisher, 1996).

By using the results of a large number of global and regional climate models the existing uncertainty about the climate system and the effects of various emission scenarios was, as much as possible, quantified. The uncertainty in the estimated change of the climate variables can be qualitatively assessed from

- the consistence between different models (both global and regional): a strong consensus about the sign of a change is more certain than large differences between model projections;
- the level of understanding of the underlying processes: if it can be well explained why changes occur, the uncertainty is reduced; and
- the signature of the change in observations: if the changes can be clearly distinguished from natural variability, the change is more certain to occur under the climate scenario assumptions.

In general, projected changes have an increasing uncertainty when following the series of variables from temperature via sea level rise, precipitation and wind. Wintertime precipitation is more certain than changes of precipitation in summer. The mean changes are more certain than changes in the extremes. This chain is partly dictated by the complexity of the underlying physical processes.

9.5   Reference year and reference period

Often a period of 30 years is used to describe a climate in order to include most of the natural variation. As reference for the KNMI'06 scenarios the climate in 1990 is used, which is described with observations from 1976 – 2005. This period is called the reference period or baseline period. The climate scenarios present the possible climate change between 1990 (or 1976 – 2005) and 2050 (or 2036 – 2065) or 2100 (or 2086 – 2115). When a different reference period is chosen, the climate change signals should be corrected for the difference with the reference period used for the KNMI'06 scenarios.
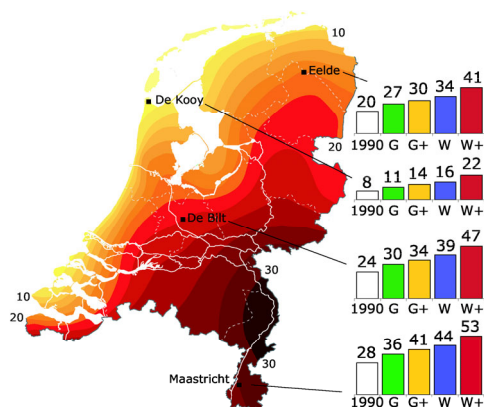
Figure 9-2: Map with observed number of summer days per year (maximum temperature > 25 ℃) for the period 1971 – 2000 (= reference), and for four places in the Netherlands according to the climate scenarios for 2050.

9.6   Spatial variability

The KNMI'06 scenarios present the possible climate change for the Netherlands as a whole. No distinction in regions with varying climate change is made. The Netherlands comprise a relatively small area. On the basis of the results of the GCMs and RCMs it is not justified to subdivide the Netherlands into regions with different climate change.

However, observations do show some trends within the Netherlands, e.g. higher summer temperatures inland. By combining these observations with the general KNMI'06 climate scenarios, maps for possible future climates can be made with spatial differentiation within the Netherlands (see example in Figure 9-2). However, users always should keep in mind that the KNMI'06 scenarios do not provide spatial differentiation in climate change within the Netherlands.

9.7   Interannual variability

The KNMI'06 climate scenarios present climatological mean values of a range of climate variables. The scenario value quantifies the change of the 30 year mean around 2050 relative to 1990. Since the scenarios are deduced from GCM calculations in which both natural variability and an anthropogenic forcing is included, the scenario values are considered to express both sources of variability on climatological (30 year) time scales.
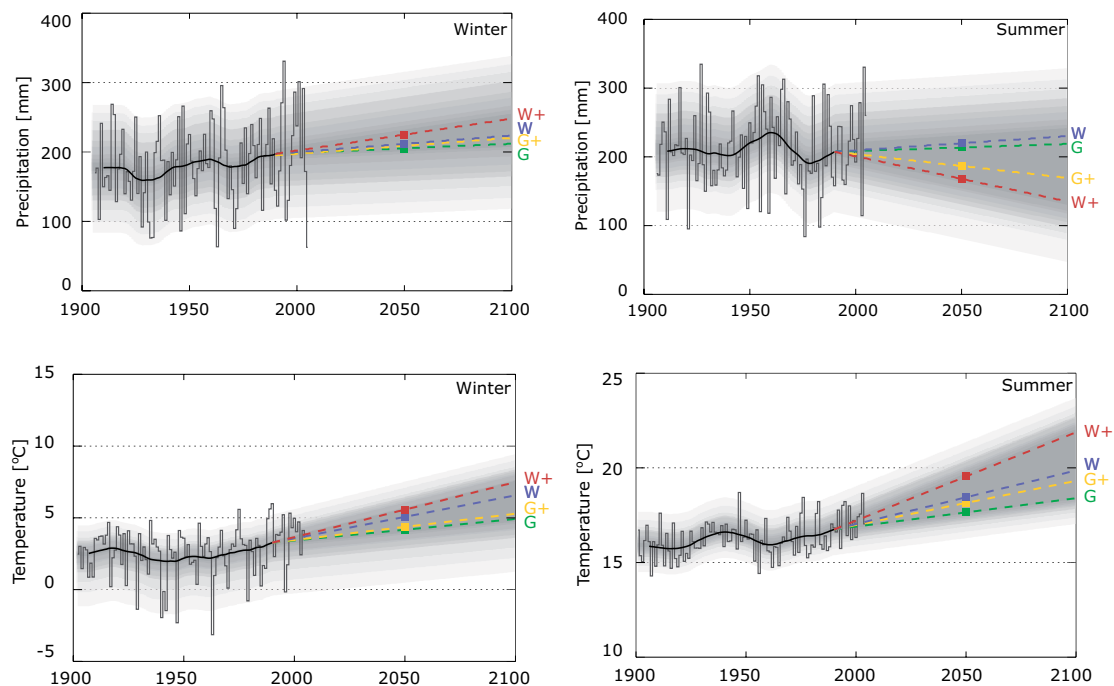
Figure 9-3: Time series of observed precipitation (mm/3 months; top) and temperature (°C; bottom) in DJF (left) and JJA (right), and the scenarios in coloured dashed lines. The background shading represents the interannual variability derived from the observations over the entire 20th century. See text for further details.

The 30-year means do not allow an interpretation of the typical interannual variability or changes therein: this interannual variability is averaged out in the 30-year climatological time frames. However, for various climate variables the seasonal mean changes foreseen in the scenarios is considerably smaller than the typical interannual variability seen in the

observational record during the 20th century. An illustration of this is given in Figure 9-3 and Figure 9-4, where time series of observed seasonal mean precipitation, temperature and wind speed are shown in combination with the scenario values. To put the mean scenario changes in the context of the interannual variability, quantile values of the climate variables have been added in shaded colours as well in both figures. The quantiles have been calculated from the *observed* time series in the entire observational period (1901 – 2005 for temperature and precipitation, 1955 – 2005 for wind). For the observational period, these mean quantiles are plotted relative to the 30 yr running mean. For the scenarios the same quantile values have been used: no changes in interannual variability have been included quantitatively. The quantiles are plotted relative to the highest scenario for quantiles higher than the median, and relative tot the lowest scenario for the lower quantiles. This artificially enhances the shading area representative for the quantile range around the median.

For temperature the 2050 scenario values seem to be significant compared to the observed interannual variability. For precipitation and wind the 2050 scenario values are relatively close to the 1990 reference value, and natural variability at interannual time scales alone may already give rise to these values. It must be kept in mind, however, that the scenario values are calculated from an ensemble of GCM output, by effectively averaging the response from the suite of GCMs. Within a single GCM, the ration between the anthropogenic climate change signal and the interannual variability may be stronger than implied by Figure 9-3 and Figure 9-4, but this has not been analysed in detail.
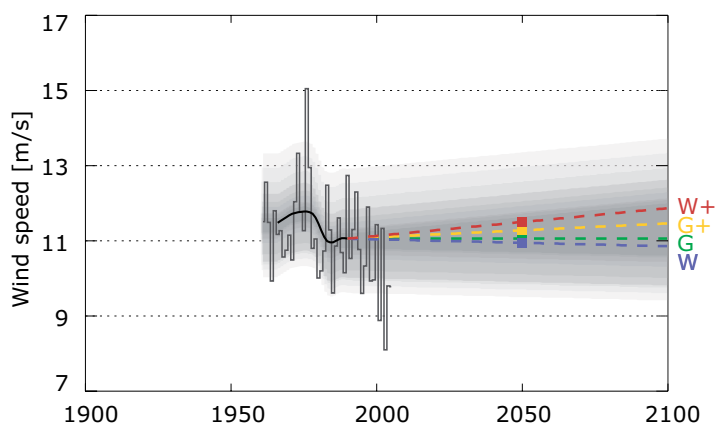
Figure 9-4: Time series of observed yearly maximum daily mean wind speed (m/s) in De Bilt, plus the scenario values for 2050 in colour coding as in Figure 9-3. The background shading represents the interannual variability derived from the observations over the entire 20th century. See text for further details.

While the figures are produced with a constant value of the interannual variability throughout the scenario time period, analysis of GCM output shows that the interannual variability of seasonally mean temperature may change (Figure 9-5). Wintertime temperature variability is seen to decrease in GCM runs with a strong increase of the zonal wind: extremely cold seasons are less frequent for relatively strong westerly wind conditions. In summer circulation change (more easterly flow) enhances the likelihood of soil drying, thereby increasing the temperature variability (Schär et al., 2004). When circulation change is small, the effects are still seen but less pronounced.

The change in interannual variability can also be deduced from changes in the slopes of the seasonally mean temperature versus mean zonal geostrophic forcing (cf. Figure 4-7).

Assuming no change in the interannual variability of seasonally mean U_{geo}, a steeper slope is associated with a stronger interannual variability. Analysis of the PRUDENCE results (indicative for the W+ scenario) indicate an increase of standard deviation of seasonally mean summer time temperature of approximately 10%/°C global temperature rise, whereas standard deviation of wintertime mean temperature decreases by 7%/°C.

For precipitation the signals are less clear. Models giving a circulation change do indicate an increase in wintertime interannual variability (see also Van Ulden and Van Oldenborgh, 2006), which is somewhat expected considering the similarity between the changes of mean and extreme precipitation (Table 4-6). For summertime the variations of the standard deviation as shown in Figure 9-5 indicate an erratic and non-systematic behaviour.
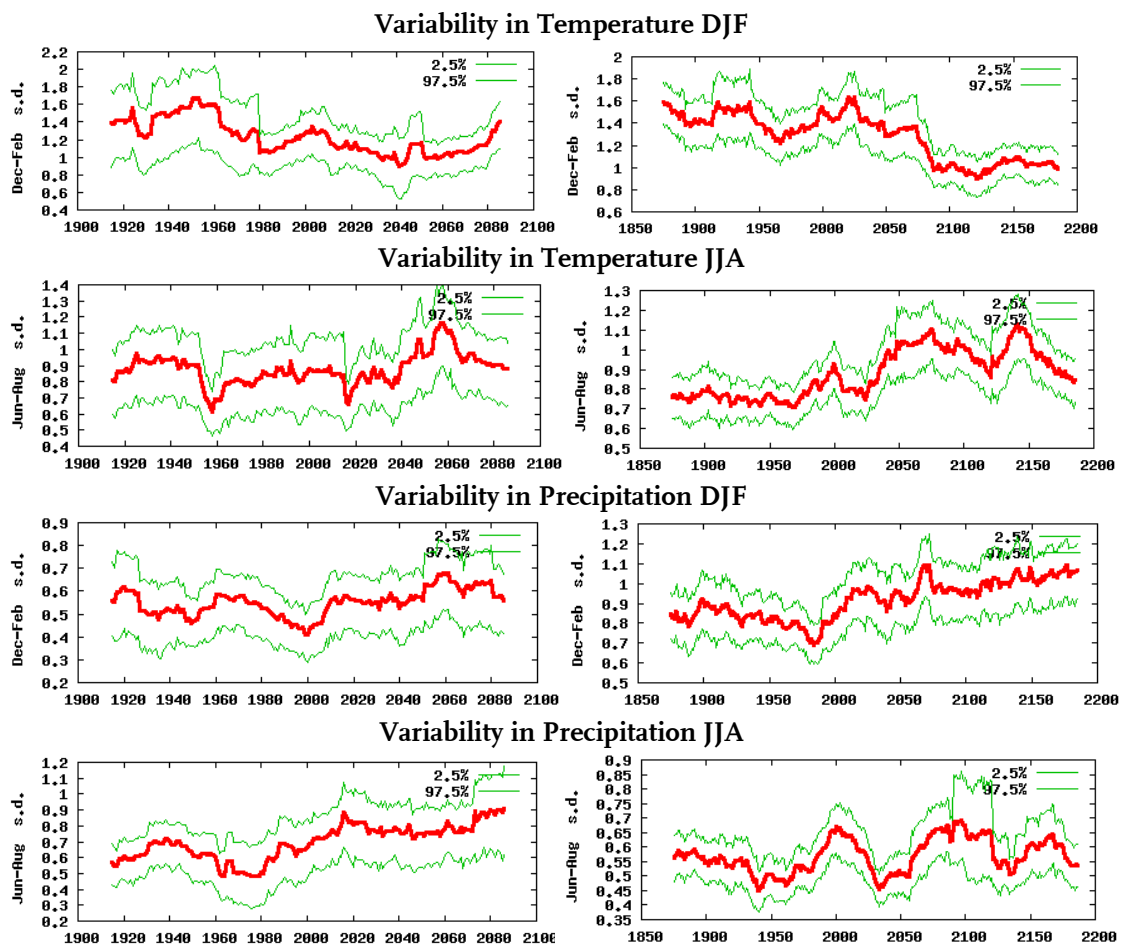
Figure 9-5: Examples of the change of interannual variability of wintertime and summertime temperature and precipitation, derived from filtered time series of output for the grid point at (7 °E, 51 °N) for two models: MIROCHi (indicative for a relatively small circulation change; left) and ECHAM5 (large circulation change; right). The central red line is the standard deviation of a 30yr running mean, the green lines mark the 2.5% and 97.5% confidence limits.

A quantitative estimate of the change of the variability of seasonal means requires a thorough understanding of all relevant processes. Effects of changes in snow cover, soil drying, vegetation response, decadal variability of SST, and other processes have not been analysed

systematically in the whole scenario definition chain including RCMs and observations. In addition, the variability of atmospheric dynamics on longer timescales is not well understood. Table 9-2 gives a qualitative assessment of the changes in interannual variability of some climate variables, but quantitative changes are not included in the scenarios.

Table 9-2: Qualitative assessment of the expected change of interannual variability of temperature and precipitation, for two different KNMI'06 scenarios.'– ' indicates a strong reduction of interannual variability, '++' a strong increase, and '+/–' a small change.

Variable	variability change in W scenario	variability change in W+ scenario
Temperature JJA	+	++
Temperature DJF	–	– –
Precipitation JJA	+/–	+/–
Precipitation DJF	+	+

9.8   Example of a full annual cycle: Potential precipitation deficit

An example of the scenario implications for the potential precipitation deficit is shown in Figure 9-6. The figure shows the median and 90% percentile value of $E_{pot} – P$ cumulative for the entire year based on the historical record of the 20th century, plus the results for the W and W+ scenarios after transformation of this historical data set using the precipitation and potential evaporation changes in the scenarios. Note that only precipitation and potential evaporation changes for summer, and precipitation changes for winter (DJF) and summer (JJA) are explicitly retrieved from the scenarios. The remaining input for the other seasons is obtained by a further (preliminary) analysis of the RCM results and a few simple interpolations; they are specifically designed for this purpose, and they are not intended for general use. Details are described below.
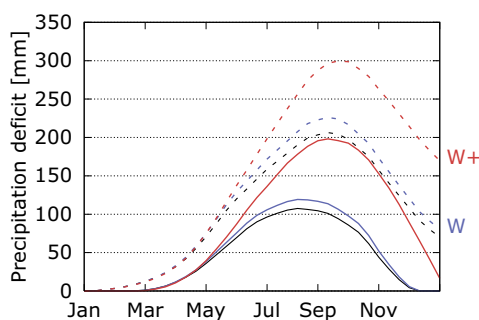
Figure 9-6: Cumulative potential precipitation deficit ($E_{pot} – P$) for The Netherlands. Shown are seasonal cycles of the historical record (1901-2000), plus the records based on a transformation of the observed time series following the W and W+ scenarios. Both median and 90%-percentile values are shown. See text for more details.

With the exception of the autumn for the G/W scenario, all values are obtained with the rescaling technique described in Section 4 using the PRUDENCE RCM ensemble driven by HadAM3H boundaries (all weighted equally). Both ECHAM4 driven runs are neglected because relatively large changes in the geostrophic vorticity appeared to lead to problems with the RCM downscaling technique for those runs. For the change in the circulation we used no change in spring and change of ΔU_{geo} = -0.6 *m/s* in autumn (half the value in summer). The latter is chosen because the circulation change in September in the GCMs is similar to the

summer response (see Figure 4-4). For autumn in the W scenario this procedure leads to rather high values of the change in potential evaporation, and low values for the precipitation change. We suspect that the results are probably affected by the hydrological memory of the soil: a dry JJA summer season will result in advection of dry air in the subsequent period, in particular September. The RCM rescaling technique cannot correct for this effect, which is not realistic in a W scenario (with on average a much wetter summer). Therefore, for autumn we simply averaged the results of the summer and winter in the W scenario.

The results are listed in Table 9-3 and Figure 9-6. In the W scenario precipitation satisfies 3%/°C for all seasons, and thus also for the annual mean. This scaling relation of the annual mean agrees well with the GCM results. For the W+ scenario a small decrease in annual mean precipitation of -1% occurs, also in fair agreement with scaling behaviour in the GCM results (see Figure 4-3).

Table 9-3: Precipitation and potential evaporation scenarios(% change) used for calculating an annual cycle of $E_{pot} - P$. DJF and JJA are directly retrieved from the scenarios, and MAM and SON numbers are discussed in the main text.

Variable	Scenario	DJF	MAM	JJA	SON
precipitation	W	7	6	6	6
precipitation	W+	14	6	−19	-6
potential evap.	W	0	6	7	4
potential evap	W+	0	6	15	10

From Figure 9-6 it clearly can be seen that the $E_{pot} - P$ evolution in the W scenario resembles the historical record, since both P and E_{pot} are increasing (and grossly balancing each other) in this scenario. The extreme years are shown to have similar evolutions. For the W+ scenario, precipitation is severely reduced in summer, leading to a significant increase of the maximum potential precipitation deficit later in the year. The historical deficit at its maximum in August (approximately 100 *mm*) is already reached in early June in an average W+ year. Also, the precipitation deficit reached in one out of 10 years increases from 200 to 300 *mm* in the W+ scenario.

10 Future research

Throughout the description of the KNMI'06 climate scenarios various hints were given for directions of future research and methodological development of the quantitative assessment of future climate conditions. This section provides an overview of recommendations for further developments.

First of all, many relevant aspects of the physical mechanism of (regional) climate change are still only poorly understood. The wide range of GCM projections for a given greenhouse gas emission scenario (Figure 3-2) illustrates this. Three aspects are particularly relevant for climate change scenarios for Western Europe.

The circulation response to elevated greenhouse gas concentrations is crucial but only marginally understood. In fact, different circulation responses in different GCMs maintain the degrees of freedom to combine increased *and* decreased summertime precipitation within a single set of climate change scenarios. But also the magnitude of seasonal mean temperature and precipitation, and the change in extreme weather events is highly linked to changes in circulation. The role of natural variability, physical mechanisms behind shifts in

storm tracks (Yin, 2005), and the role of changed land-sea temperature contrast urgently need additional research.

Also a significant range of sea level scenarios is induced by poor correspondence between GCM results and deficiencies in our knowledge on dynamics of large ice sheets, changes in precipitation climate at high altitudes, and changes in glacier length or seasonal dynamics. The basic observational records from which long term sea level rise from melting ice caps and glaciers can be deduced is very short (e.g. Rignot and Kanagaratnam, 2006). A thorough analysis of this contribution to future sea level rise for the Netherlands will be carried out in the next few years, possibly leading to an update of the sea level scenarios in a couple of years time.

A third group of poorly understood processes that generates strong regional climate variability is the role of the land surface in the (regional) climate system. Summer drying and complex feedbacks associated with snow cover can give rise to strong interactions with large scale dynamical flow patterns, and the physical processes contain many features that are able to generate positive feedbacks in the coupled system. For instance, actual evaporation scenarios (in addition to potential evaporation) can only be constructed with adequate insight in the role of the terrestrial soil water storage in present and future climate conditions. The wide range of model results in this respect hints at a poor level of understanding of the relevant processes (Van den Hurk et al., 2005a).

The KNMI'06 scenarios were constructed by means of a set of scaling rules, to circumvent the lack of available RCM runs for an optimal set of GCM projections. Had PRUDENCE been replanned for the purpose of supporting the KNMI'06 climate scenarios, the RCM ensemble would have been spread more evenly over a wider range of GCMs. Also, transient simulations covering at least the 1990 – 2050 period would have been executed. This RCM exercise is partially planned in the context of the ongoing ENSEMBLES project (see `http://www.ensembles.org`), and active involvement of the KNMI RCM team in these developments is warranted.

But even with improved climate models or downscaling methods, deterministic climate prediction will always remain impossible. The use of a limited set of discrete scenarios is a useful alternative for this, but it does not help in situations where a quantitative assessment of the likelihood of individual scenarios is urgent. Also in the context of the ENSEMBLES project, scientific methodological research is being carried out regarding the construction of probabilistic climate forecasts, weighing ensemble members, combining climate model output with impact assessment applications etc.

Also the list of variables to be analysed in further detail is considerable. First, the KNMI'06 climate scenarios basically only addressed DJF and JJA seasons, whereas in many applications scenarios must be given for the entire annual cycle. Climate change in transition seasons has an extra level of complexity. Projected changes in these seasons are very sensitive to complex non-linear climate processes, and processes with time scales longer than a single season (snow albedo, sea ice dynamics, extensive continental drying). Further analysis of these transition seasons is needed prior to constructing consistent and plausible climate change scenarios.

Another desirable variable, mentioned before in Section 9.7, is the interannual variability. For applications where long multiyear time series of climate variables are needed, a superposition of background (natural) variability on annual time scale, mean change induced by anthropogenic forcings, and day-to-day variability must be merged within a single time

series. A systematic analysis of the projected changes of interannual variability, along the suggestive lines listed in Table 9-2, is needed for all relevant variables.

Finally, the user consultation and information process remains an issue that deserves additional attention. Our experience has supported the extreme importance of clarity of presentation of the rationale, implication and limitations of the scenarios. The user group is rather diverse, and different preferences about included variables or their presentation remain. These even lead to different ways of presenting different groups of variables. For instance, there is a discrepancy between the presentation of precipitation and temperature variables (single numbers per scenario, based on a best quantitative guess of the representative value within an uncertainty range), wind variables (where quantiles of a given uncertainty range are listed as scenario values) and sea level (where a range of values is given instead of single numbers). This discrepancy may easily lead to confusion and misinterpretation if the argumentation of these choices remains unclear. The communication between the scenario constructors and users deserves continuous attention, and a solid scientific basis.

11 Annex: Statements in the scenario brochure – a reference guide

This chapter contains supplementary comments and references supporting the statements that are made in the brochure "Climate in the 21st century: Four scenarios for the Netherlands" (KNMI, 2006). The structure follows that of the brochure.
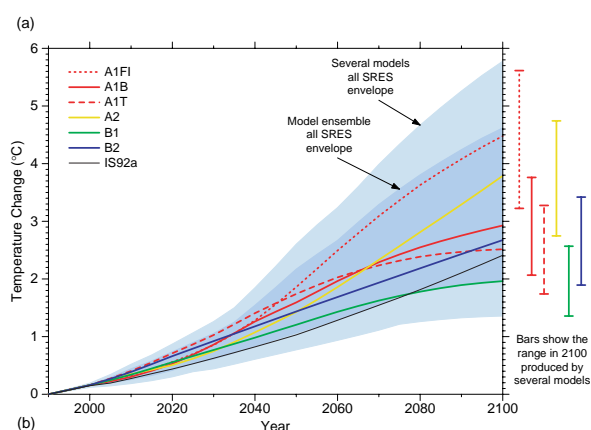
Figure 11-1: Projections of global temperature, calculated with a simplified climate model calibrated to a range of state of the art GCMs. Colored lines show the temperature evolution for six representative SRES scenarios, averaged over seven GCMs. The error bands on the right show the spread of the GCMs for each emission scenario. The grey area shows the spread of all temperature projections (IPCC TAR, 2001).

11.1 Introduction

Climate models differ considerably in their calculation of global temperature rise. This is caused by uncertainty regarding future emissions of greenhouse gasses and our limited understanding of the complex processes in the climate system. Besides, there are fundamental limits to the predictability of complex systems, such as the climate system.

Differences between global temperature projections by GCMs driven by various SRES emission scenarios indicate that the model spread up to 2050 is larger than the spread in mean model output for given emission scenarios (Figure 11-1). This implies that model uncertainty is larger than uncertainty due to unknown future greenhouse gas emissions.

After 2050 differences in emissions start to become distinguishable in the temperature projections.

> *Temperature in the Netherlands will continue to rise. Mild winters and hot summers will become more common.*

All scenarios for the Netherlands are based on AR4 GCMs, of which none projects a decrease of the mean temperature for Western Europe for the coming 50 years (see Section 4). These increases obviously do not include unforeseen events, such as a complete shutdown of the THC (see Section 7), which may cause a reduction of mean temperature. Also, the projected changes do not imply that cold years or even longer cold periods will not occur: natural variability at seasonal to decadal time scales may induce low temperature periods as well. However, averaged over the 30-year period for which the scenarios are representative, the statistical likelihood of an episodic reduction of temperature is smaller than the likelihood of a temperature increase.

> *On average winters will become wetter and extreme precipitation amounts will increase.*

In all scenarios the precipitation amount in winter increases (see Table 8-1). In the G+ and W+ scenarios this is partly due to an increase in the wet day frequency. The main effect is however the thermodynamic increase of precipitation with increasing temperature (see Section 4). Observations from synoptic stations in The Netherlands, which were the basis of the WB21 scenarios (Section 2), show a clear relationship between temperature and shower intensity (Figure 2-1).

> *The intensity of extreme rain showers in summer will increase. However, the number of rainy days in summer will decrease.*

In all scenarios the wet day frequency decreases in summer (see Table 8-1). The increase is most pronounced in the scenarios with changing atmospheric circulation. This leads to more dry weather types. The increase of precipitation intensity within showers is the result of the RCM analysis (see Section 4), and is understood as a thermodynamic effect of temperature increase on the growth of convective showers and the horizontal advection of moisture through the atmosphere.

> *The calculated change in wind is small compared to the natural fluctuations.*

Changes in wind speed and storm activity are directly derived from the GCM analysis (see Section 6). An indication of observed trends and natural fluctuations follows from the analysis of observed wind speed records in the Netherlands (Smits et al., 2005).

> *The sea level will continue to rise, however at a lower rate than predicted earlier.*

For sea level rise, the IPCC AR4 GCMs are analyzed both worldwide and for the North Atlantic sector. From these analyses the thermosteric component of sea level rise has been estimated (see Section 7.4). The other major components of sea level rise (melting of glaciers and the Greenland and Antarctic ice sheet) have been estimated from the literature, including IPCC TAR (2001). The scenarios do not account for unexpected sea level rise due to sudden melting of large portions of Antarctic Ice or Greenland glaciers. It is argued that the model predictions for such catastrophic events are very uncertain and observational support is absent (see Section 7).

11.2 Temperature

> *Since 1900 the global mean temperature has increased on average by 0.8°C. In the past 30 years this warming was mainly anthropogenic.*

The global temperature increase has been derived from the updated global temperature series by CRU/UKMO (available at `climexp.knmi.nl`), which is also used in IPCC assessment reports. The statement on the anthropogenic influence on temperature rise in the past 30 years is based on model studies of global temperature rise (see IPCC TAR, 2001).

Temperature rise was largest above the continents in the Northern Hemisphere.

Gridded datasets of temperature observations at meteorological stations clearly show that largest warming in the 20th century occurred over the continents in the Northern Hemisphere (Jones and Moberg, 2003).

In the Netherlands the temperature has risen, on average, by 1.6°C since 1900. During the past 20 years, the months February and March have seen the largest increases in temperature. Apart from global warming, this was also due to an increase of the number of days with south-westerly winds.

The value of 1.6°C is derived from fitting a linear regression line to the observed annual temperature series of station De Bilt between 1901 and 2005. This station has been regarded as representative station for temperature in the Netherlands in earlier KNMI publications (KNMI, 2003). The effect of changes in wind direction on temperature rise in De Bilt has been studied by Van Oldenborgh and Van Ulden (2003). For this report they extended the analysis period, up until February 2006.

In Europe the average temperature will probably increase slightly faster than the world average. In the Scandinavian countries especially winter temperatures will increase more rapidly than the global average, and in Southern Europe summer temperatures will increase more rapidly.

The global and regional temperature projections are based on our analysis of AR4 GCM simulations (see Section 4).

Most climate models simulate a relatively slow temperature increase over the Atlantic Ocean.

This is based on our analysis of AR4 GCM simulations. A hint of the slower warming over the North Atlantic ocean is seen in Figure 4-1, where warming patterns are shown for five representative GCMs. The Atlantic Ocean is not shown fully on these graphs, but the hint for the slower temperature increase is clearly displayed. See also Van Ulden and Van Oldenborgh (2006).

The observed temperature rise between 1990 and 2005 is comparatively high: on average 0.7°C for winter and 0.8°C for summer. This does not mean necessarily that the scenarios for 2050 are too conservative.

The +1°C climate scenarios G and G+ result in temperature increases in the Netherlands in 2050 that are not far above the observed increases between 1990 and 2005. The +1°C scenarios are based on the low end of the range of AR4 GCM projections. Indeed, the results shown in Figure 3-2 and Figure 3-3 seem to indicate that +1°C is too low, but its choice is also motivated by the desire to use round numbers, to maintain correspondence with the older WB21 scenarios, and to discriminate between the two temperature values (+1°C and +2°C). The observed temperature trend since 1990 is an indication that presently temperature is rising faster than foreseen in the +1°C scenarios. However, the origin of this rapid increase is not necessarily human and can be partly the result of natural variability. Both in the reference year (1990) and in the scenario target year (2050) the high-frequency (annual time scale) contribution of natural variability is concealed in the use of a climatological mean in a reference period of 30 yrs instead of using the temperature in a

single year (1990). Since natural fluctuations will continue in the future, it is possible that in the coming decades we will temporarily experience a period with relatively colder weather.

11.3 Precipitation

Precipitation in the temperate regions in the Northern Hemisphere has increased, on average by 5 to 10% during the 20th century. This is partly due to an increase of the strength of the westerly circulation.

Station observations show much more spatial variability in precipitation trends than temperature trends. The trends shown in Figure 11-2 are based on data from the ECA data set (Klein Tank et al., 2002). However, averaged over large regions of the northern hemisphere an increase in precipitation is observed in the order of 5-10% over the 20th century (New et al., 2000). Averaged over Europe, precipitation has also increased since 1946 (Klein Tank and Können, 2003). Part of the increase is related to the observed increase in the North Atlantic Oscillation index in winter (Thompson et al., 2000).
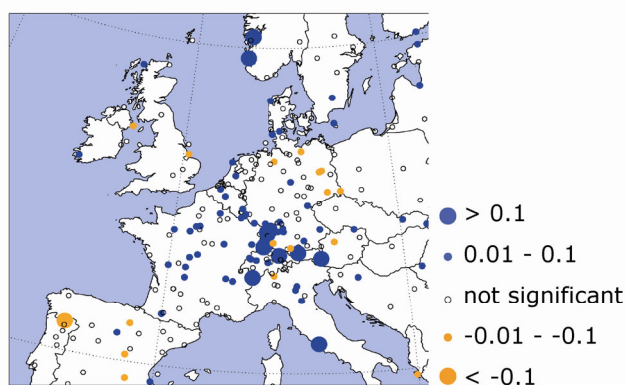
Figure 11-2: Trends in number of days per year with at least 20 mm precipitation, measured at European weather stations between 1946 and 2004. Source: eca.knmi.nl.

For Europe as a whole, the intensity of extreme precipitation has increased in the past 50 years.

Station trends in extreme precipitation show spatial variability with both increases and decreases scattered over Europe (Klein Tank and Können, 2003). Averaged over Europe, most indices of extreme precipitation have increased since 1946. In particular, the contribution of extreme precipitation to the precipitation totals has increased. This behaviour is also observed in many other midlatitude regions of the world (Alexander et al., 2006).

In the Netherlands, the annual precipitation amount increased by 20% since 1900.

Observed precipitation trends in the Netherlands are based on an analysis of 13 stations equally spread over the Netherlands. The same set of stations has also been used in earlier KNMI publications to describe precipitation change in the Netherlands (KNMI, 2003).

Climate models calculate an increase in total annual precipitation for the temperate regions and a decrease in the subtropics. For Southern Europe nearly all climate models calculate a decrease in summer precipitation and an increased chance for drought. For Northern Europe the change in precipitation is less consistent. For Europe as a whole, an increased chance of prolonged heavy precipitation and short intense showers is calculated

The regional temperature projections are based on our analysis of AR4 GCM simulations (see Section 4). Both in summer and winter, the GCMs project a clear north-south gradient in the precipitation change signal across Europe as seen in Figure 4-2.

11.4 <u>Wind and storms</u>

> *In previous decades, above the Northern part of the Atlantic Ocean the western circulation has become stronger and more northerly than it was before.*

This is illustrated for example by Yin (2005).

> *Measurements at KNMI-stations in the Netherlands show that the total number of "storms" (≥ 7 Bft along the coast, or ≥ 6 Bft inland) has decreased since 1962.*

This is published by Smits et al. (2005), and discussed in chapter 6.1 (see for instance Figure 6-2).

> *Climate models project on average a slight decrease in the number of storms in the Northern Hemisphere. However, locally the number of storms may increase.*

This finding is published by Lambert and Fyfe (2006), and further illustrated in Figure 6-5.

> *Climate models indicate that the strength of the heaviest storms could increase, but these indications are highly uncertain.*

This is also based on indications by Lambert and Fyfe (2006) and supported by our analysis of AR4 GCMs as illustrated by the GEV plots in Figure 6-4. Further support is provided by Leckebusch et al. (2006).

> *The model calculations used for the four scenarios hardly show any changes in the number of storms coming from north-west directions, relevant for surges near the Dutch coast.*

This is demonstrated by the analyses of AR4 GCMs shown in Section 6.3 (see for instance Figure 6-10).

11.5 <u>Sea level rise</u>

> *According to measurements in coastal areas and with sea-based buoys, the sea level rose by 1 to 2 mm per year since 1900. Especially between 1930 and 1960 and in the past decade the increase was relatively large. Satellite measurements since 1993 show a global average sea level rise of approximately 3 mm per year, with strong local variations between -20 up to +20 mm per year.*

Observed change in sea level based on buoys and satellite observations is discussed in Church and White (2006) and Leuliette et al. (2004). See also Section 7.

> *During the 20th century subsidence in the Netherlands varied on average between 0 and 4 mm per year, depending on the exact location.*

A source for the observed subsidence in the Netherlands is for instance
`www.geofoon.nl/Bodemdaling.html` (in Dutch).

> *After 2050 global temperature rise plays a stronger role in the sea level rise.*

The insensitivity of sea level rise on global temperature rise up to 2050 is illustrated in Figure 7-2, and discussed in Section 7.4.

> *If also large scale melting of the large ice caps takes place, a sea level rise of few meters within a few centuries can be expected.*

See for instance Otto-Bliesner et al. (2006). From this and other publications, it becomes clear that the likelihood of such catastrophic events to occur in the time frame of the present scenarios (2050 and 2100) is very low. Neither climate models nor recent observations do provide support for this. As explained in Section 7.6, the uncertainty in the melting rate of Greenland and Antarctica is considerable. Around 2100, a contribution to sea-level rise of 5

mm/yr from Greenland and Antarctica cannot be excluded. After 2100, this contribution might increase even more for some time, but the contribution from thermal expansion will level off and decrease, and we estimate sea-level rise in 2300 to be in the range between 1 and 2.5 *m* (Section 7.9). This range excludes the possibility of catastrophic events with an extremely low probability such as the collapse of the West-Antarctic ice sheet.

> *The absolute sea level rise in the new KNMI climate scenarios is almost the same as the sea level rise compared to NAP.*

Absolute sea level rise is identical to sea level rise relative to NAP, apart from slight changes in the NAP-marks over time.

11.6 Examples of applications

> *The expected increase in winter precipitation will be accompanied by increased peak discharges*

Relationships between precipitation and river discharge of Meuse and Rhine are studied for high flow conditions in winter among others by Booij et al. (2005) and for low flow conditions in summer by De Wit et al. (2006).

> *More precipitation in the Alps will occur in the form of rain rather than snow. This increases the Rhine discharge in winter.*

See for instance Beniston et al. (2003) and Keller and Goyette (2005).

> *Summertime river discharge will decrease.*

Summertime river flow is dependent on the precipitation, the discharge from deeper soil water reservoirs, and the actual evaporation. The actual evaporation does not have the same signature as the potential evaporation: in particular later in the summer season potential evaporation can still be high while actual evaporation is reduced by limited soil water availability. However, in particular for the changes in E_{pot} and P in the scenario W+ (Table 8-1) it can be expected that evaporation early in the season will reduce the soil water content that otherwise would have discharged into the river.

> *The maximum potential energy production of the wind turbines has decreased.*

Analysis of station records by Smits et al. (2005) showed a downward trend in wind in the Netherlands for events which occur several times every week up to events that occur only once a year. The reduction in averaged wind speed in recent decades is illustrated in Figure 6-1. This figure also shows that average wind speed in the sixties and seventies increased. Since wind energy yield is a non-linear function of wind speed, and wind turbine efficiency changes over time the observed wind speed changes do not straightforwardly translate to changes in energy production.

> *Energy consumption for heating is positively correlated with the number of degree days. The number of degree days decreases in each scenario.*

See for the relation between heat consumption and degree days Bessembinder (2005). The number of degree days according to the G+ and W+ scenarios is calculated using the perturbed time series for De Bilt, as outlined in Section 4. Figure 11-3 shows the observed and projected number of degree days.

> *The scenarios do not give reason to believe that wind energy production will remain lower in the future.*

The wind scenarios (Table 8-1) show small changes of the daily mean wind with a one year return probability. Given the small change and the large natural fluctuations in the

observations, future wind energy yield will be more dependent on the natural fluctuations than on the climate change scenarios. The short time series of observations of these fluctuations does not support a continuous downward trend of wind energy gain.
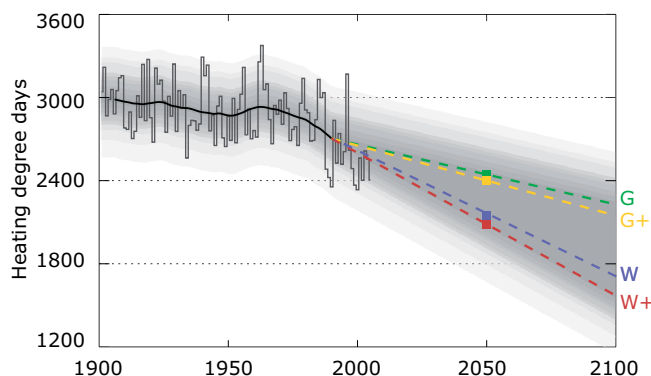
Figure 11-3: Number of heating degree days (cumulative temperature on days below a threshold) below 17 °C in De Bilt. Shown are the observations and the evolution according to the four KNMI'06 scenarios. The shading indicates the interannual variability as seen in the observations.

Periods with summer smog coincide with heat waves. Winter smog is less pronounced with westerly circulations.

An analysis of summer smog is given by RIVM (2004). Ozone-related summer smog conditions are discussed by Vautard et al. (2004). Winter smog especially occurs during conditions with high pressure systems above central Europe, advecting polluted air from eastern areas. A reference is Rombout et al. (1999).

In all four scenarios the expected number of "Eleven cities tours" decreases.

The decrease in mean winter temperature in the scenarios indicates that the chance of long periods with frost decrease. According to Brandsma (2001) this implies a decrease in the number of Eleven cities skating tours.

11.7 Justification

The band width in global temperature rise by 2100 (+1°C up to +6°C compared to 1990) of recent GCM simulations is only slightly broader than the band width presented in the third report of the Intergovernmental Panel on Climate Change (IPCC, 2001; +1.4°C up to +5.8°C).

The band width of global temperature rise shown in Figure 3-2 contains only a portion of the total ensemble of GCM simulations produced for AR4. Taking into account other uncertainties than those parameterized by the 4AR coupled climate models, the band extends from +1°C up to +6°C compared to 1990. The motivation for this (slight) extension of the band width comes from studies being referred to in the (upcoming) AR4 report, for instance Knutti et al. (2006) and Annan et al. (2005).

The increase of +4°C in 2100 is close to the value that the European Environment Agency expects in case of unchanged climate policy.

The reference for this EEA result is EEA (2005).

The simulation of the frequency distribution of daily precipitation averaged over the Rhine catchment area by RACMO2 resembles the observations well.

This is demonstrated by Figure 11-4 and explained further in the figure caption.
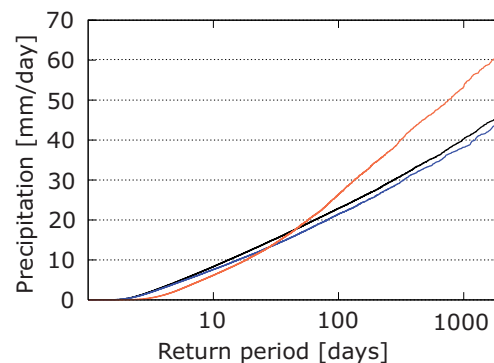
Figure 11-4: Comparison between simulated (blue) and measured (black) precipitation on summer days in the Rhine river basin. For the simulations the KNMI regional climate model RACMO2 was used. The figure shows the relation between the precipitation amount and a certain return period. The precipitation amount for a return period of 100 indicates that once every 100 days this amount is exceeded. Model calculations for 1961-1990 exhibit a good match with the observations. Therefore, the simulations for the future (red) are also considered rather reliable. The simulations for 2071-2100 show a slight decrease in low precipitation amounts, and a strong increase in larger precipitation amounts. Other climate models project the same trends. This information is the basis for the increase of the extreme precipitation in summer in all scenarios.

Most of the used GCM's (selected on the basis of a good representation of the present climate air pressure patterns above Europe), show either hardly any change in air circulation in summer and winter, or a clear change in both seasons.

This is based on our analysis of AR4 GCMs. In this case only 5 GCMs could be analysed (see Section 4 and in particular Figure 4-4). It is, however, possible to construct scenarios in which strong circulation change in one season is combined with weak or no circulation change in the other. This is the reason of grouping winter and summer changes together in Table 8-1, and avoiding changes over the whole year to be presented in the scenarios.

The simulation of abrupt climate change, for example as a result of a complete collapse of the "warm gulf stream" or the unexpectedly fast melting of large ice caps in Greenland and West Antarctica is relatively poor in climate models.

GCMs do not model the ice-sheets explicitly. For instance, Overpeck et al. (2006) use indirect evidence for melting of the West Antarctic ice sheet in the Eemien based on simulated warming of the Southern Oceans. Otto-Bliesner et al. (2006) use GCM output to run an ice sheet model off-line. The thermohaline circulation ("gulf stream" for laymen) and the oceanic western boundary currents are poorly simulated in GCMs due to low resolution. None of the models show a collapse of the THC under global warming. To come to a collapsed state unrealistic large (sub) arctic fresh water fluxes need to be prescribed in models (e.g. Stouffer et al., 2006).

The G and G+ scenarios are more in agreement with the MNP B1 and B2 scenarios, and the W and W+ scenarios with the MNP A1 and A2 scenarios.

This is explained in the 'Guidance for use' section and Table 9-1.

Acknowledgements

References

Alexander, L.V., X. Zhang, T.C. Peterson, J. Caesar, B. Gleason, A.M.G. Klein Tank, M. Haylock, D. Collins, B. Trewin, F. Rahimzadeh, A. Tagipour, P. Ambenje, K. Rupa Kumar, J. Revadekar en G. Griffiths, 2006. Global observed changes in daily climate extremes of temperature and precipitation. *J. Geophys. Res.* **111** (D05109), doi:10.1029/2005JD006290

Allen, M., P. Stott, J. Mitchell, R. Schnur & T. Delworth, 2000. Quantifying the uncertainty in forecasts of anthropogenic climate change. *Nature* **407**, 617-620.

Alley, R.B., et al., 2005. Ice-sheet and sea-level changes. *Science* **310**, 456-460.

Annan, J.D., J. C. Hargreaves, R. Ohgaito, A. Abe-Ouchi and S. Emori, 2005. Efficiently Constraining Climate Sensitivity with Ensembles of Paleoclimate Simulations. SOLA **1**, 181-184, doi: 0.2151/sola. 2005-047

Antonov, J. I., S. Levitus and T.P. Boyer, 2002. Steric sea level variations 1957-1994: importance of salinity. *J.Geoph. Res.* **107**, doi:10.1029/2001JC000964

Arnell N. W., Hudson D A, Jones R, 2005. Climate change scenarios from a regional climate model: Estimating change in runoff in southern Africa. *Journal of Geophysical Research-Atmospheres.* **108**(D16): art. no.-4519.

Asselman, N.E.M., H. Buiteveld, M. Haasnoot, F.J.P.M. Kwaad, J.C.J. Kwadijk, H. Middelkoop, W.P.A. van Deursen, P.M. van Dijk, J.A.P.H. Vermulst, C. Wesseling, 2000. *The impact of climate change on the river Rhine and the implications for water management in the Netherlands.* Summary report of the NRP project 952210, RIZA report 2000.010, 156 pp.

Beersma, J.J. and T.A. Buishand, 2002. *Droog, droger, droogst*; KNMI Scientific Report 199.

Beersma, J.J., B.J.J.M. van den Hurk and G.P. Konnen, 2001. *Weer en Water in de 21e eeuw*; Brochure KNMI (see www.knmi.nl/klimaatverandering_en_broeikaseffect/factsheets/weer_en_water_inde_21e_eeuw.pdf) (In Dutch)

Beniston, M., F. Keller and S. Goyette, 2003. Snow pack in the Swiss Alps under changing climatic conditions: an empirical approach for climate impact studies; *Theor. Appl. Climatology* **74**, 19-31.

Bessembinder, J., 2005. *Klimaatverandering en planning van capaciteit en volume*. KNMI Technical report TR-283.

Boer, G.J., G. Flato and D. Ramsden, 2000. A transient climate change simulation with greenhouse gas and aerosol forcing: projected climate to the twenty-first century. *Climate Dynamics* **16**, 427-450.

Booij, M.J., 2005. Impact of climate change on river flooding assessed with different spatial model resolutions. *J. Hydrol.* **303**, doi 10.1016/j.hydrol.2004.07.013.

Brandsma, T., 2001. How many "Elfstedentochten" in the 21st century? *Zenit* **28**, 194-197. In Dutch.

Buishand, T.A. and A.M.G. Klein Tank, 1996. Regression model for generating time series of daily precipitation amounts for climate change impact studies. *Stochastic Hydrology and Hydraulics*, **10**, 87-106.

Buizza, R., P.L. Houtekamer, Z. Toth, G. Pellerin, M. Wei and Y.A. Zhu, 2005. Comparison of the ECMWF, MSC, and NCEP Global Ensemble Prediction Systems. *Monthly Weather Review,* **133**, 1076-1097.

Christensen, J. H., O. Christensen, P. Lopez, E. van Meijgaard, and M. Botzet, 1996. *The HIRHAM4 regional atmospheric climate model*. Technical Report 96-4, DMI.

Christensen, J.H., T. Carter and F. Giorgi, 2002. PRUDENCE employs new methods to assess European climate change. *EOS* **83**, 147.

Christensen, J.H. and O.B. Christensen, 2003. Severe summertime flooding in Europe. *Nature* **421**, 805-806.

Christensen, J. H., O. B. Christensen, 2006: A summary of the PRUDENCE model projections of changes in the European climate by the end of this century. *Climatic Change*, in press.

Church, J.A. and N.J. White, 2006. A 20th century acceleration in global sea-level rise. *Geophys. Res. Lett.* **33** (L01602) doi:10.1029/2005GL024826.

Church, J.A., et al., 2001. *Chapter 11, Changes in sea level*. In: Climate Change 2001: The scientific basis. Contribution of Working Group I to the Third Assessment Report of the Intergovernmental Panel on Climate Change. J.T. Houghton et al. (eds), pp 639-693, Cambridge University Press.

CLIVAR Scientific Steering Group, 1995. *CLIVAR Science Plan*. World Climate Research Programme publication WCRP-89, WMO/TD No. 690, WMO, Geneva, Switzerland, 157 pp.

Covey, C., K. M. Achuta Rao, U. Cubasch, P. Jones, S. J. Lambert, M. E. Mann, T. J. Phillips, and K. E. Taylor, 2003. An overview of results from the Coupled Model Intercomparison Project. *Global Planet. Change* **37**, 103–133.

Dawson R., Hall J, Bates P, Nicholls R., 2005. Quantified analysis of the probability of flooding in the Thames Estuary under imaginable worst case sea-level rise scenarios. *Int. J. Water Resources Development* **21**, 577 - 591.

Delworth, T.L. and CoAuthors, 2006. GFDL's CM2 global coupled climate models – Part 1: Formulation and simulation characteristics, *J. Climate* **19**, 643-674

Déqué, M. D.P. Rowell, D. Lüthi, F. Giorgi, J. H. Christensen, B. Rockel, D. Jacob, E. Kjellström, M. de Castro, and B. van den Hurk, 2006: An intercomparison of regional climate simulations for Europe: assessing uncertainties in model projections. *Climatic Change*, in press.

EEA, 2005. *European Environment Outlook*. EEA report 4/2005. European Environment Agency, Copenhagen, Denmark.

Fisher, R. W., 1996. Future Energy Use. *Future Research Quarterly* **31**, 43-47.

Flato, G. M, 2005: The third generation coupled global climate model (CGCM3). www.cccma.bc.ca/modelscgcm2.shtml

Frei, C., 2004. *Die Klimazukunft der Schweiz – Eine probabilistische Projektion*. Institut für Atmosphäre und Klima, ETH Zürich.

Frei, C., R. Schöll, S. Fukutome, J. Schmidli en P.L. Vidale, 2006. Future change of precipitation extremes in Europe: an intercomparison of scenarios from regional climate models. *J.Geophys.Res.*, in press.

Giorgi, F., C. Shields Brodeur and G.T. Bates, 1994. Regional Climate Change Scenarios over the United States Produced with a Nested Regional Climate Model. *Journal of Climate* **7**, 375–399.

Giorgi, F. and L. O. Mearns, 1999. Introduction to special section: Regional climate modeling revisited. *J. Geophys. Res.* **104**, 6335-6352.

Gregory, J. M. and J. Oerlemans, 1998. Simulated future sea-level rise due to glacier melt based on regionally and seasonally resolved temperature changes. *Nature* **391**, 474-476.

Gregory J. M., et al., 2005. A model intercomparison of changes in the Atlantic thermohaline circulation in response to increasing atmospheric CO 2 concentration. *Geophys. Res. Lett.* **32**, L12703

Gregory, J.M., and P. Huybrechts, 2006. Ice sheet contributions to future sea-level change. *Phil. Trans. Roy. Soc. A*, in press.

Hazeleger, W., 2005. Can global warming affect tropical ocean heat transport? *Geophys.Res.Lett.* **32**, L22701. doi:10.1029/2005GL023450.

Holgate, S.J. and P.L. Woodworth, 2004. Evidence for enhanced coastal sea level rise during the 1990's. *Geophys. Res. Lett.* **31** (L07305), doi:10.1029/2004GL019626.

Hulme, M., G. Jenkins, X. Lu, J. R. Turnpenny, T. D. Mitchell, R. G. Jones, J.Lowe, J. M. Murphy, D. Hassell, P. Boorman, R. McDonald, and S. Hill, 2002. *Climate Change Scenarios for the United Kingdom: The UKCIP02 Scientic Report*. Technical report, Tyndall Centre for Climate Change Research.

Huybrechts, P., et al., 2004. Modelling Antarctic and Greenland volume changes during the 20th and 21st centuries forced by GCM time slice integrations. *Glob. Planet. Change* **42**, 83-105.

IPCC, 2000. *Special report on emissions scenarios*, 599 pp., Cambridge University Press, Cambridge.

IPCC, 2001. *Climate Change 2001: The scientific basis. Contribution of Working Group I to the Third Assessment Report of the Intergovernmental Panel on Climate Change.* J.T. Houghton et al. (eds), Cambridge University Press.

Jacob, D., 2001. A note to the simulation of the annual and inter-annual variability of the water budget of the Baltic Sea drainage basin. *Meteor. Atm. Phys.* **77**, 61-73.

Jacob, D., L. Bärring, O.B. Christensen, J.H. Christensen., M. de Castro, M. Déqué, F. Giorgi, S. Hagemann., M. Hirschi, R. Jones, E. Kjellström, G. Lenderink, B. Rockel, E. Sánchez Sánchez, C. Schär, S.I. Seneviratne, S. Somot, A. van Ulden and B van den Hurk, 2006. An inter-comparison of regional climate models for Europe: Design of the experiments and model performance. *Climatic Change*, in press.

Johns, T. et al., 2004. *HadGEM1 — Model description and analysis of preliminary experiments for the IPCC Fourth Assessment Report.* Tech. Rep. 55, U.K. Met Office, Exeter, U.K.

Jones, P. D., T. D. Davies, D. H. Lister, V. Slonosky, T. Jonsson, L. Barring, P. Jonsson, P. Maheras, F. Kolyva-Machera, M. Barriendos, J. Martin-Vide, R. Rodriquez, M. J. Alcoforado, H. Wanner, C. Pfister, J. Luterbacher, R. Rickli, E. Schuepbach, E. Kaas, T. Schmith, J. Jacobeit, and C. Beck, 1999. Monthly mean pressure reconstructions for Europe for the 1780 – 1995 period. *Int. J. Climatol.* **19**, 347–364.

Jones, R. G., J. M. Murphy, D. Hassell, and R. Taylor, 2001. *Ensemble mean changes in a simulation of the European climate 2071-2100 using the new Hadley Centre regional modelling system HadAM3H/HadRM3H.* Technical report, Hadley Centre.

Jones, P.D. and A. Moberg, 2003. Hemispheric and large-scale surface air temperature variations: An extensive revision and update to 2001. *J. Climate* **16**, 206–223.

K-1 model developers, 2004. *K-1 coupled model (MIROC) description.* Tech. Rep. 1, Center for Climate System Research, University of Tokyo.

Kabat, P., W. van Vierssen, J. Veraart, P. Vellinga and J. Aerts, 2005. Climate proofing the Netherlands. *Nature* **438**, 283-284

Keller, F. and S. Goyette (2005): *Snowmelt under different temperature increase scenarios in the Swiss Alps*; In: de Jong et al. (Eds), *Climate and Hydrology in Mountain Areas*, J.Wiley & Sons, pp 277-289.

Kjellstrom, E., L. Bärring, D. Jacob, R. Jones, G. Lenderink and C. Schär, 2006. Variability in daily maximum and minimum temperatures: Recent and future changes over Europe. *Climatic Change* (in press).

Kjellstrom, E., 2004. Recent and future signatures of climate change in Europe. *Ambio* **33**, 193-198.

Klein Tank, A.M.G. and T.A. Buishand, 1995. *Transformation of precipitation time series for climate change impact studies.* KNMI Scientific Report WR 95-01, De Bilt.

Klein Tank, A.M.G., T.A. Buishand, J.J. Beersma and G.P. Können, 1995. *Climate Change scenarios for impact studies in The Netherlands.* In: Zwerver et al. (Eds), *Climate Change Research: Evaluation and Policy Implications*; Elsevier.

Klein Tank, A.M.G. and G.P. Können, 1997. Simple temperature scenario for a Gulf Stream induced climate change. *Climatic Change* **37**, 505-512.

Klein Tank, A.M.G. and G.P. Können, 2003. Trends in indices of daily temperature and precipitation extremes in Europe, 1946–1999. *J. Climate* **16**, 3665–3680.

Klein Tank, A.M.G., J.B. Wijngaard et al., 2002. Daily dataset of 20th-century surface air temperature and precipitation series for the European Climate Assessment. *Int. J. Climatology* **22**, 1441-1453.

KNMI, 2003. *Climate Change in the Netherlands; Fourth National Climate Report.* De Bilt, the Netherlands, 32pp. (in Dutch; available at www.knmi.nl)

KNMI, 2006. *Climate in the 21st century: Four scenarios for the Netherlands*; Brochure (16 pp). Available from KNMI, PO Box 201, 3730 AE De Bilt, The Netherlands.

Knutti, R., G.A. Meehl, M.R. Allen and D.A. Stainforth, 2006. Constraining climate sensitivity from the seasonal cycle in surface temperature. *J.Climate.*, in press.

Komen, G.J. 1994. *An expert-opinion approach to the prediction problem in complex systems.* In: J. Grasman and G. Van Straten (eds), *Predictability and Nonlinear Modelling in Natural Sciences and Economics.* Kluwer, Dordrecht, p432-438.

Komen, G.J. (2001): *Lente in de broeikas – over begrijpen en voorspellen van klimaatveranderingen*; Oration lecture; KNMI, De Bilt (48 pp) (In Dutch)

Können, GJ (2001): Climate Scenarios For Impact Studies In The Netherlands; see www.knmi.nl/onderzk/klimscen/scenarios/Scenarios2001_Web.htm

Kors, A.G., F.A.M. Claessen, J.W. Wesseling and G.P. Können, 2000. *Scenario's externe krachten voor WB21*; WL|Delft Hydraulics; Koninklijk Nederlands Meteorologisch Instituut (KNMI) ; Ministerie van Verkeer en Waterstaat, Rijkswaterstaat, Rijksinstituut voor Integraal Zoetwaterbeheer en Afvalwaterbehandeling (RWS, RIZA) (in Dutch).

Krabill, W., et al., 2004. Greenland Ice Sheet: Increased coastal thinning. *Geophys. Res. Lett.* **31** (L24402) doi:10.1029/2004GL021533.

Lambert, S.J. and J.C. Fyfe, 2006. Changes in winter cyclone frequencies and strengths simulated in enhanced greenhouse warming experiments; results from the models participating in the IPCC diagnostic exercise; *Climate Dynamics* doi 10.1007/s00382-006-0110-3.

Lawrence, D.M. and A.G. Slater, 2005. A projection of severe near-surface permafrost degradation during the 21th century. *Geophys. Res. Lett.* **32** (L24401), doi:10.1029/2005GL025080.

Leander, R. en T.A. Buishand, 2006. Combining regional climate model output and resampling - can it provide realistic input for the simulation of extreme river flows? Submitted *J. Hydrol.* (see www.knmi.nl/publications/fulltexts/hydrol4965_copy1.pdf)

Leckebusch, G.C., B.U. Ulbrich, J.G. Pinto, T. Spangehl and S. Zacharias, 2006. Analysis of frequency and intensity of winter storm events in Europe on synoptic and regional scales from a multi-model perspective. *Climatic Research* (in press).

Lenderink, G., B. van den Hurk, E. van Meijgaard, A. van Ulden and H. Cuijpers, 2003. *Simulation of present-day climate in RACMO2: first results and model developments.* KNMI TR 252, 24 pp.

Lenderink, G., A. van Ulden, B. van den Hurk and E. van Meijgaard, 2006. Summertime inter-annual temperature variability in an ensemble of regional model simulations: analysis of the surface energy budget. *Climatic Change*, in press.

Leuliette, E.W., R.S. Nerem and G.T. Mitchum, 2004. Calibration of Jason altimeter data to construct a continuous record of mean sea level change. *Marine Geodesy* **27**, 79-94. Data at: sealevel.colorado.edu

Levermann, A. et al., 2005. Dynamic sea level changes following changes in the thermhohaline circulation. *Climate Dynamics* **24**, 347-354

Lorenz, E.N., 1969. Atmospheric predictability as revealed by naturally occurring analogues. *Journal of the Atmospheric Sciences* **26**, 636-646.

Lorenz, E.N., 1975. *Climate predictability: The physical basis of climate modeling.* GARP Publication series, Vol. 16, WMO, 132–136.

MacCracken, M.C., E.J. Barron, D.R. Easterling, B.S. Felzer and T.R. Karl, 2003. Climate change scenarios for the U.S. National Assessment. Bull.Am.Met.Soc. **84**, 1711-1723, doi: 10.1175/BAMS-84-12-1711

Makkink, G.F., 1957. Testing the Penman formula by means of lysimeters; *J.Int.Water Eng.* **11**, 277-288.

Manabe, S., and R.J. Stouffer, 1988. Two stable equilibria of a coupled ocean-atmosphere model. *J. Climate* **1**, 841-866.

Meehl, G. A., G.J. Boer, C. Covey, M. Latif and R.J. Stouffer, 2000. The Coupled Model Intercomparison Project (CMIP). *Bulletin of the American Meteorological Society* **81**, 313–318.

Meehl, G.A., C. Covey, B. McAvaney, M. Latif, and R.J. Stouffer, 2005. Overview of the Coupled Model Intercomparison project. *Bulletin of the American Meteorological Society* **86**, p89 – 93.

Meehl, G.A., et al., 2005. How much more global warming and sea level rise? *Science* **307**, 1769-1772.

Molteni, F., R. Buizza, T.N. Palmer and T. Petroliagis, 1996. The ECMWF Ensemble Prediction System: Methodology and validation. *Quarterly Journal of the Royal Meteorological Society* **122**, 73-119.

Murphy, J.M., D.M.H. Sexton, D.N. Barrett, G.S. Jones, M.J. Webb, M. Collins and D.A. Stainforth, 2004. Quantification of modelling uncertainties in a large ensemble of climate change simulations. *Nature* **430**, 768-772.

Müller, P., and H. von Storch, 2004. *Computer Modelling in Atmospheric and Oceanic Sciences - Building Knowledge.* Springer Verlag Berlin – Heidelberg - New York, 304pp, ISN 1437-028X

New, M., Hulme, M. and Jones, P.D., 2000. Representing twentieth century space-time climate variability. Part 2: development of 1901-96 monthly grids of terrestrial surface climate. *J. Climate* **13**, 2217-2238.

Ohmura, A., 2004. Cryosphere during the Twentieth Century, The State of the Planet. *IUGG Geophys. Monograph* **150**, 239-257.

Overpeck, J.T., B.L. Otto-Bliesner, G.H. Miller, D.R. Muhs, R.B. Alley, and J.T. Kiehl, 2006. Paleoclimatic Evidence for Future Ice-Sheet Instability and Rapid Sea-Level Rise. *Science* **311**, 1747-1750.

Otto-Bliesner, B.L., S.J. Marshall, J.T. Overpeck, G.H. Miller, A. Hu, CAPE Last Interglacial Project members, 2006. Simulating Arctic climate warmth and icefield retreat in the last interglaciation. *Science* **311**, 1751-1753.

Palmer, T. N., 1993. Extended-range atmospheric prediction and the Lorenz model. *Bull. Amer. Meteor. Soc.* **74**, 49-65.

Palmer, T. N. F. J. Doblas-Reyes, and R. Hagedorn, A. Alessandri and S. Gualdi, U. Andersen and H. Feddersen, P. Cantelaube and J.-M. Terres, M. Davey and R. Graham, P. Délécluse and A. Lazar, M. Déqué, and J.-F. Guérémy, E. Díez and B. Orfila, M. Hoshen and A. P. Morse, N. Keenlyside and M. Latif, E. Maisonnave and P. Rogel, ,V. Marletto, M. C. Thomson, 2004. Development of a European Multimodel Ensemble System for Seasonal-to-Interannual Prediction (Demeter). *Bulletin of the American Meteorological Society* **85**, 853–872.

Peltier, W.L., 2002. On eustatic sea level history: Last Glacial Maximum to Holocene. *Quarternary Science Reviews* **21**, 377-396.

Raisanen, J., U. Hansson, A. Ullerstig, R. Doscher, L. P. Graham, C. Jones, H. E. M. Meier, P. Samuelsson, and U. Willen, 2004. European climate in the late twenty-first century: regional simulations with two driving global models and two forcing scenarios. *Climate Dynamics* **22**, 13-31.

Raper, S., and R.J. Braithwathe, 2005. The potential for sea level rise: New estimates from glacier and ice cap area and volume distribution. *Geophys. Res. Lett.* **32** (L05502) doi:10.1029/2004GL02181.

Raper, S. and R.J. Braithwathe, 2006. Low sea level rise projections from mountain glaciers and icecaps under global warming. *Nature* **439**, 311-313.

Rial, J.A., R.A. Pielke Sr., M. Beniston, M. Claussen, J. Canadell, P. Cox, H. Held, N. De Noblet-Ducoudré, R. Prinn, J.F. Reynolds and J.D. Salas, 2005. Nonlinearities, Feedbacks And Critical Thresholds Within The Earth's Climate System. *Climatic Change* **65**, 11–38.

Ridley, J.K., et al., 2005. Elimination of the Greenland ice sheet in a high CO_2 climate. *J. Clim.* **17**, 3409-3427.

Rignot, E. and R.H. Thomas, 2002. Mass balance of polar ice sheets. *Science* **297**, 1502-1506.

Rignot, E.G., et al., 2005. Recent ice loss from the Fleming and other glaciers, Wordie Bay, West Antarctic Peninsula. *Geophys. Res. Lett.* **32**, 1-4.

Rignot, E. and P. Kanagaratnam, 2006. Changes in the Velocity Structure of the Greenland Ice Sheet. *Science* **311**, 986-990.

RIVM, 2004. *Zomersmog 2004*. Report 20041223.Bilthoven: (in Dutch).

RIZA, HKV, Arcadis, KIWA, Korbee en Hovelynck, Durk Klopstra, Rudolf Versteeg, Timo Kroon, 2005. *Aard, ernst en omvang van watertekorten in Nederland - Eindrapport Droogtestudie Nederland.* Riza rapport 2005.016 (In Dutch) (see also www.droogtestudie.nl).

Rombout PJA, Bloemen HJTh, Bree L van, Buringh E, Eerens HC, Fischer PH, Marra M, 1999. *Wintersmog en verkeersmaatregelen, effecten op luchtkwaliteit en gezondheid* [Winter-type smog and traffic, effects on air quality and health]. RIVM Rapport 650010012, 42 p. (In Dutch).

Schaeffer, M.; Selten, F. M.; Opsteegh, J. D.; Goosse, H., 2002. Intrinsic limits to predictability of abrupt regional climate change in IPCC SRES scenarios. *Geophysical Research Letters* **29**, 14-19.

Schär, C., D. Luthi, U. Beyerle and E. Heise, 1999. The soil-precipitation feedback: a process study with a regional climate model. *J. Climate* **12**, 722-741.

Schär, C., P.-L. Vidale, D. Luethi, C. Frei, C. Haeberli, M.A. Liniger and C. Appenzeiler, 2004. The role of increasing temperature variability inEuropean summer heatwaves. *Nature* **427**, 332-336.

Schmittner, A., M. Latif and B. Schneider, 2005. Model projections of the North Atlantic thermohaline circulation for the 21st century assessed by observations. *Geophys. Res. Lett.* **32** (L23710), doi:10.1029/2005GL024368.

Selten, F.M., G. Branstator, M. Kliphuis en H.A. Dijkstra, 2004. Tropical origins for recent and future Northern Hemisphere climate change. *Geophys. Res. Lett.* **31**, doi:10.1029/2004GL020739.

Shukla, J., 1998. Predictability in the Midst of Chaos: A Scientific Basis for Climate Forecasting. *Science* **23**, 728-731.

Smits, A., A.M.G. Klein Tank en G.P. Können, 2005. Trends in storminess over the Netherlands, 1962-2002. *Int. J. Climatology* **25**, 1331-1344.

Steppeler, J., G. Doms, U. Schattler, H. W. Bitzer, A. Gassmann, U. Damrath, and G. Gregoric, 2003. Meso-gamma scale forecasts using the nonhydrostatic model LM. *MAP* **82**, 75-90.

Stott, P.A., S.F. Tett, G.S. Jones, M.R. Allen, J.F. Mitchell, G.J. Jenkins, 2000. External control of 20th century temperature by natural and anthropogenic forcings. *Science* **290**, 2133-2137.

Stott, P.A., D.A. Stone and M.R. Allen, 2004. Human contribution to the European heatwave of 2003. *Nature* **432**, 610-613.

Stouffer, and coauthors, 2006. Investigating the causes of the response of the thermohaline circulation to past and future climate changes. *J. Climate* **19**, 1365-1387.

Tennekes, H., 1990. A sideways look at climate research. *Weather* 1990, 67-68.

Thompson, D.W.J., J.M. Wallace, and G.C. Hegerl, 2000. Annular modes in the extratropical circulation. Part II: Trends. *J. Climate* **13**, 1018–1036.

Van den Brink, H.W., 2005. *Extreme winds and sea-surges in climate models*. Thesis Universiteit Utrecht, 122p.

Van den Hurk, B., M. Hirschi, C. Schär, G. Lenderink, E. van Meijgaard, A. van Ulden, B. Rockel, S. Hagemann, L. Graham, E. Kjellstrom and R. Jones, 2005a. Soil Control on Runoff Response to Climate Change in Regional Climate Model Simulations. *Journal of Climate* **18**, 3536–3551.

Van den Hurk, B. J. Beersma en G. Lenderink, 2005b. Hydrological simulations in the Rhine basin; *Water Science and Technology* **51**, 5, 1-4

Van de Wal, R.S.W. and M. Wild, 2001. Modelling the response of glaciers to climate change, applying volume-area scaling in combination with a high resolution GCM. *Clim. Dyn.* **18**, 359-366.

Van der Schrier, G., S.L. Weber, S.S. Drijfhout and J.A. Lowe, 2004. Low-frequency Atlantic sea-level variability. *Global and Planetary Change* **43**, 129-144

Van Oldenborgh, G.J. and A. van Ulden, 2003. On the relationship between global warming, local warming in the Netherlands and changes in circulation in the 20th century. *Int. J. Climatology* **23**, 1711-1723, doi:10.1002/joc.966

Van Ulden, A., G. Lenderink, B. van den Hurk and E. van Meijgaard, 2006. Circulation statistics and climate change in Central Europe: Prudence simulations and observations. *Climatic Change*, in press.

Van Ulden, A.P. and G.J. van Oldenborgh, 2006. Large-scale atmospheric circulation biases and changes in global climate model simulations and their importance for climate change in Central Europe. *Atmos. Chem. Phys.* **6**, 863-881. www.atmos-chem-phys.net/6/863/2006/

Vautard R., C. Honore, M. Beekmann, and L. Rouil, 2005. Simulation of ozone during the August 2003 heat wave and emission control scenarios. *Atmos. Environ.* **39**, 3291-3303.

Velicogna, I. and J. Wahr, 2005. Greenland mass balance from GRACE. *Geophys. Res. Lett.* **32**, L18505.

Vidale, P. L., D. Lüthi, C. Frei, S. I. Seneviratne, and C. Schär, 2003. Predictability and uncertainty in a regional climate model. *J. Geophys. Res.* **108**, 4586 doi:10.1029/2002JD002810.

Vidale, P. L., D. Lüthi, R. Wegmann and C. Schär, 2006. European climate variability in a heterogeneous multi-model ensemble. *Climatic Change* (in press).

Von Storch, H., 2006. *Klimaänderungsszenarien*. In: Gebhardt, H., R. Glaser, U. Radtke & P. Reuber (Hrsg.): *Lehrbuch Geographie*, Spektrum Verlag, Heidelberg (in German).

Wit, M.J.M. de, P.M.M. Warmerdam, P.J.J.F. Torfs, B. van den Hurk, E. Roulin and W.P.A. van Deursen, 2006. Impact of climate change on low flows in the river Meuse. Submitted to *Climatic Change*.

Yin, J.H., 2005. A consistent poleward shift of the storm tracks in simulations of 21st century climate. *Geophys. Res. Lett.* **32**, L18701, doi:10.1029/2005GL023684.

Zwally, H.J., et al., 2006. Mass changes of the Greenland and Antarctic ice sheets and shelves and contributions to sea level rise: 1992-2002. *J. Glac.*, in press.